Deep Eutectic Solvents as Extraction, Reaction and Detection Media for Inorganic Compounds

Dissertation

Zur Erlangung des Doktorgrades der Naturwissenschaften

(Dr. rer. nat.)

an der Fakultät für Chemie und Pharmazie

der Universität Regensburg

vorgelegt von

Anika Söldner

(geb. Kolb)

aus Pegnitz

2019

This work has been carried out between December 2013 and April 2019 under the supervision of Prof. Dr. Burkhard König at the University of Regensburg, Institute of Organic Chemistry.

Date of submission:	04.04.2019
Date of colloquium:	10.05.2019

Board of examiners:	Prof. Dr. Alexander Breder	(chair)
	Prof. Dr. Burkhard König	(1st referee)
	Prof. Dr. Arno Pfitzner	(2nd referee)
	Prof. Dr. Frank-Michael Matysik	(examiner)

"A philosopher once said: 'It is necessary for the very existence of science that the same conditions always produce the same results'. – *Well… they do not."*

Richard P. Feynman

(Nobel Prize in Physics in 1965)

TABLE OF CONTENTS

1 DEEP EUTECTIC SOLVENTS AS EXTRACTION MEDIA FOR PHOSPHATES FROM INCINERATED SEWAGE SLUDGE ASH 1

1.1 Introduction 3

1.2 Results and Discussion 5

1.2.1 Solubility of Metal Salts and Metal Oxides in Different DESs 5

1.2.2 Extraction of Phosphorus from ISSA with DESs 15

1.3 Conclusion 20

1.4 Experimental 21

1.4.1 General Procedures and Materials 21

1.4.2 Procedures and Analytical Methods for Solubility Experiments 22

1.4.3 Procedures and Analytical Methods for the Extraction of Phosphates from ISSA 23

1.5 References 24

2 PREPARATION OF MAGNESIUM, COBALT AND NICKEL FERRITE NANOPARTICLES FROM METAL OXIDES USING DEEP EUTECTIC SOLVENTS 29

2.1 Introduction 31

2.2 Results and Discussion 32

2.2.1 Dissolving Properties and Incineration Behavior of DESs 32

2.2.2 Synthesis of Different Spinel-Type Ferrites with DESs 36

2.2.3 Characterization of the Synthesized Ferrite Nanoparticles 44

2.3 Conclusion 46

2.4 Experimental 46

2.4.1 General Procedures and Materials 46

2.4.2 Thermal Process for the Synthesis of Spinel-Type Ferrites with DESs 47

2.4.3 Characterization Methods 47

2.5 References 49

3 DEEP EUTECTIC SOLVENTS AS POTENTIAL MEDIA FOR OPTICAL ANALYSIS AND SEPARATION OF TRIVALENT LANTHANIDES 53

3.1 Introduction 55

3.2 Results and Discussion 58

3.2.1 Spectroscopic Studies of Trivalent Lanthanides in DESs 60

Europium(III) 61

Terbium(III) 71

Further Trivalent Lanthanides (Sm^{3+}, Dy^{3+}) 73

3.2.2 Solubility and Separation Experiments of Trivalent Lanthanide Oxides in DESs 73

3.3 Conclusion 79

3.4 Experimental 79

3.4.1 General Procedures and Materials 79

3.4.2 Spectroscopic Methods for Luminescence Studies 80

3.4.3 Procedures and Analytical Methods for Solubility and Separation Experiments 80

3.5 References 82

4 SUMMARY 89

5 ZUSAMMENFASSUNG 93

6 APPENDIX 97

6.1 References for Renewable DES Compounds 97

6.2 Degree of Inversion of the Prepared $MgFe_2O_4$ Nanoparticles 97

6.3 Concentration Dependence of the Fluorescence Intensity 99

6.4 Fluorescence Spectra of Samarium(III) and Dysprosium(III) Chlorides in DESs 103

6.5 Abbreviations 105

7 DANKSAGUNG 111

CHAPTER 1

1 Deep Eutectic Solvents as Extraction Media for Phosphates from Incinerated Sewage Sludge Ash

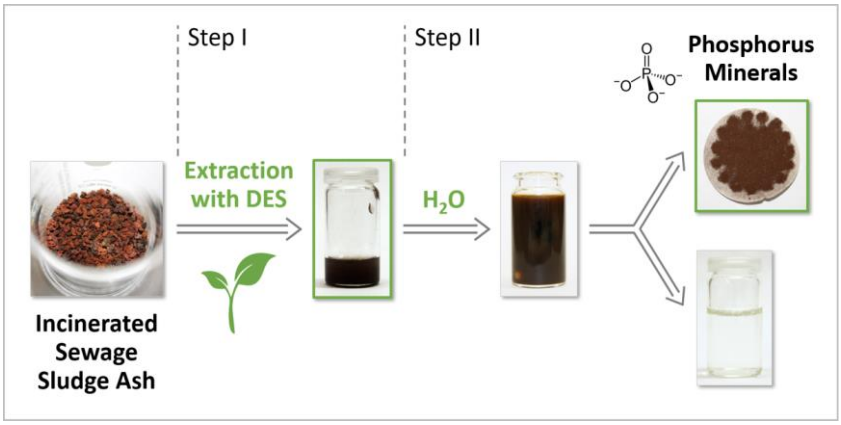

This chapter has been published as:

A. Söldner, J. Zach and B. König, *Green Chem.*, **2019**, 21, 321-328.

A. Söldner performed the solubility experiments, carried out all measurements and wrote the manuscript. J. Zach accomplished the phosphorus extraction experiments. B. König supervised the project and is the corresponding author.

1.1 Introduction

The extraction of phosphates from a nearly inexhaustible secondary resource using renewable solvents based on natural products would imply a great step towards sustainability. Besides phosphate rock as a primary but a limited source for phosphorus compounds, the main secondary but hardly used resource is sewage sludge, whose availability would be ensured for decades. The difficulties of sewage sludge workup are the complexity and inhomogeneity of its composition.[1] While some batches of sewage sludge can be used as manure for agriculture, the bulk is combusted to incinerated sewage sludge ash (ISSA) or used as landfill.[2] The incineration of sewage sludge has several advantages as it removes the relatively high water content, reduces the mass and volume by up to 90%, and concentrates the mineral fraction, which increases the processing capacities required.[3, 4] In addition, pathogenic agents get destroyed, organic compounds are oxidized (*e.g.* residues of pharmaceuticals and personal care products),[5-8] and thermal energy is generated that can be used.[9-11]

Due to the fact that all modern agricultural systems depend on the continual application of phosphate fertilizers[12] and the predicted phosphorus scarcity by the end of this century,[13-15] it is crucial to find effective (and ideally environmentally friendly) extraction processes for phosphate compounds from renewable resources. Furthermore, the European Union (EU) has no natural mining sites of phosphate rock and is entirely dependent on imports. Therefore, the legal regulations in EU countries intensify. For example, in Germany, the new Ordinance for the Recovery of Sewage Sludge came into force on October 2, 2017, which bounds the operators of sewage sludge treatment plants for municipal districts with more than 50 000 citizens to the recovery of phosphorus from sewage sludge and ISSA by 2032 at the latest.[16, 17] As a result, countries such as the United Kingdom, the Netherlands, Austria and Germany increasingly support research on the recovery of phosphates.[2, 18-20]

Several methods for achieving the goal have been reported, but so far, none of these processes has become established as a standard for phosphate recycling for industry and municipalities or offers a low-energy and environmentally friendly procedure under mild

extraction conditions, as far as we know. Recovery of phosphorus by acid leaching is one of the extensively studied approaches. A major challenge is the separation or precipitation of metals that are also soluble in the respective acidic solution. Several acids were investigated: H_2SO_4,[21-26] H_3PO_4,[27, 28] HCl,[22, 24, 29-31] HNO_3,[27, 28, 32] citric acid and oxalic acid.[22] For many of these processes, high amounts of acids are required and the amount of wet solid residues for disposal is higher than the amount of ISSA that was treated. One process tested at a large scale is the REMONDIS TetraPhos procedure, which has phosphoric acid and gypsum as its final products.[33] The main alternative for P recovery so far is *via* thermal methods below or above the melting point of ISSA at around 1300 °C dependent on the composition. Thermochemical treatment at 900–1000 °C and the addition of nutrients nitrogen, phosphorus, and potassium or chlorinating agents (*e.g.* Cl_2, $MgCl_2$, KCl_2, $CaCl_2$, and $NaCl_2$) to ISSA lead to a high percentage removal of undesirable compounds by volatilization,[34-36] but also 30% of P can be lost in fine ashes carried out with exhaust gases.[24] The P-recovery process developed within the framework of the European FP6-project SUSAN is based on this procedure and has already been tested on an industrial scale.[37] At temperatures above 1450 °C, phosphorus can be transferred into a metallurgical slag by reductive smelting[38] or reduced to elementary phosphorus and separated *via* the gas phase.[39] However, both types of thermochemical processes are accompanied by high energy costs and the necessity of an appropriate composition of ISSA. Furthermore, less intensively studied methods are using base[29] or supercritical fluids[40] as an extractant or electrodialytic separation in acids.[41, 42]

One class of extractants that has not been considered so far is ionic liquids (ILs) and deep eutectic solvents (DESs). An IL is a salt in the liquid state, whereas DESs consist of a hydrogen-bond acceptor (HBA) and a hydrogen-bond donor (HBD) forming a mixture with a melting point that is significantly lower than that of the two single components – ideally around room temperature.[43, 44] DESs share many properties with ILs but, in addition, DESs are facile to prepare, based on readily available and inexpensive starting materials, and do not accumulate in the environment. Both types of liquids have previously been reported as extraction media for a variety of compounds from complex matrices. DESs and ILs provide a high solvation potential without the presence of water, an organic

solvent, or the highly basic/acidic conditions that are needed in most analogous aqueous systems. This is exemplified by the extraction of metals from different waste streams including slag, filter cakes and battery waste,[45-47] natural products from plant materials,[48-52] and lipids from primary sewage sludge.[53] In this chapter, we present a comprehensive study of the extraction potential of DESs based on natural products for a variety of metal salts and metal oxides, as well as a new approach for phosphorus mineral extraction from ISSA.

1.2 Results and Discussion

In many papers and reviews, DESs and ILs are discussed as solvents that are fully adjustable to many requirements and separation problems due to the wide variety of composition possibilities. However, the prediction of *e.g.* specific extraction properties is still a challenge. Furthermore, DESs and ILs have poor transport properties compared to molecular solvents such as water. They are at least an order of magnitude more viscous than molecular solvents, which leads to slow transport of the diffusing species and complicated handling. Nonetheless, DESs and ILs provide a high solvation potential even for hardly soluble metal oxides under relatively mild conditions.

1.2.1 Solubility of Metal Salts and Metal Oxides in Different DESs

In the first part of this report, we discuss the solvation potential of 12 different DESs with respect to metal salts and metal oxides. The used metal compounds are either main or valuable trace components of ISSA or at least of interest regarding prior workup.[1] As HBA components for the DESs choline chloride (ChCl) and *N,N'*-dimethyl urea (DMU) were used (Figure 1). Both compounds form low viscosity melts with a variety of HBDs at temperatures up to 100 °C in a viscosity range of 20 to 750 cP, which is crucial for further extraction experiments.[54, 55]

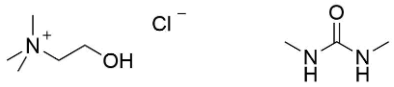

Figure 1. Hydrogen-bond acceptors (HBAs) for DESs used as extraction media: choline chloride (ChCl, *left*) and *N,N'*-dimethyl urea (DMU, *right*).

The HBD component of the DESs varies from sugars and sugar alcohols to organic acids and urea (Table 1). The majority of the compounds for the presented DESs are easily available and inexpensive as well as readily biodegradable and renewable (for detailed references on the renewability of the used DES compounds see Table A.1 in Appendix 6.1).[56, 57] For each metal salt and oxide, an oversaturated mixture was prepared with the DESs at a processing temperature of 80 or 90 °C (Table 1), which was chosen according to the following aspects: high enough to ensure low viscosity and maximum solubility due to heat exposure; low enough to avoid decomposition, sublimation or vaporization of the DES components and easy handling.

Table 1. DESs 1–12 based on choline chloride (ChCl) or *N,N'*-dimethyl urea (DMU) as hydrogen-bond acceptor (HBA) with sugars, sugar alcohols, organic acids, urea and vanillin as hydrogen bond donor (HBD), and the respective melting point (T_m) or solidification point (T_s).[43, 58, 59]

Entry	HBA	HBD	Structure [c]	Molar ratio	*T* [°C]	
1	ChCl	D-sorbitol [b]	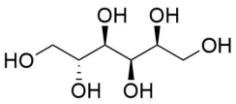	1 : 1	T_m	liquid at r.t.
2	ChCl	tartaric acid [b]	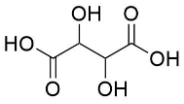	2 : 1	T_m	47
3	ChCl	citric acid monohydrate [a]	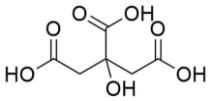	2 : 1	T_s	69
4	ChCl	urea [a]	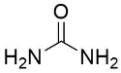	1 : 2	T_s	12
5	DMU	D-fructose [a]	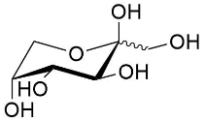	3 : 1	T_m	80
6	DMU	mannose [a]	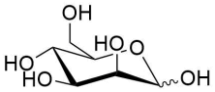	5 : 1	T_m	75
7	DMU	citric acid monohydrate [a]	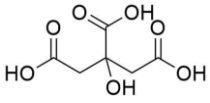	7 : 2	T_m	65
8	ChCl	D-fructose [a]	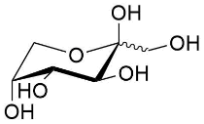	1 : 2	T_m	*n.a.*

9	ChCl	D-glucose [a]	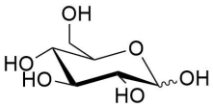	1 : 2	T_m	*n.a.*
10	ChCl	malonic acid [a]	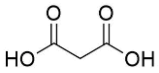	1 : 1	T_m	*n.a.*
11	ChCl	xylitol [a]	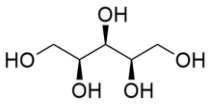	1 : 1	T_m	*n.a.*
12	ChCl	vanillin [a]	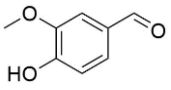	1 : 2	T_m	*n.a.*

Processing temperature: (*a*) 80 °C or (*b*) 90 °C. (*c*) Structures do not contain hydrate molecules.
Abbreviation: n.a. = not available.

The appearance of the obtained samples ranged from slightly turbid for colloidal solutions or suspensions to completely clear, indicating that the metal compound was largely dissolved (Figure 2).

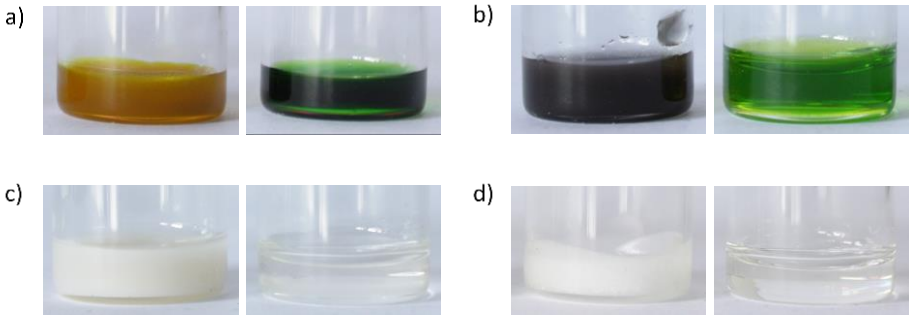

Figure 2. Turbid and clear saturated solutions of a) $CuCl_2$ in ChCl/citric acid monohyd. (turbid, *left*) and DMU/citric acid monohyd. (clear, *right*), b) CuO in ChCl/D-sorbitol (turbid, *left*) and ChCl/citric acid monohyd. (clear, *right*), c) ZnO in ChCl/D-sorbitol (turbid, *left*) and ChCl/citric acid monohyd. (clear, *right*), and d) MoO_3 in ChCl/D-mannose (turbid, *left*) and ChCl/citric acid monohyd. (clear, *right*) after hot filtration.

The amount of the dissolved metal in the DESs was determined *via* inductively coupled plasma optical emission spectroscopy (ICP-OES) (inductively coupled plasma optical emission spectroscopy) or reweighing after the complete combustion of the organic components. The obtained values for the mass fraction ω_{max} of the maximum dissolved metal salt or oxide are listed in Table 2 for DESs 1–12 and are depicted in Figure 3, Figure 4, Figure 5, and Figure 6 for DESs 1–7. The values for DESs 1–7 represent an average of three independent measurements.

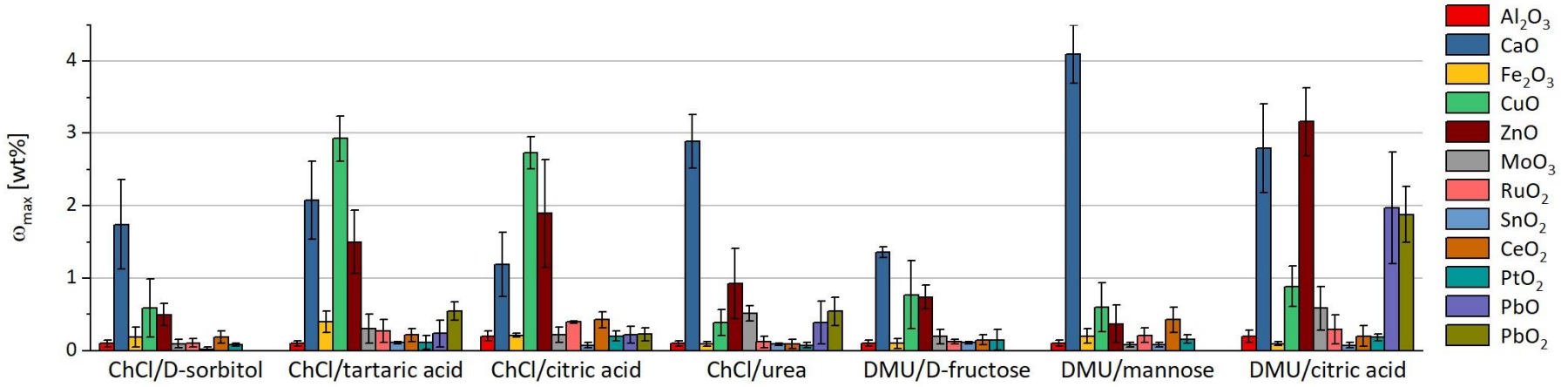

Figure 3. Maximum solubility as the mass fraction ω_{max} [wt%] of metal oxides in DESs 1–7.

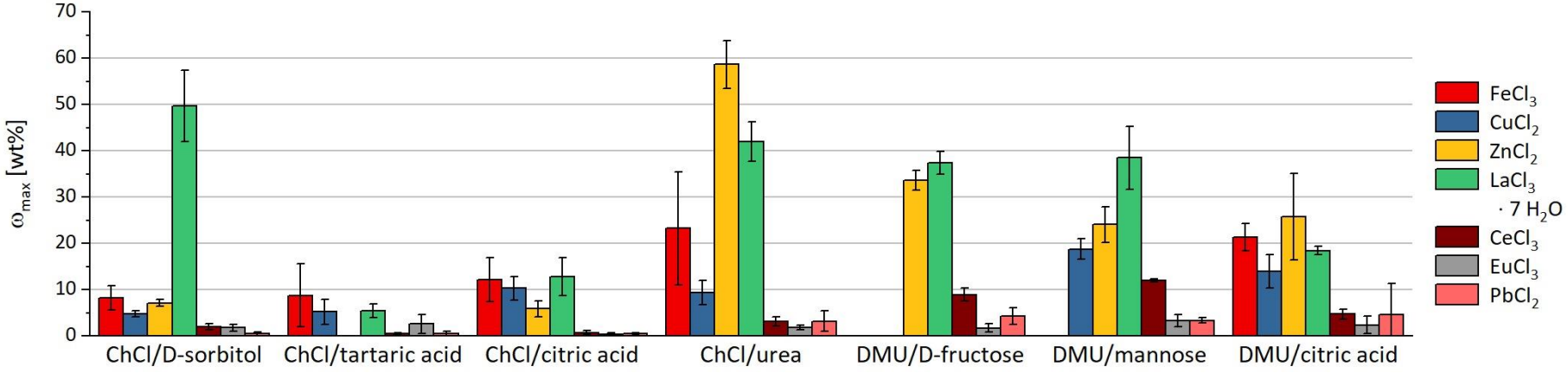

Figure 4. Maximum solubility as the mass fraction ω_{max} [wt%] of metal chlorides in DESs 1–7.

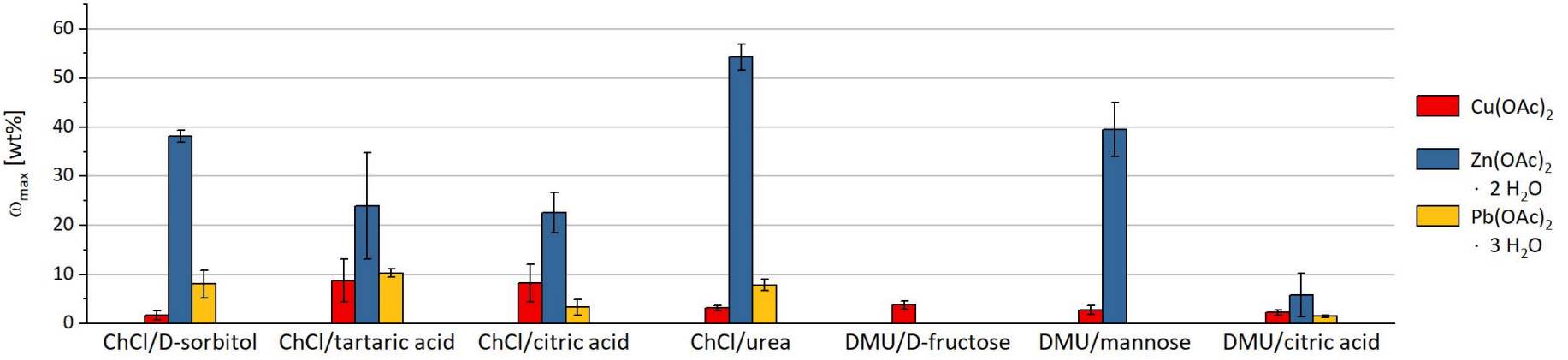

Figure 5. Maximum solubility as the mass fraction ω_{max} [wt%] of metal acetates in DESs 1–7.

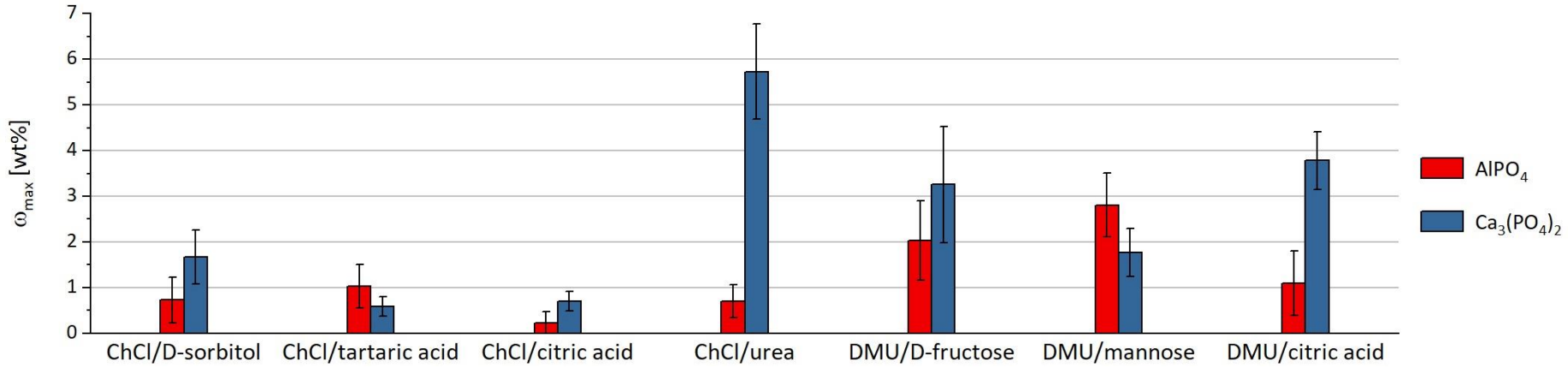

Figure 6. Maximum solubility as the mass fraction ω_{max} [wt%] of metal phosphates in DESs 1–7.

Table 2. Mass fraction ω_{max} [wt%] of 26 different metal salts and oxides in DESs 1–12.

ω_{max} [wt%]	ChCl/ D-sorbitol	ChCl/ tartaric acid	ChCl/ citric acid monohyd.	ChCl/ urea	DMU/ D-fructose	DMU/ mannose	DMU/ citric acid monohyd.	ChCl/ D-glucose*	ChCl/ D-fructose*	ChCl/ vanillin*	ChCl/ malonic acid*	ChCl/ xylitol*
Al_2O_3 [b]	0.1±0.0	0.1±0.0	0.2±0.1	0.1±0.0	0.1±0.0	0.1±0.0	0.2±0.1	---	---	0.1	0.1	0.1.
$AlPO_4$ [a]	0.7±0.5	1.0±0.5	0.2±0.2	0.7±0.4	2.0±0.9	2.8±0.7	1.1±0.7	---	---	0.6	1.5	1.0
$CaCO_3$ [a]	2.1±0.4	2.5±0.7	2.0±0.5	4.4±2.5	4.0±1.1	3.5±1.8	4.1±0.5	---	---	4.5	5.1	3.8
CaO [a]	1.7±0.6	2.1±0.5	1.2±0.4	2.9±0.4	1.4±0.1	4.1±0.4	2.8±0.6	---	---	4.1	2.9	2.9
$Ca_3(PO_4)_2$ [a]	1.7±0.6	0.6±0.2	0.7±0.2	5.7±1.0	3.3±1.3	1.8±0.5	3.8±0.6	---	---	3.5	2.6	0.9
$CaSO_4$ [a]	2.6±0.6	2.5±0.6	3.1±2.0	3.1±1.1	3.8±0.7	2.4±0.9	4.2±1.3	---	---	1.8	4.5	2.1
Fe_2O_3 [b]	0.2±0.1	0.4±0.2	0.2±0.0	0.1±0.0	0.1±0.1	0.2±0.1	0.1±0.0	0.2	0.2	---	---	---
$FeCl_3$ [a]	8.2±2.6	8.8±6.8	12.1±4.8	23.3±12.2	dec.	dec.	21.4±3.0	dec.	dec.	---	---	---
CuO [a]	0.6±0.4	2.9±0.3	2.7±0.2	0.4±0.2	0.7±0.5	0.6±0.3	0.9±0.3	0.4	dec.	---	---	---
$Cu(OAc)_2$ [a]	1.7±0.9	8.8±4.3	8.2±3.9	3.2±0.5	3.8±0.8	2.7±0.9	2.2±0.5	dec.	dec.	---	---	---
$CuCl_2$ [a]	4.8±0.7	5.3±2.7	10.3±2.6	9.4±2.6	dec.	18.8±2.3	14.0±3.7	dec.	dec.	---	---	---
ZnO [a]	0.5±0.2	1.5±0.4	1.9±0.7	0.9±0.5	0.7±0.2	0.4±0.3	3.2±0.5	0.6	dec.	---	---	---
$Zn(OAc)_2 \cdot 2\ H_2O$ [a]	38.2±1.2	24.0±10.8	22.6±4.1	54.2±2.7	dec.	39.6±5.5	5.9±4.4	dec.	dec.	---	---	---
$ZnCl_2$ [a]	7.2±0.7	dec.	5.9±1.8	58.7±5.2	33.6±2.1	24.1±3.8	25.8±9.4	dec.	dec.	---	---	---
MoO_3 [b]	0.1±0.1	0.3±0.2	0.2±0.1	0.5±0.1	0.2±0.1	0.1±0.0	0.6±0.3	0.2	dec.	---	---	---
RuO_2 [b]	0.1±0.1	0.3±0.2	0.4±0.0	0.1±0.1	0.1±0.0	0.2±0.1	0.3±0.2	0.5	dec.	---	---	---
SnO_2 [b]	0.0±0.0	0.1±0.0	0.1±0.0	0.1±0.0	0.1±0.0	0.1±0.0	0.1±0.0	0.0	dec.	---	---	---

$LaCl_3 \cdot 7\ H_2O$ [a]	49.7±7.7	5.5±1.5	12.8±4.2	42±4.3	37.4±2.4	38.5±6.8	18.4±0.9	dec.	dec.	---	---	---
CeO_2 [b]	0.2±0.1	0.2±0.1	0.4±0.1	0.1±0.1	0.2±0.1	0.4±0.2	0.2±0.1	0.3	dec.	---	---	---
$CeCl_3$ [a]	2.1±0.6	0.5±0.2	0.7±0.4	3.1±1.0	8.9±1.4	12.0±0.3	4.8±1.1	dec.	dec.	---	---	---
$EuCl_3$ [a]	1.8±0.8	2.6±2.1	0.4±0.3	1.8±0.5	1.8±0.9	3.3±1.3	2.4±1.9	0.8	dec.	---	---	---
PtO_2 [b]	0.1±0.0	0.1±0.1	0.2±0.1	0.1±0.0	0.1±0.1	0.2±0.1	0.2±0.0	0.2	dec.	---	---	---
PbO [b]	dec.	0.2±0.2	0.2±0.1	0.4±0.3	dec.	dec.	2.0±0.8	dec.	dec.	---	---	---
PbO_2 [b]	dec.	0.5±0.1	0.2±0.1	0.6±0.2	dec.	dec.	1.9±0.4	dec.	dec.	---	---	---
$Pb(OAc)_2 \cdot 3\ H_2O$ [a]	8.1±2.8	10.3±0.8	3.3±1.5	7.9±1.2	dec.	dec.	1.5±0.3	dec.	dec.	---	---	---
$PbCl_2$ [a]	0.5±0.4	0.5±0.5	0.5±0.3	3.2±2.2	4.3±1.8	3.3±0.6	4.7±6.6	0.4	0.3	---	---	---

Determination of metal contend in the filtered DES: (*a*) *via* ICP-OES of a solution with half-concentrated fuming nitric acid (10.7 M) or (*b*) *via* reweighing after complete combustion of the organic components in a muffle furnace. Abbreviations: dec. = decomposition of the DES; --- = experiment was not performed; * = unpublished results.

If an entry is stated as *dec*., it indicates that the eutectic melt solidified or decomposed after the addition of the metal compound and the sample was unusable for further investigations.

The DESs are able to dissolve or at least highly disperse up to 50 wt% of some metal compounds. The low melting mixtures are even capable of processing up to 0.4 wt% of metal oxides (*e.g.* Al_2O_3 and Fe_2O_3) that are hardly soluble in harsh acids. Furthermore, the solubility of a metal salt or oxide can vary depending on the DES by an order of magnitude (*e.g.* $Ca_3(PO_4)_2$, $ZnCl_2$, CuO, and $CeCl_3$). In particular, eutectic melts that contain urea or its derivative DMU show a high tendency to dissolve especially metal chlorides and phosphates compared to other DESs (Figure 4 and Figure 6). For acetates, melts with ChCl provide a preferable extraction medium (Figure 5), whereas carboxylic acids such as tartaric acid or citric acid as a melt component result in a DES with high potential to dissolve metal oxides (Figure 3). Hydrates show a significant increase in solubility that may be explained by the contained water of crystallization (Figure 4 and Figure 5). The corresponding metal salts of the herein used hydrates possess a high solubility in water. By heating the hygroscopic DES mixture, water molecules are released, which may support the solvation of the metal salt in the eutectic melt.

To gain further insight into the properties of DESs used for extraction, the pH value was measured in aqueous solution (2 M) of DESs based on ChCl, choline bitartrate (ChBt), urea or DMU as HBA (Figure 7). The pH value of eutectic melts cannot be determined without the addition of water as the melts are completely anhydrous, which means that the actual pH conditions in DESs can only be approximated. For comparison, the pH values of the DESs from Table 1 and Table 3 as well as all related single components were determined under the same conditions. The values are depicted in Figure 8.

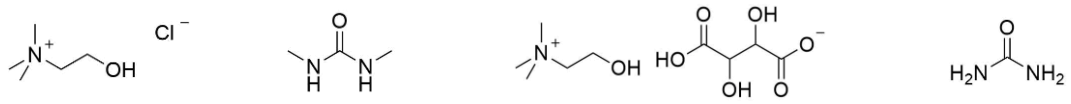

Figure 7. Hydrogen-bond acceptors (HBA) for DESs used as extraction media: choline chloride (ChCl) and *N,N'*-dimethyl urea (DMU), and for further investigations of the pH value: choline bitartrate (ChBt) and urea (*from left to right*).

Table 3. DESs 13–22 based on choline chloride (ChCl), choline bitartrate (ChBt), urea or *N,N'*-dimethyl urea (DMU) as hydrogen-bond acceptor (HBA) with different hydrogen-bond donors (HBD) and the respective molar ratio [n:n].[43, 58, 59]

Entry	HBA	HBD	Structure [a]	Molar ratio
13	ChCl	maleic acid	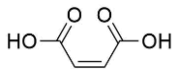	1 : 1
14	ChCl	malic acid	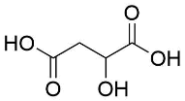	1 : 1
15	ChCl	oxalic acid dihydrate	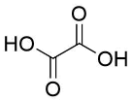	1 : 1
16	ChBt	DMU	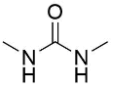	1 : 2
17	ChBt	maleic acid		1 : 1
18	ChBt	oxalic acid dihydrate	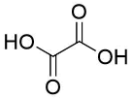	1 : 1
19	urea	D-fructose	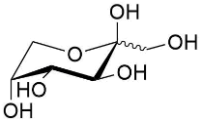	4 : 1
20	urea	D-glucose	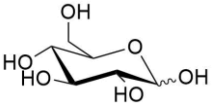	9 : 2
21	urea	galactose	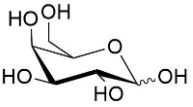	7 : 1
22	DMU	ChCl	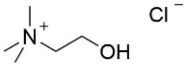	2 : 1

(*a*) Structures do not contain hydrate molecules.

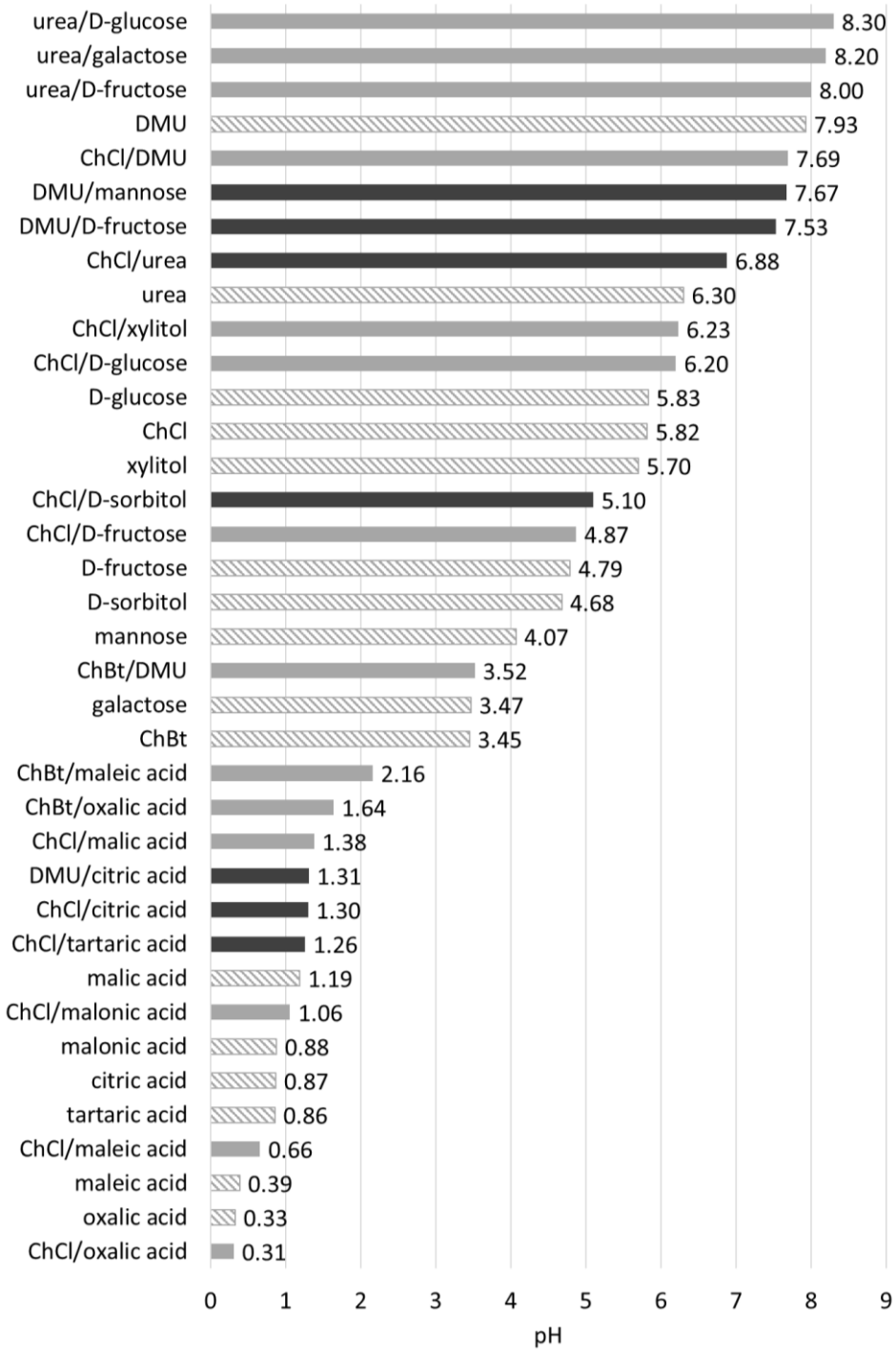

Figure 8. pH values of herein used DESs (*black*), further eutectic melts (*grey*), and single components (*striped*) for comparison; determined for 2 M solutions with water.

The low melting mixtures show pH values from acidic to basic, and the values do not necessarily correspond to the pH of the single components or their average. For example, the pH value of 2 M aqueous sugar solutions is in the range between 4 and 6 and for urea at 6.3, whereas the urea–sugar melts are weakly basic around pH 8. DESs containing an organic acid as an HBD are strongly acidic with a pH between 2 and 0, which explains why metal oxides are especially dissolved or incorporated by those melts. In accordance with the results for the pH values of eutectic mixtures favorable for metal chlorides, these compounds dissolve in neutral or slightly basic media. Also, phosphates tend to dissolve preferably in neutral to low basic DESs, although this finding does not correlate with the general behavior of $AlPO_4$ and $Ca_3(PO_4)_2$.

The results of the solubility experiments provide the extraction selectivity characteristics that are essential for separation procedures. The data imply that an effective separation of different metal salts and metal oxides with DESs is possible. Furthermore, the selectivity can be partly correlated with the pH values of the DESs. The high variation of the determined values shows on the other hand that for each separation problem, the applicability of a DES as an extractant has to be tested separately and that the suitable eutectic solvent has to be adjusted empirically.

1.2.2 Extraction of Phosphorus from ISSA with DESs

ISSA is a particularly promising and at the same time challenging target for extraction investigations of phosphorus: phosphate-based compounds are embedded in a highly complex matrix with a wide variety of main and trace components with similar solubility properties in common solvents and extraction media. Furthermore, the amount of phosphorus can reach from 3 up to 15 wt% (≙ 30–150 g/kg dry matter) from batch to batch, which makes extensive investigations necessary.

In the following section, we present first promising results for the accumulation of phosphorus from ISSA with a simple and low-energy extraction process using DESs as extraction media. All measurements were performed following German DIN standards for the characterization of sludge, soil, or water. This includes aqua regia digestion of all samples and analysis by ICP-OES, inductively coupled plasma mass spectrometry (ICP-MS),

or atomic absorption spectrometry (AAS) depending on the concentration of the element in the sample.

The solubility behavior of the single main components (whitlockite $Ca_3(PO_4)_2$, aluminum phosphate $AlPO_4$, quicklime CaO, calcite $CaCO_3$, anhydrite $CaSO_4$, and hematite Fe_2O_3) and many possible trace metal salts and oxides of ISSA in DESs was already investigated in the first section. Referring to Figure 6, the investigated phosphates, whitlockite and aluminum phosphate, accumulate selectively in DESs that contain urea or its derivative DMU. Furthermore, the solvation of metal oxides, which constitute a large share of ISSA and are to separate from the phosphates, is preferred in acidic DESs. Consequently, neutral to slightly basic DESs with a urea derivative as a component may provide suitable extraction conditions for whitlockite and aluminum phosphate. Based on the herein investigated DESs, this limits the selection of extraction media to the following three: ChCl/urea (1:2), DMU/D-fructose (3:1), and DMU/mannose (5:1). In addition, ChCl/D-sorbitol was used as a reference medium for slightly acidic conditions and as a DES without a urea derivative as a component.

As a real specimen, ISSA from the sewage sludge incineration plant in Straubing, Germany was used. In the herein used batch, the amount of phosphorus of 95 500 mg/kg is high compared to those of other samples from German incineration plants of about 65 000–70 000 mg/kg.[1] This value constitutes the calculation basis for following extraction investigations.

The procedure for the extraction of phosphorus from ISSA comprises two steps: 1. extraction of ISSA with the DES, and 2. precipitation by water addition. In the first step, 2.0 wt% of ISSA were added to two samples of each DES at 80 or 90 °C according to Table 1. For comparison, one sample was stirred for 2 h and the other for 24 h at the respective temperature from Table 1. Afterwards, the mixtures were filtered through hot filtration apparatus. In the second step, water was added to the filtered mixtures. In this way, the DES gets dissolved in water and the extracted but not water-soluble components, which were highly dispersed or dissolved in the DES, deposit. The mass fraction of phosphorus was analyzed before and after the filtration to obtain the yield of the first and second

extraction steps. In addition, the concentration of phosphorus in the water–DES phase was determined. The results are presented in Figure 9, Figure 10, and Table 4.

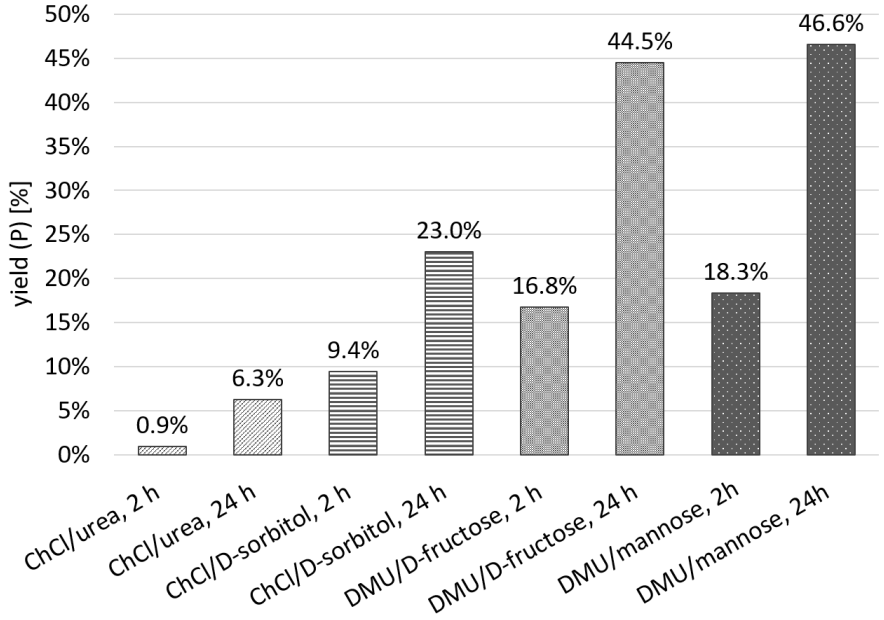

Figure 9. Yield [%] of phosphorus after the extraction step with four different DESs after 2 and 24 h: ChCl/urea, ChCl/D-sorbitol, DMU/D-fructose, and DMU/mannose.[60]

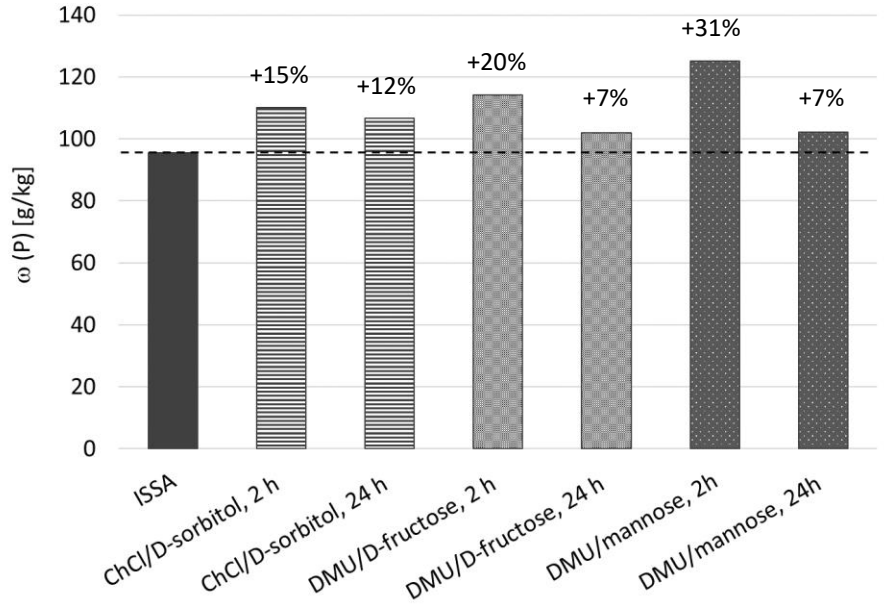

Figure 10. Mass fraction ω [mg/kg] of phosphorus in ISSA and in the extraction products.[60]

Table 4. Mass fraction ω [mg/kg] of phosphorus in ISSA and in the precipitates of the extraction experiments (see Figure 10) and the remaining concentration c [mg/L] of phosphorus in the separated water–DES phase.[60]

	ω (P) [g/kg] Extraction product	c (P) [mg/L] Water–DES phase
ISSA Straubing	**95.5**	**---**
ChCl/D-sorbitol, 2 h	110.0	2.2
ChCl/D-sorbitol, 24 h	106.6	2.6
DMU/D-fructose, 2 h	114.1	6.8
DMU/D-fructose, 24 h	101.9	12
DMU/mannose, 2 h	125.0	4.2
DMU/mannose, 24 h	102.1	5.6

The yield shown in Figure 9 represents the amount of overall phosphorus that was extracted from the ISSA sample. In accordance with the expectations, the more effective extraction media are the eutectic melts with a neutral to slightly basic pH value and a urea derivative as a constituent, namely DMU/mannose and DMU/D-fructose, extracting up to 47% of phosphorus from the ISSA sample (Figure 9). These melts are able to accumulate twice the amount of phosphorus in the same time as the other two DESs. However, more phosphorus is extracted with the melt of ChCl/D-sorbitol than with ChCl/urea, even if the former does not contain a urea derivative and shows a lower pH value in the acidic range. Furthermore, the graphical representation of the yields in Figure 9 emphasizes the high time dependency of the extraction process. After 2 h of stirring, only up to 18% of phosphorus was extracted by the DESs, whereas up to 47% of phosphorus was absorbed by the melts after 24 h. The samples prepared with the DES ChCl/urea were not considered for further analysis in the second step because of the low yield of extracted phosphorus (0.9% and 6.3%).

Table 4 and Figure 10 show the degree of accumulation of phosphorus in the extraction products in comparison with the crude ISSA and the resulting amount of phosphorus in the water–DES phase. For all analyzed extraction products, an increase of phosphorus was observed, from 95 500 mg/kg in ISSA up to 125 g/kg in the precipitate from extraction with DMU/mannose. This represents a rise in phosphorus by 30.9%. In

accordance with the general solubility experiments, phosphorus was accumulated preferably with DMU-containing DESs. However, the mass fraction of phosphorus was not decreased by the DES ChCl/D-sorbitol, which had no urea or urea derivative as a component nor provided a neutral to low basic pH value in contrast to the other two DESs. The results for the water–DES phase (Table 4) showed that the amount of phosphorus that remained in the water–DES phase was negligible compared to the amount in the final product.

When correlating the accumulation with the overall yield, it is observed that a larger relative fraction of phosphorus was accumulated for a shorter extraction time, even if the overall yield of the samples that were stirred for 24 h was two times that of the samples stirred for 2 h. For DMU/mannose as extraction media and an extraction time of 2 h, 18.2% of phosphorus was extracted from the initial ISSA and the mass fraction was increased by 0.9%, whereas 46.6% of phosphorus was extracted after a 24 h extraction time and the mass fraction was increased by only 7.0%. Similar results were obtained for DMU/D-fructose as the extraction medium. This leads to the assumption that the accumulation of phosphorus occurs faster than that for other main components. Further investigations of the extraction time may lead to optimum values for both accumulation and yield.

After demonstrating the feasibility to accumulate phosphorus by the developed extraction procedure using biodegradable DESs, it is of interest whether the extraction products comply with the requirements of the new German Ordinance for the Recovery of Sewage Sludge regarding their content of toxic heavy metals.[16, 61] Thus, we measured the amounts of toxic heavy metals in the crude ISSA and in the extraction product and compared them with the limiting values (Table 5). The herein used crude ISSA contains a relatively low amount of toxic heavy metals and even does not reach the limiting value for all toxic heavy metals. For all three types of investigated DESs, the amounts of toxic heavy metals do not decrease to a lower level; the amounts of cadmium and nickel were even accumulated. The amount of thallium was not quantifiable for the extraction products, as the amounts are below the limit of detection of the analytical method. In previous ICP-OES

measurements, we also observed that traces of the DES in the analyte can cause an increase of the noise and, therefore, raise the limit of quantification.

Table 5. Mass fraction ω [mg/kg] of arsenic, lead, cadmium, chromium, nickel, mercury and thallium in ISSA and in the products of the extraction experiments in comparison to the limiting values of the German fertilizer ordinance.[61]

ω [mg/kg]	As	Pb	Cd	Cr	Ni	Hg	Tl
Limiting value	*40*	*150*	*1.5*	*900*	*80*	*1.0*	*1.0*
ISSA Straubing	**6.0**	**59**	**0.9**	**88**	**68**	**<0.1**	**0.7**
ChCl/D-sorbitol, 2 h	15	95	1.0	130	215	<0.1	n.q.
ChCl/D-sorbitol, 24 h	15	110	1.8	143	217	<0.1	n.q.
DMU/D-fructose, 2 h	16	118	1.6	130	201	<0.1	n.q.
DMU/D-fructose, 24 h	8.0	120	1.3	100	91	<0.1	n.q.
DMU/mannose, 2 h	17	114	1.7	176	188	<0.1	n.q.
DMU/mannose, 24 h	13	79	1.2	95	99	<0.1	n.q.

Abbreviation: n.q. = not quantifiable; < = below the limit of quantitation.[60]

Although extraction trends for salts and oxides can be predicted based on the pH values of the DESs, a selectivity for individual metal salts cannot be derived from the DES composition at present. Therefore, the use of DESs for phosphorus mineral extraction from ISSA does not solve the challenge of phosphorus separation from unwanted toxic metal salts unless more selective DESs are identified. Until this goal is reached, the precipitation of toxic heavy metals from the extract by Na_2S or other additional separation steps may be still necessary for ISSA containing higher amounts of such metal salts.

1.3 Conclusion

In conclusion, we have shown that the extraction of phosphorus containing minerals from ISSA is possible using DESs. The extraction procedure avoids strong acids and high temperatures, which may allow for more efficient and energetically less demanding recycling strategies for phosphorus from ISSA. With the introduced two-step extraction procedure, we were able to demonstrate the feasibility of the approach: a rational choice of the deep eutectic extraction media leads to a significant accumulation of phosphorus from ISSA. DESs with DMU as a component and neutral to less basic pH values were found

to be suitable media for the extraction of phosphorus from this highly complex matrix. The kinetics of the phosphorus extraction varies with the compositions of the DESs and the ISSA, which makes an individual optimization necessary to reach the desired efficiency and selectivity.

The extent of metal salt and metal oxide extraction into the investigated DESs strongly depends on the DES composition as shown by an extensive study. Future investigations using further DESs and ISSA samples from different batches and sewage sludge incineration plants aim at higher phosphate extraction and the reduction of toxic heavy metals in the extraction product.

1.4 Experimental

1.4.1 General Procedures and Materials

Chemicals and materials. All chemicals were of analytical reagent grade and used as received without further purification except for choline chloride ($HOC_2H_4N(CH_3)_3^+Cl^-$ or ChCl), which was dried at 130 °C *in vacuo* and stored under nitrogen prior to use. All metal salts and oxides were at least of grade ≥99.9% on the trace metal basis. The ISSA sample was taken from the sewage sludge incineration plant in Straubing, Germany. The ISSA material for all extraction experiments was taken from the same batch and the coarse granulate was ground *via* a planetary ball mill and dried in an oven at 105 °C before use to ensure the homogeneity of the feedstock and better accessibility of the constituents.

DES preparation. The DESs were formed by mixing the two components in the respective molar ratios (Table 1 and Table 3) in a glass vial in batches of 10 g. The mixtures were heated up to 80 or 90 °C (according to the footnote in Table 1) in an aluminum heating block until a homogeneous, colorless liquid was obtained.

Hot filtration. For hot filtration, an extruder (LiposoFastBasic) by Avestin was adapted: the original PTFE-blocks (polytetrafluoroethylene) of the extruder were exchanged with PEEK-blocks (polyetheretherketone). The outlet was widened up to 1.60 mm and adjusted to 1 mL Hamilton Gastight syringes with Luer-Lock and shortened HSW ECO cannulas (1.60 × 3.00 mm) from Henke-Sass, Wolf GmbH. We used No. 41

Whatman filter paper as filters with a pore size of 20–25 µm and a filter net by Avestin as a pre-filter. The filter apparatus was equipped with a fitted heating block and a control panel.

1.4.2 Procedures and Analytical Methods for Solubility Experiments

Saturation experiments. The metal salt or oxide was added gradually to the DES in proportions of 5.0 mg. The mixture was stirred at the processing temperature of 80 or 90 °C (according to the footnote in Table 1) for 2 h before further addition of the next proportion. After saturation of the melt was reached, the mixture was filtered using the hot filtration apparatus at the processing temperature and analyzed *via* ICP-OES. The mass fractions listed in Table 2 represent an average of three independent measurements.

ICP-OES measurements. The concentration of elements in DESs was determined using a SpectroFlame-EOP, FSMEA85C S/N 4G/0002 from SPECTRO Analytical Instruments in solutions with half-concentrated fuming nitric acid (10.7 M).

Determination of metal oxide content by reweighing. The mass fraction of metal oxides that were not soluble in half-concentrated nitric acid was determined by the following process: a defined amount of the DES mixture was filled in a crucible and the sample combusted in a muffle furnace (L 3/11/B 170, Nabertherm) under an excess of oxygen. The residue was reweighed and the phase characterized by X-ray powder diffraction (STOE STADI P X-ray diffractometer, Stoe & Cie GmbH) with a germanium monochromator and Cu$K\alpha_1$ radiation (λ = 1.54059 Å) to find out if the obtained compound had the same crystal structure as the starting material; this was the case for all analyzed samples.

Determination of the pH value. An aqueous solution of each DES and of all single components with Milli-Q water in a concentration of 2 M (for DESs, the summarized molar amounts of both components – HBA and HBD) was prepared. For the measurements, a 691 pH-meter from Metrohm was used. The pH values reported in Figure 8 represent an average of three independent measurements.

1.4.3 Procedures and Analytical Methods for the Extraction of Phosphates from ISSA

Ball milling. A planetary ball mill (Pulverisette-6) from Fritsch was used for fine grinding of the coarse-grained ISSA with polished agate grinding balls (diameter 10 mm). The weight ratio of ISSA to grinding balls was 3 : 4 and the material was ground for 1 h at 400 rpm.

Extraction procedure. 5.0 g of the respective DES was prepared for each experimental setup. In the first step, two samples of DES 1 and 4–6 were prepared at 80 or 90 °C (Table 1) and 2.0 wt% of ground and dried ISSA was added. For each type of DES, one sample was stirred for 2 h and the other for 24 h at the respective temperature. Afterwards, the mixtures were filtered through the hot filtration apparatus at 90 °C according to the general procedure. In the second step, 10 mL of Milli-Q water per 1.0 g of the filtrate were added and the mixture was stirred for 30 min. The suspension was centrifuged and the precipitate was dried in an oven at 80 °C.

Methods for analysis. The determination of phosphorus and trace elements was performed following German DIN standards for the characterization of sludge, soil, or water. All samples were digested with aqua regia (DIN EN 13 346) prior to analysis. The trace elements arsenic, lead, cadmium, chromium, nickel, and thallium were determined *via* ICP-MS (DIN EN ISO 17294-2). The trace element mercury was determined *via* AAS with and without enrichment (DIN EN ISO 12846) or in aqua regia extracts by cold-vapor atomic spectrometry (DIN ISO 16772). The amount of phosphorus was determined by ICP-OES (DIN EN ISO 11885) and ICP-MS. The analytical method was chosen depending on the concentration of the element in the sample.

1.5 References

[1] C. Adam and O. Krüger, *VDI Wissensforum*, **2012**.

[2] J. E. Hall, *Water Environ. J.*, **1995**, *9*, 335-343.

[3] T. Chen and B. Yan, *Waste Manag.*, **2012**, *32*, 957-964.

[4] O. Hjelmar, *J. Hazard. Mater.*, **1996**, *47*, 345-368.

[5] T. L. Jones-Lepp and R. Stevens, *Anal. Bioanal. Chem.*, **2007**, *387*, 1173-1183.

[6] B. Wiechmann, C. Dienemann, C. Kabbe, S. Brandt, I. Vogel and A. Roskosch, *Sewage sludge management in Germany*, Umweltbundesamt, **2015**.

[7] C. vom Eyser, K. Palmu, T. C. Schmidt and J. Tuerk, *Sci. Total Environ.*, **2015**, *537*, 180-186.

[8] O. Zuloaga, P. Navarro, E. Bizkarguenaga, A. Iparraguirre, A. Vallejo, M. Olivares and A. Prieto, *Anal. Chim. Acta*, **2012**, *736*, 7-29.

[9] W. Rulkens, *Energy Fuels*, **2008**, *22*, 9-15.

[10] M. Barz, *Int. J. Renew. Energy*, **2009**, *4*, 1-12.

[11] T. R. Bridle and D. Pritchard, *Water Sci. Technol.*, **2004**, *50*, 169-175.

[12] V. Smil, *Annu. Rev. Energy Env.*, **2000**, *25*, 53-88.

[13] T.-S. Neset, D. Cordell, S. Mohr, F. VanRiper and S. White, *Front. Nutr.*, **2016**, *3*, 47.

[14] J. D. Edixhoven, J. Gupta and H. H. G. Savenije, *Earth Syst. Dynam.*, **2014**, *5*, 491-507.

[15] D. Cordell, J.-O. Drangert and S. White, *Global Environ. Chang.*, **2009**, *19*, 292-305.

[16] Bundesgesetzblatt, *Verodnung zur Neuordnung der Klärschlammverwertung*, Bonn, Part I, vol. 65, 3465, **2017**.

[17] Federal Ministry for the Environment Nature Conservation and Nuclear Safety, New Sewage Sludge Ordinance in force, www.bmu.de/en/law/sewage-sludge-ordinance, (accessed July 23, 2018).

[18] D. Cordell, A. Rosemarin, J. J. Schröder and A. L. Smit, *Chemosphere*, **2011**, *84*, 747-758.

[19] EU Commission, *The 2017 list of Critical Raw Materials for the EU*, **2017**.

[20] P. Walan, S. Davidsson, S. Johansson and M. Höök, *Resour. Conserv. Recycl.*, **2014**, *93*, 178-187.

[21] S. Petzet, B. Peplinski and P. Cornel, *Water Res.*, **2012**, *46*, 3769-3780.

[22] B. K. Biswas, K. Inoue, H. Harada, K. Ohto and H. Kawakita, *J. Environ. Sci. (China)*, **2009**, *21*, 1753-1760.

[23] M. Franz, *Waste Manag.*, **2008**, *28*, 1809-1818.

[24] S. Donatello and C. R. Cheeseman, *Waste Manag.*, **2013**, *33*, 2328-2340.

[25] B. G. Oliver and J. H. Carey, *Water Res.*, **1976**, *10*, 1077-1081.

[26] M. Takahashi, S. Kato, H. Shima, E. Sarai, T. Ichioka, S. Hatyakawa and H. Miyajiri, *Chemosphere*, **2001**, *44*, 23-29.

[27] K. Gorazda, B. Tarko, Z. Wzorek, H. Kominko, A. K. Nowak, J. Kulczycka, A. Henclik and M. Smol, *Environ. Res.*, **2017**, *154*, 171-180.

[28] K. Gorazda, B. Tarko, Z. Wzorek, H. Kominko, A. K. Nowak, J. Kulczycka, A. Henclik and M. Smol, *Environ. Res.*, **2017**, *158*, 815.

[29] K. Stark, E. Plaza and B. Hultman, *Chemosphere*, **2006**, *62*, 827-832.

[30] C. Schaum, P. Cornel and N. Jardin, *Phosphorus recovery from sewage sludge ash–a wet chemical approach*, **2007**.

[31] C. Schaum and P. Cornel, *Vom Wasser*, **2009**, *107*, 7-12.

[32] A. Sano, M. Kanomata, H. Inoue, N. Sugiura, K.-Q. Xu and Y. Inamori, *Chemosphere*, **2012**, *89*, 1243-1247.

[33] J. Lehmkuhl and M. Lebek, *Germany Pat.,* DE102014006278B3, **2014**.

[34] C. Vogel, R. M. Exner and C. Adam, *Environ. Sci. Technol.*, **2012**, *47*, 563-567.

[35] C. Adam, B. Peplinski, M. Michaelis, G. Kley and F. G. Simon, *Waste Manag.*, **2009**, *29*, 1122-1128.

[36] H. Herzel, O. Krüger, L. Hermann and C. Adam, *Sci. Total Environ.*, **2016**, *542*, 1136-1143.

[37] H. Mattenberger, G. Fraissler, T. Brunner, P. Herk, L. Hermann and I. Obernberger, *Waste Manag.*, **2008**, *28*, 2709-2722.

[38] K. Scheidig, *KA - Korrespondenz Abwasser, Abfall*, **2009**, *11*, 1138-1146.

[39] A. Schöneberg, K. Samiei, H. Kern and H. Raupenstrauch, *Österr. Wasser Abfallw.*, **2014**, *60*, 403-407.

[40] E. Yabalak and A. Gizir Murat, *J. Serb. Chem. Soc.*, **2013**, *78*, 1013-1022.

[41] P. Guedes, N. Couto, L. M. Ottosen and A. B. Ribeiro, *Waste Manag.*, **2014**, *34*, 886-892.

[42] L. M. Ottosen, P. E. Jensen and G. M. Kirkelund, *Sep. Sci. Technol.*, **2014**, *49*, 1910-1920.

[43] C. Ruß and B. König, *Green Chem.*, **2012**, *14*, 2969-2982.

[44] A. P. Abbott, D. Boothby, G. Capper, D. L. Davies and R. K. Rasheed, *J. Am. Chem. Soc.*, **2004**, *126*, 9142-9147.

[45] J. R. Harjani, T. Friscic, L. R. MacGillivray and R. D. Singer, *Dalton Trans.*, **2008**, 4595-4601.

[46] T. V. Hoogerstraete, B. Onghena and K. Binnemans, *J. Phys. Chem. Lett.*, **2013**, *4*, 1659-1663.

[47] Reconif, Nickel Recovery from Filter Cake, www.reconif.co.uk, (accessed July 23, 2018).

[48] Y. Dai, J. van Spronsen, G.-J. Witkamp, R. Verpoorte and Y. H. Choi, *J. Nat. Prod.*, **2013**, *76*, 2162-2173.

[49] F. Chemat, M. A. Vian and G. Cravotto, *Int. J. Mol. Sci.*, **2012**, *13*, 8615.

[50] M. G. Bogdanov, in *Alternative Solvents for Natural Products Extraction*, eds. F. Chemat and M. A. Vian, Springer Berlin, Heidelberg, **2014**, 127-166.

[51] T. Bosiljkov, F. Dujmić, M. Cvjetko Bubalo, J. Hribar, R. Vidrih, M. Brnčić, E. Zlatic, I. Radojčić Redovniković and S. Jokić, *Food Bioprod. Process.*, **2017**, *102*, 195-203.

[52] S. Bajkacz and J. Adamek, *Talanta*, **2017**, *168*, 329-335.

[53] M. Olkiewicz, N. V. Plechkova, A. Fabregat, F. Stüber, A. Fortuny, J. Font and C. Bengoa, *Sep. Purif. Technol.*, **2015**, *153*, 118-125.

[54] A. Popescu, C. Donath and V. Constantin, *Density, viscosity and electrical conductivity of three choline chloride based ionic liquids*, **2014**.

[55] F. S. Mjalli and J. Naser, *Asia-Pac. J. Chem. Eng.*, **2015**, *10*, 273-281.

[56] Q. Wen, J.-X. Chen, Y.-L. Tang, J. Wang and Z. Yang, *Chemosphere*, **2015**, *132*, 63-69.

[57] K. Radošević, M. Cvjetko Bubalo, V. Gaurina Srček, D. Grgas, T. Landeka Dragičević and I. Radojčić Redovniković, *Ecotoxicol. Environ. Saf.*, **2015**, *112*, 46-53.

[58] Y. Dai, J. van Spronsen, G.-J. Witkamp, R. Verpoorte and Y. H. Choi, *Anal. Chim. Acta*, **2013**, *766*, 61-68.

[59] V. Fischer, Doctor of Philosophy dissertation, Universität Regensburg, **2015**.

[60] *The general error of the method is 15-20% due to reproducability, volumetric errors, and handling.*

[61] Bundesgesetzblatt, *Verordnung über das Inverkehrbringen von Düngemitteln, Bodenhilfsstoffen, Kultursubstraten und Pflanzenhilfsmitteln (Düngemittelverordnung - DüMV)*, Bonn, Part I, vol. 58, 2482, **2012**.

CHAPTER 2

2 Preparation of Magnesium, Cobalt and Nickel Ferrite Nanoparticles from Metal Oxides using Deep Eutectic Solvents

This chapter has been published as:

A. Söldner, J. Zach, M. Iwanow, T. Gärtner, M. Schlosser, A. Pfitzner and B. König, *Chem. Eur. J.* **2016**, *22*, 13108-13113.

A. Söldner performed the synthesis of all compounds, powder X-ray diffraction measurements, thermogravimetric analysis, Williamson-Hall analysis and wrote the manuscript. J. Zach carried out the UV/Vis diffuse reflectance measurements. M. Iwanow executed the SEM measurements. M. Schlosser achieved the cation distribution measurements and calculations. A. Pfitzner and B. König supervised the project. B. König is the corresponding author.

2.1 Introduction

Replacing highly corrosive inorganic acids or hazardous organic solvents in chemical processes is a step towards more sustainable chemistry. The optimization of the process we are focusing on within this report, is the synthesis of spinel-type ferrites with the general formula MFe_2O_4 (M = Mg, Zn, Co, Mn, Ni). These particles are of high interest due to their magnetic and electrical properties and have been investigated for technological applications including hyperthermia,[1] information storage systems,[2] ferrofluids,[3] photocatalysts,[4] humidity sensors,[5, 6] radar-absorbent materials,[7] and green anode materials.[8, 9] The structure of spinel-type ferrites can be described as a cubic close-packed arrangement of oxygen atoms with M^{II} and Fe^{III} ions occupying either tetrahedral or octahedral sites.[10]

Usually, nanoparticles of spinel-type ferrites are prepared from metal salts such as nitrates, chlorides, or acetates. Various methods for synthesizing nanoparticles have been reported, such as ball milling,[11] co-precipitation,[12] reverse micelle,[13] hydrothermal,[14] sol-gel,[15, 16] microemulsion,[10, 17] or microwave combustion techniques.[18] The disadvantage for many of these methods is difficult upscaling owing to expensive and complicated procedures, high reaction temperatures, pH sensitivity, long reaction times, toxic reagents, as well as unselective side reactions. Simple metal oxides are seldom employed as starting materials, because they require excessive reaction temperatures and normally do not yield phase-pure spinel ferrites.[19]

One class of possible reaction media for this type of inorganic synthesis are deep eutectic solvents (DESs). DESs based on natural compounds were intensively studied over the last decade as nontoxic, inexpensive and completely biodegradable alternative to common solvents. DESs usually consist of choline chloride (ChCl) as a hydrogen-bond acceptor (HBA) and an appropriate hydrogen-bond donor (HBD) forming a mixture with a melting point that is significantly lower than that of the two single components – ideally around room temperature.[20, 21] These melts are related to ionic liquids but, in addition, DESs are facile to prepare, are based on readily available and inexpensive starting materials, and do not accumulate in the environment according to literature.[22, 23]

DESs have previously been used as reaction media for standard organic reactions as C–C coupling and cycloaddition.[24-27] Also, enzyme-catalyzed reactions have been carried out in these solvents.[28, 29] Another field of application for DESs is the processing of metals, based on the ability to solvate a wide range of transition metal species, including metal oxides and hydroxides, without the highly acidic conditions that are needed in analogous aqueous systems. Further, the incorporation of metal ions in deep eutectic solvents for metal electrodeposition, metal electropolishing, and metal extraction have been published.[30-33] The decisive benefits of this type of solvent system over aqueous electrolytes are the absence of water, high solubility, and high conductivity compared to other non-aqueous solvents.

Extensive studies have been performed on the solubility of metal oxides in a variety of DESs. In particular, DESs containing well-known chelating agents such as malonic acid, tartaric acid, citric acid and oxalic acid are able to solubilize relatively high amounts of metal oxides.[34, 35] However, the ability of DESs to dissolve compounds like zinc oxide, magnetite, or copper oxide is not fully understood yet. But it was found that classical solubility models cannot be applied to this kind of solvent system. The solvation process is presumably based on complexation without breaking the metal–oxide bond.[36, 37]

We report the use of DESs as solvation and reaction media for metal oxides to successfully synthesize phase-pure spinel-type ferrite nanoparticles MFe_2O_4 (M = Mg, Co, Ni) by a thermal process.

2.2 Results and Discussion

2.2.1 Dissolving Properties and Incineration Behavior of DESs

For preliminary investigations, the general qualitive solubility of the metal oxides used as potential starting materials for the process, namely iron(III) oxide (α-Fe_2O_3), magnesium oxide (MgO), cobalt(II) oxide (CoO), nickel(II) oxide (NiO), and zinc oxide (ZnO), was tested. Approximately 0.05 wt% of the respective metal oxide was added to the DES from Table 6 and stirred for 2 h at 80 °C. The mixtures with Fe_2O_3 were additionally stirred for 24 h due to its poor solubility. The herein used eutectic melts are based on

organic acids as HBD, because these DESs are known from previous studies to preferably dissolve metal oxides.[34] The chemical structures of the HBAs are shown in Figure 11.

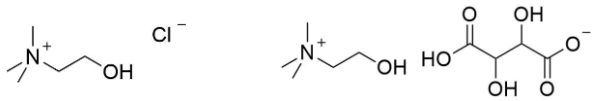

Figure 11. Hydrogen-bond acceptors choline chloride (ChCl, *left*) and choline bitartrate (ChBt, *right*).

Table 6. DESs based on choline chloride (ChCl) or choline bitartrate (ChBt) as hydrogen-bond acceptor (HBA) with organic acids as hydrogen bond donor (HBD).

Entry	HBA	HBD	Structure [a]	Molar ratio
1	ChCl	oxalic acid dihydrate	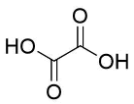	1 : 1
2	ChCl	malonic acid	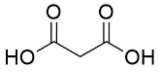	1 : 1
3	ChCl	maleic acid	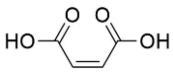	1 : 1
4	ChCl	malic acid	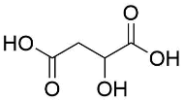	1 : 1
5	ChCl	tartaric acid	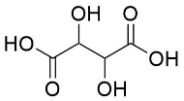	2 : 1
6	ChCl	citric acid monohydrate	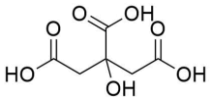	2 : 1
7	ChCl	vanillin	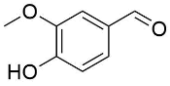	1 : 2
8	ChBt	oxalic acid dihydrate	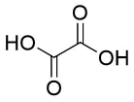	1 : 1

(*a*) Structures do not contain hydrate molecules.

The qualitative solubility was evaluated by the appearance of the melts after stirring and classified into three categories: soluble, partly soluble, and not soluble. The looks of the obtained samples ranged from turbid for suspensions or colloidal solutions to completely clear, indicating that the metal oxide was largely dissolved by the DESs (Figure 12 and Figure 13). The results for the qualitative solubility are given in Table 7.

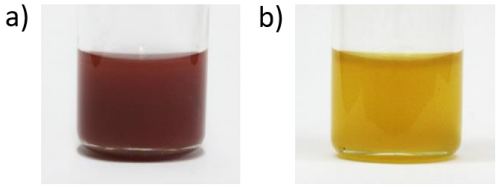

Figure 12. Highly and slightly turbid suspensions/solutions of Fe_2O_3 in ChCl/oxalic acid dihydrate after a) 2 h (highly turbid) and b) 24 h of stirring (slightly turbid) at 80 °C.

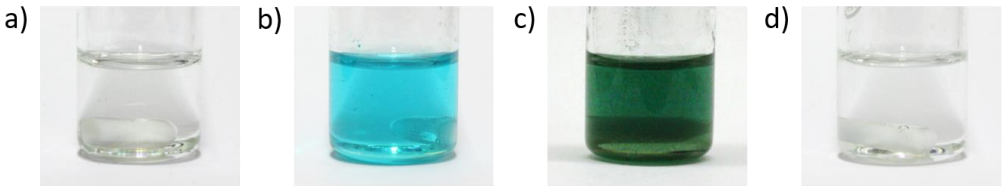

Figure 13. Turbid and clear solutions of a) MgO in ChCl/malic acid (clear), b) CoO in ChBt/oxalic acid dihyd. (clear), c) NiO in ChCl/malic acid (turbid), and d) ZnO in ChCl/citric acid monohyd. (clear).

Table 7. Qualitative solubility of Fe_2O_3, MgO, CoO, NiO, ZnO (ca. 0.05 wt%) in DESs.

Entry	DES	Fe_2O_3	MgO	CoO	NiO	ZnO
1	ChCl/oxalic acid dihydrate	p.s.	**sol.**	p.s.	-	p.s.
2	ChCl/malonic acid	p.s.	-	-	-	-
3	ChCl/maleic acid	n.s.	**sol.**	**sol.**	**sol.**	**sol.**
4	ChCl/malic acid	n.s.	**sol.**	n.s.	n.s.	**sol.**
5	ChCl/tartaric acid	n.s.	**sol.**	p.s.	-	p.s.
6	ChCl/citric acid monohydrate	n.s.	**sol.**	**sol.**	-	**sol.**
7	ChCl/vanillin	p.s.	-	-	-	-
8	ChBt/oxalic acid dihydrate	n.s.	p.s.	**sol.**	-	**sol.**

Abbreviations: **sol.** = soluble, p.s. = partly soluble, n.s. = not soluble, - = not tested.

The metal oxides MgO, CoO, NiO, and ZnO were readily soluble in several eutectic melts. Fe_2O_3 was hardly soluble in any DESs after stirring for 2 h at 80 °C and stayed dark red and turbid. However, it was observed for Fe_2O_3 that the appearance of the melts with ChCl/oxalic acid dihydrate, ChCl/malonic acid, and ChCl/vanillin changed to yellow and almost clear after stirring for 24 h at 80 °C. These three melts may be potential media for

dissolving Fe_2O_3 under relatively mild conditions compared to conventional inorganic solvents or solvent systems like hydrochloric acid or aqua regia.

Further, thermogravimetric analysis (TGA) and differential TGA (DTGA) were carried out to provide an insight into the behavior of DESs during incineration. Figure 14 shows the results of the DESs ChCl/maleic acid and ChCl/malic acid in the temperature range of 25–500 °C with a heating rate of 10 °C/min in air.

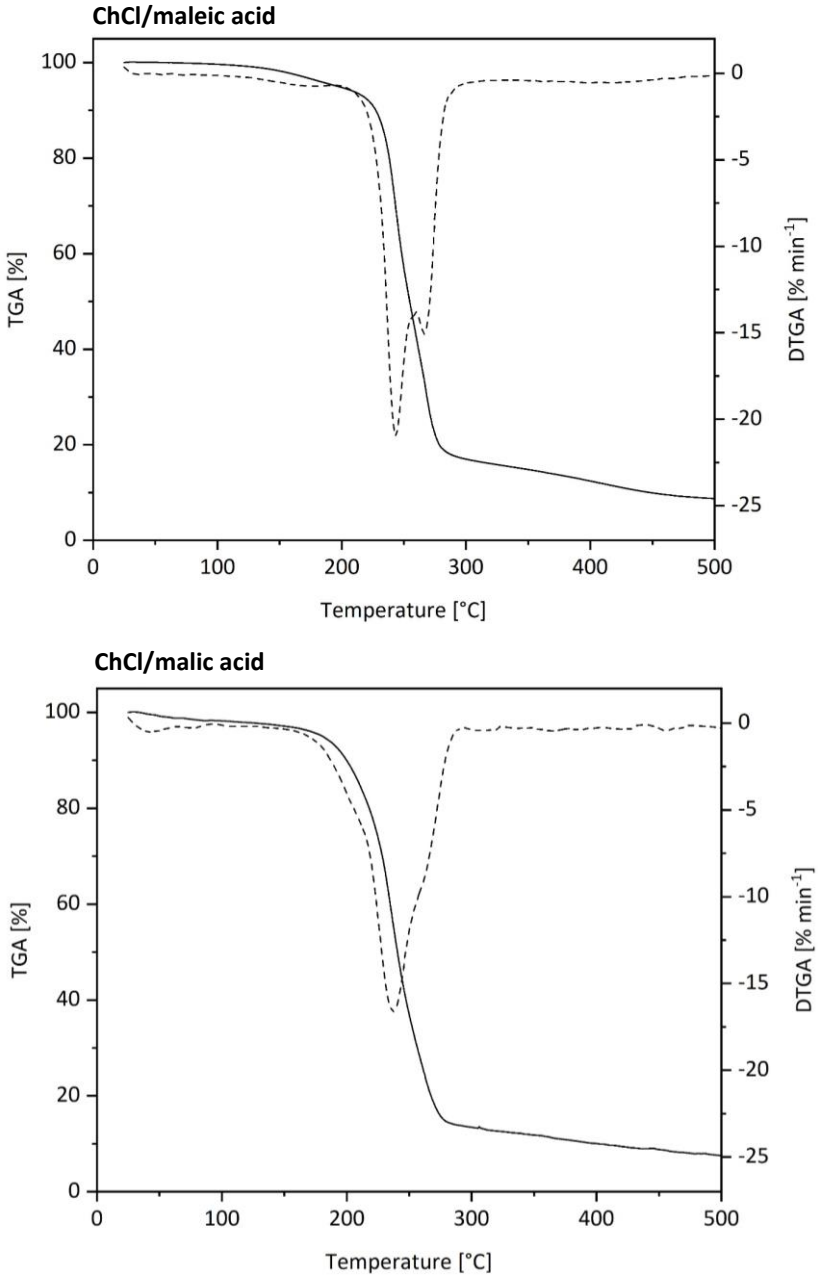

Figure 14. TGA (*solid line*) and DTGA (*dashed line*) curves of DESs composed of ChCl/maleic acid and ChCl/malic acid.

The decay for both analyzed DESs is characterized by a significant weight loss of around 85% in one major step in the temperature range 200–280 °C. Complete combustion to 0% was not obtained, which can be explained by either an excessive heating rate or the abrupt termination of the incineration.

2.2.2 Synthesis of Different Spinel-Type Ferrites with DESs

Initial investigations for ferrite formation with DESs were made for the synthesis of magnesium ferrite $MgFe_2O_4$. In the general procedure, Fe_2O_3 and MgO were added in a molar ration of 1:1 to the DES, stirred at 80 °C, and the mixture was calcinated in a muffle furnace in air.

To investigate the influence of the reaction parameters on the outcome of the reaction and the phase purity, the conditions of the general procedure were varied as followed: Ten different DESs were used, based on either ChCl, urea, or *N,N'*-dimethylurea (DMU) as HBA (Figure 15) and organic acids, sugars, or vanillin as HBD (Table 8); the overall mass fraction of starting material in the DES was tested for 0.25 wt%, 0.50 wt%, and 1.00 wt%; the stirring time was chosen for 2, 24, and 72 h; the calcination was performed at 400, 500, and 600 °C for 6, 12, or 36 h.

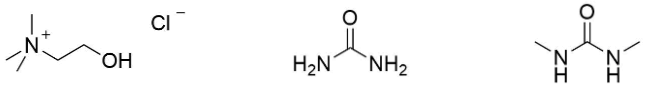

Figure 15. Hydrogen-bond acceptors (HBAs) choline chloride (ChCl, *left*), urea (*middle*) and *N,N'*-dimethylurea (DMU, *right*).

Table 8. DESs based on choline chloride (ChCl) or choline bitartrate (ChBt) as hydrogen-bond acceptor (HBA) with organic acids as hydrogen bond donor (HBD).[20, 38]

Entry	HBA	HBD	Structure [a]	Molar ratio
1	ChCl	maleic acid	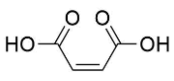	1 : 1
2	ChCl	malic acid	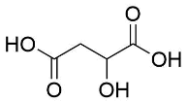	1 : 1
3	ChCl	DMU	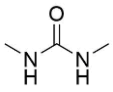	1 : 2

4	ChCl	oxalic acid dihydrate	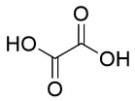	1 : 1
5	ChCl	vanillin	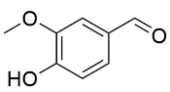	1 : 2
6	DMU	citric acid monohydrate	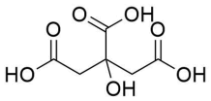	7 : 2
7	DMU	D-mannose	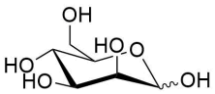	5 : 1
8	DMU	D-fructose	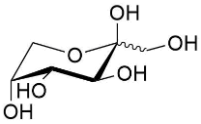	3 : 1
9	urea	D-fructose	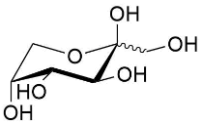	4 : 1
10	urea	D-glucose	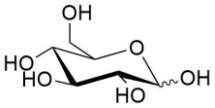	9 : 2

(*a*) Structures do not contain hydrate molecules.

The black or red to orange powders were analyzed by powder X-ray diffraction (XRD) regarding their crystalline phases. The results are ordered by the calcination temperature and listed in Table 9 for 400 °C, Table 10 for 500 °C, and Table 11 for 600 °C. In addition, the products were tested for magnetism as $MgFe_2O_4$ is highly magnetic in contrast to the starting materials.

Table 9. Resulting phases for the calcination of Fe_2O_3 and MgO at 400 °C using different DESs as reaction media. Mass fraction of the overall amount of starting material in the DES was varied.

Entry	DES	Mass fraction [wt%]	Stirring time [h]	Calcination time [h]	Crystalline phases
1	ChCl/maleic acid	0.25	2	6	*no reflexes*
2	ChCl/malic acid	0.25	2	6	*no reflexes*
		0.50	2	6	*no reflexes*
5	ChCl/vanillin	0.50	2	6	$MgFe_2O_4$, Fe_2O_3, MgO

The products for the calcination at 400 °C with ChCl/maleic acid and ChCl/malic acid were bulky black powders that did not show any diffraction patters for the XRD measurement nor magnetism. This leads to the assumption that the DES was not completely combusted at this temperature and thus, no crystalline phases could be formed at all. However, the dark red powder for the calcination with ChCl/vanillin was slightly magnetic and traces of $MgFe_2O_4$ were displayed in the diffractogram.

Table 10. Resulting phases for the calcination of Fe_2O_3 and MgO at 500 °C using different DESs as reaction media. Mass fraction of the overall amount of starting material in the DES, stirring time, and calcination time were varied.

Entry	DES	Mass fraction [wt%]	Stirring time [h]	Calcination time [h]	Crystalline phases
1	ChCl/maleic acid	0.25	2	6	**$MgFe_2O_4$**
		0.50	2	6	**$MgFe_2O_4$**
		0.50	2	12	**$MgFe_2O_4$**
		0.50	2	36	**$MgFe_2O_4$**
		1.00	2	6	$MgFe_2O_4$, Fe_2O_3, MgO
2	ChCl/malic acid	0.25	2	6	**$MgFe_2O_4$**
		0.50	2	6	$MgFe_2O_4$, Fe_2O_3, MgO
		0.50	24	6	**$MgFe_2O_4$**
		0.50	72	6	**$MgFe_2O_4$**
		0.50	2	12	$MgFe_2O_4$, Fe_2O_3, MgO
		0.50	2	36	$MgFe_2O_4$, Fe_2O_3, MgO
		1.00	2	6	$MgFe_2O_4$, Fe_2O_3, MgO
3	ChCl/DMU	0.50	2	6	$MgFe_2O_4$, Fe_2O_3, MgO
		0.50	24	6	$MgFe_2O_4$, Fe_2O_3, MgO
		0.50	72	6	$MgFe_2O_4$, Fe_2O_3, MgO
4	ChCl/oxalic acid dihydrate	0.50	2	6	$MgFe_2O_4$, Fe_2O_3, MgO
		0.50	24	6	$MgFe_2O_4$, Fe_2O_3, MgO
		0.50	72	6	$MgFe_2O_4$, Fe_2O_3, MgO

5	ChCl/vanillin	0.50	2	6	$MgFe_2O_4$, Fe_2O_3, MgO
		0.50	2	12	$MgFe_2O_4$, Fe_2O_3, MgO
		0.50	2	36	$MgFe_2O_4$, Fe_2O_3, MgO
		1.00	2	6	$MgFe_2O_4$, Fe_2O_3, MgO
6	DMU/citric acid monohydrate	0.50	2	6	Fe_2O_3, MgO
7	DMU/D-mannose	0.50	2	6	Fe_2O_3, MgO
8	DMU/D-fructose	0.50	2	6	Fe_2O_3, MgO
9	urea/D-fructose	0.50	2	6	Fe_2O_3, MgO
10	urea/D-glucose	0.50	2	6	Fe_2O_3, MgO

For the combustion at 500 °C, with the DESs ChCl/maleic acid and ChCl/malic acid phase-pure $MgFe_2O_4$ was synthesized. These results are in accordance to previously reported methods using organic acid complexes as precursors for the preparation of phase-pure spinel-type ferrites.[19, 39, 40] Also, with other DESs $MgFe_2O_4$ was formed, but these DESs exclusively contained ChCl and no urea or DMU. All products showing only $MgFe_2O_4$ in the diffractogram were voluminous red to orange solids with a foam-like structure (Figure 16), which proved to be highly magnetic. Furthermore, it has been found by the variation of the mass fraction and stirring time that the higher the amount of starting material in the DES the more stirring or solvation time is necessary to yield a phase-pure product.

Table 11. Resulting phases for the calcination of Fe_2O_3 and MgO at 600 °C using different DESs as reaction media. Mass fraction of the overall amount of starting material in the DES was varied.

Entry	DES	Mass fraction [wt%]	Stirring time [h]	Calcination time [h]	Crystalline phases
1	ChCl/maleic acid	0.25	2	6	**$MgFe_2O_4$**
		0.50	2	6	**$MgFe_2O_4$**
2	ChCl/malic acid	0.25	2	6	**$MgFe_2O_4$**
		0.50	2	6	$MgFe_2O_4$, Fe_2O_3, MgO
5	ChCl/vanillin	0.50	2	6	$MgFe_2O_4$, Fe_2O_3, MgO

Figure 16. Phase-pure $MgFe_2O_4$ synthesized *via* the DES method with ChCl/maleic acid.

Calcination at 600 °C delivered the same results as at 500 °C and also prolonging of the calcination time had no influence on the purity of the reaction product.

Summing up the findings for the synthesis of $MgFe_2O_3$ by the DES method, it was demonstrated that the outcome of the reaction is controlled by the degree of dispersion of the starting materials in the reaction medium as well as the composition of the DES and less by the temperature or the calcination time – if the DES gets fully combusted.

Based on these results, the syntheses of various other spinel ferrites by the DES method, namely $MnFe_2O_4$, $CoFe_2O_4$, $NiFe_2O_4$, and $ZnFe_2O_4$ were investigated. For each mixed oxide, the DES ChCl/maleic acid and ChCl/malic acid were prepared and the oxides Fe_2O_3 and MO (M = Mn, Co, Ni, Zn) added in a molar ratio of 1:1, leading to an overall amount of metal oxide in the melt of 0.5 wt%. All mixtures were stirred for 2 h at 80 °C and the calcination was carried out at 400, 500, and 600 °C for 6 h. The results were compared with the solid-state reaction of Fe_2O_3 with the respective metal oxide MO (M = Mn, Co, Ni, Zn) at 900 °C for 3 days. An overview of the results evaluated by XRD, including those for $MgFe_2O_4$, is given in Table 12.

Table 12. Synthesis of spinel ferrites MFe_2O_4 (M = Mg, Mn, Co, Ni, Zn) by the DES method with two different DESs at calcination temperatures of 400, 500 and 600 °C in comparison to the solid-state reaction of Fe_2O_3 with the respective metal oxide at 900 °C. The success of the reactions is classified by: ✓ = phase-pure spinel-type ferrite, ~ = spinel-type ferrite, × = no spinel-type ferrite was formed.

Entry	Spinel ferrite	DES-method				Solid-state
		DES	400 °C	500 °C	600 °C	900 °C
1	$MgFe_2O_4$	ChCl/maleic acid	×	✓	✓	~
		ChCl/malic acid	×	~	~	
2	$MnFe_2O_4$	ChCl/maleic acid	×	×	×	×
		ChCl/malic acid	×	×	×	
3	$CoFe_2O_4$	ChCl/maleic acid	×	✓	✓	~
		ChCl/malic acid	×	~	~	
4	$NiFe_2O_4$	ChCl/maleic acid	×	✓	✓	~
		ChCl/malic acid	×	~	~	
5	$ZnFe_2O_4$	ChCl/maleic acid	×	~	~	✓
		ChCl/malic acid	×	~	~	

The spinel-type ferrites $CoFe_2O_4$, $NiFe_2O_4$, and $ZnFe_2O_4$ were successfully formed by using the DES method with simple metal oxides.[41] The results prove that applying DESs as solvent enables low-temperature synthesis of mixed oxides and that DESs provide excellent reaction media for this type of inorganic synthesis. In combination with the DES ChCl/maleic acid, highly phase-pure products were obtained for magnesium, cobalt, and nickel ferrite at 500 and 600 °C. All reactions at 400 °C resulted in amorphous black powders, in contrast to the orange to brown products yielded at 500, 600, and 900 °C, which indicates incomplete incineration at low temperature.

The DES method with Fe_2O_3 and MnO as starting material did not result in formation of the desired manganese ferrite. However, even the solid-state reaction at 900 °C did not take place for this spinel ferrite. This is in accordance with previous reports, in which the synthesis of $MnFe_2O_4$ by thermal treatment of the metal oxides required a considerably

higher energy supply than other spinel ferrites. Full conversion into manganese ferrite could therefore only be performed at temperatures above 1150 °C.[42]

The XRD patterns of $MgFe_2O_4$, $CoFe_2O_4$, and $NiFe_2O_4$ prepared by the DES method with ChCl/maleic acid and the respective solid-state reactions are shown in Figure 17, Figure 18, and Figure 19. All reflection peaks of phase-pure, as well as impure, mixed oxides match well with reference data from the Inorganic Crystal Structure Database (ICSD) of the pure phases ($MgFe_2O_4$: ICSD #152470; $CoFe_2O_4$: ICSD #193531; $NiFe_2O_4$: ICSD #192290).[43-45] The obtained patterns indicate that the prepared samples are single-phase crystalline spinel-type ferrites with cubic structure and space group $Fd\bar{3}m$. The direct comparison with the starting materials also emphasizes the high phase purity of the products obtained by the DES method, in contrast to the solid-state reactions. In addition, the broad peaks immediately indicate the small particle size of the spinel structures obtained by the DES method. Particle sizes can be estimated from line broadening by using the Williamson-Hall method.[46]

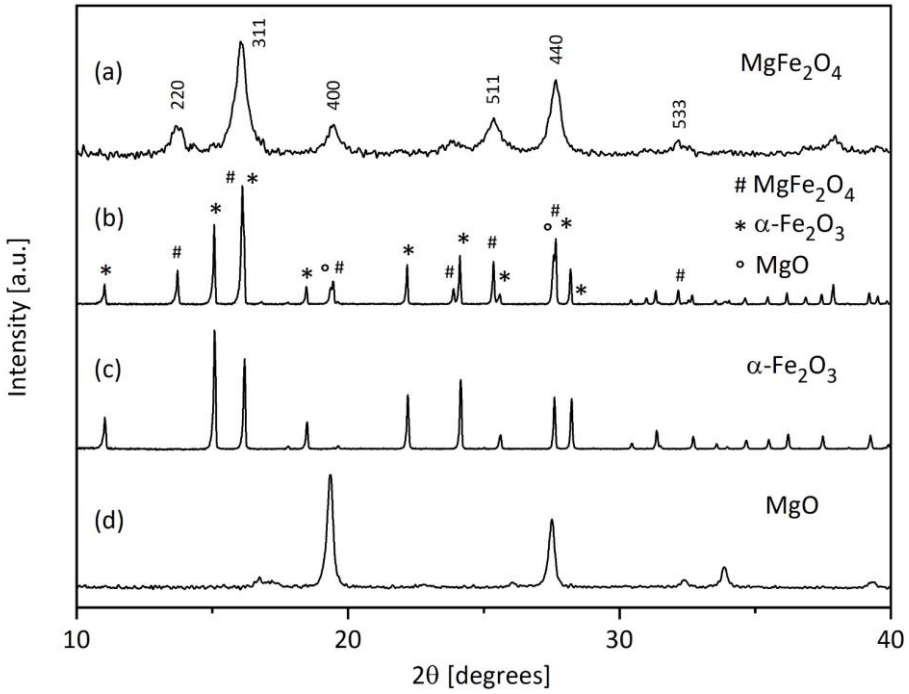

Figure 17. XRD patterns: a) $MgFe_2O_4$ prepared by DES method with ChCl/maleic acid at 500 °C; b) solid-state reaction of $MgFe_2O_4$ at 900 °C including both starting materials, α-Fe_2O_3 and MgO; c) α-Fe_2O_3; d) MgO.

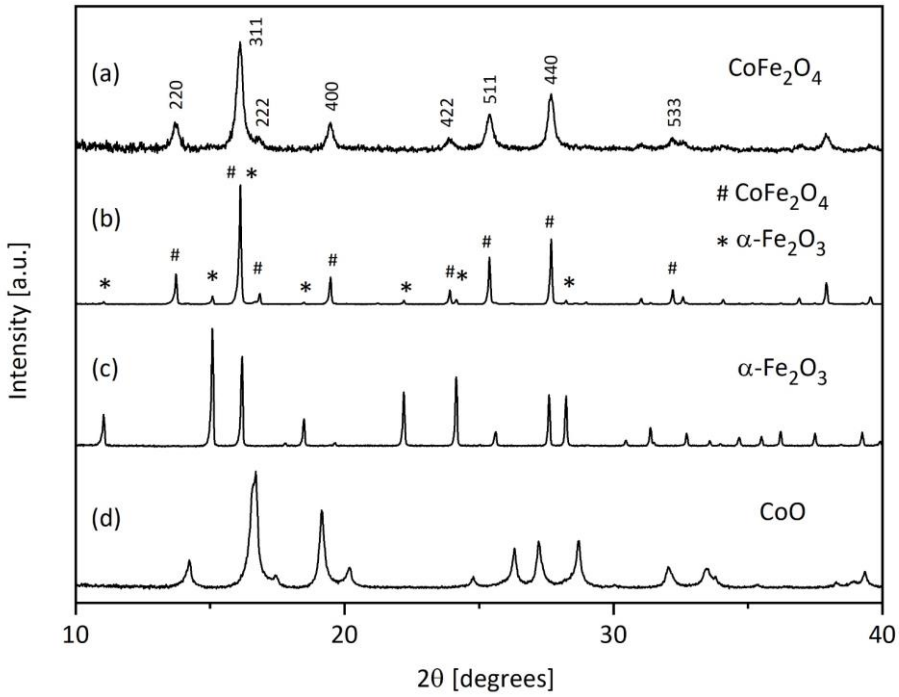

Figure 18. XRD patterns: a) $CoFe_2O_4$ prepared by DES method with ChCl/maleic acid at 500 °C; b) solid-state reaction of Co Fe_2O_4 at 900 °C including both starting materials, α-Fe_2O_3 and CoO; c) α-Fe_2O_3; d) CoO.

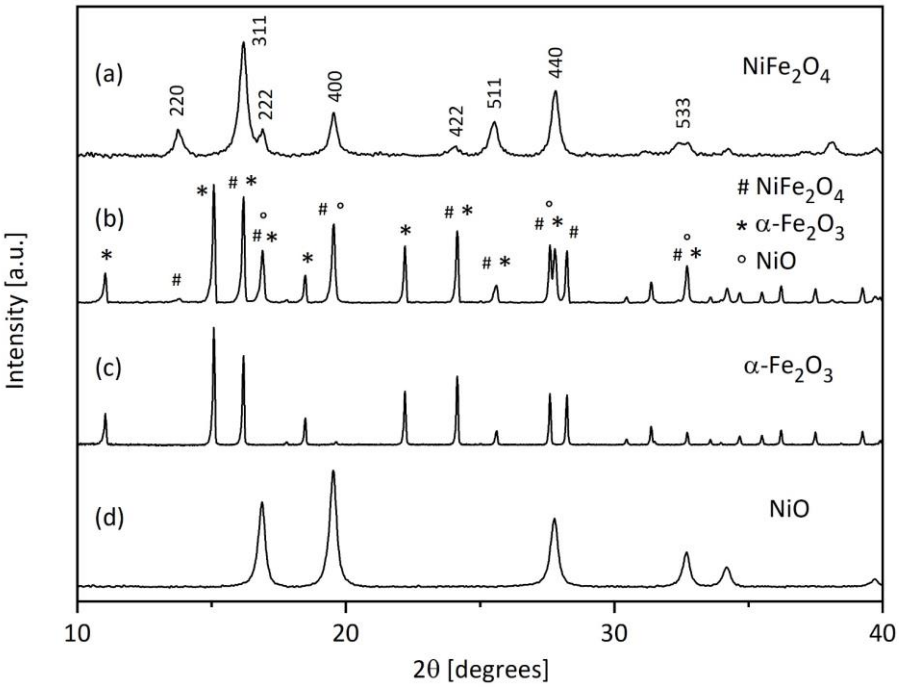

Figure 19. XRD patterns: a) $NiFe_2O_4$ prepared by DES method with ChCl/maleic acid at 500 °C; b) solid-state reaction of $NiFe_2O_4$ at 900 °C including both starting materials, α-Fe_2O_3 and NiO; c) α-Fe_2O_3; d) NiO.

2.2.3 Characterization of the Synthesized Ferrite Nanoparticles

The X-ray diffraction intensity data recorded for $MgFe_2O_4$ were used to estimate the cation distribution over the tetrahedral and octahedral voids (*i.e.*, the degree of inversion of the spinel). One can expect reasonable significance even from X-ray powder data due to the different scattering powers of Mg and Fe. Thus, calculated diffraction patterns with different degrees of inversion were compared with the measured data (see Appendix 6.2). The reflections 111, 220, 400, 331, and 422 show a pronounced sensitivity to the cation distribution. The best matching intensities were calculated for a cation distribution of $[Mg_{0.24}Fe_{0.76}]^T[Mg_{0.76}Fe_{1.24}]^OO_4$, *i.e.*, the degree of inversion is $\lambda \approx 0.76$, with $\lambda = 0$ for a normal spinel and $\lambda = 1$ for a fully inverse spinel. The reflection intensities and the lattice constant of the magnesium ferrite annealed at 600 °C fit quite well with data reported for nanocrystalline spinel-type $MgFe_2O_4$.[44]

The average crystallite size of the phase-pure mixed oxides magnesium ferrite, cobalt ferrite and nickel ferrite synthesized by the DES method was estimated using Williamson-Hall analysis based on XRD line broadening. The values for all three ferrite types were around 100 nm for the incineration at 500 °C and were increased up to about 150 nm at 600 °C (Table 13).

Table 13. Crystallite size and optical bandgap of phase-pure MFe_2O_4 (M = Mg, Co, Ni) synthesized with the DES ChCl/maleic acid at 500 and 600 °C.

Entry	Spinel ferrite	Crystallite size [nm] [a]		Band gap [eV] [b]	
		500 °C	600 °C	500 °C	600 °C
1	$MgFe_2O_4$	68	102	1.72	1.88
2	$CoFe_2O_4$	122	175	1.24	1.16
3	$NiFe_2O_4$	91	145	1.58	1.79

(*a*) Obtained by XRD; (*b*) obtained by diffuse reflectance UV/Vis spectroscopy (UV/Vis DRS).

The optical properties of the nanoparticles were investigated by measuring the spectral UV/Vis reflectance in the wavelength range 380–800 nm. To analyze the diffuse reflectance spectra, Kubelka-Munk theory was used, according to equation (1):

$$\mathrm{F}(R_\infty) = (1 - R_\infty)^2 / 2R_\infty \quad (1)$$

$\mathrm{F}(R_\infty)$ describes the remission or Kubelka-Munk function and R_∞ the reflectance.[47, 48] The bandgap energy E_g was determined by finding the intercept of the straight line in the low-energy rise of the plot of $[\mathrm{F}(R_\infty)hv]^{1/2}$ for the indirect allowed transition versus hv, where hv is the incident photon energy. For $MgFe_2O_4$, the bandgap is in the range 1.7–1.9 eV, which is about 0.2 eV lower than the literature values.[47] The difference can be attributed to several factors, as the bandgap value is influenced by crystallite size, structural parameters, carrier concentrations, and lattice strain. The bandgap energies for $CoFe_2O_4$ (1.2 eV) and $NiFe_2O_4$ (1.6–1.8 eV) corresponded to the reported values.[49-51]

The morphology and microstructure of the ferrite particles were characterized by scanning electron microscopy (SEM). The structures of $MgFe_2O_4$, $CoFe_2O_4$ and $NiFe_2O_4$ synthesized by the DES method with malic acid at 500 °C are depicted in Figure 20.

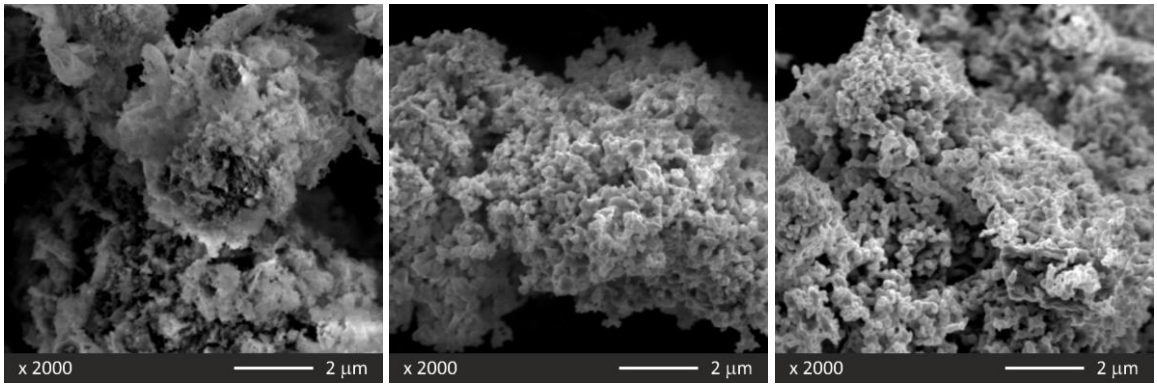

Figure 20. SEM images of $MgFe_2O_4$, $CoFe_2O_4$, and $NiFe_2O_4$ (from first to last) synthesized by DES method with ChCl/maleic acid at 500 °C for 6 h.

Cobalt and nickel ferrite are very similar in morphology and average particle size, which was found to be in the range 130–220 nm. Both ferrites consist of particles with coral-like structures. The particle size distribution of $MgFe_2O_4$ is much broader, ranging from 120–480 nm. The structures are more irregular and can be described as frayed. However, further characterization of the synthesized spinel-type ferrites by transmission electron microscopy (TEM) was not possible because of their high tendency to

agglomerate. As shown for $MgFe_2O_4$, the degree of inversion is less influenced by this synthetic procedure than by other methods.

Further, measurements of the specific surface area were made for $MgFe_2O_4$ using the BET theory (Brunauer, Emmett, Teller)[52] because of the foam-like structure of the phase-pure products. But the specific surface area was only increased from 3.03 m^2/g (±0,02) for Fe_2O_3 up to 15.24 m^2/g (±1.02) for $MgFe_2O_4$ synthesized with ChCl/malic acid at 400 °C.

2.3 Conclusion

In conclusion, magnesium, cobalt, and nickel ferrite nanoparticles were successfully prepared by the DES method, by using low-temperature synthesis from simple unmodified metal oxides as starting materials instead of metal salts. DESs provide a nontoxic and renewable reaction medium that is facile to prepare and easy to handle. The reported procedure does not require the preparation of precursors or the use of highly corrosive acids and harmful reagents, which may be an advantage over other methods. Due to the good solubility of some metal oxides in DESs, the reactions proceed at much lower temperatures than the respective solid-state reactions and at the same temperatures as syntheses with comparable calcination processes that use metal salts. The DES method therefore reduces the overall required energy for the nanoparticle synthesis. Furthermore, employing DESs may offer new possibilities for the inorganic synthesis of metal oxides.

2.4 Experimental

2.4.1 General Procedures and Materials

Chemicals. All chemicals were of analytical reagent grade and used as received without further purification except for choline chloride [$HOC_2H_4N(CH_3)_3^+Cl^-$ or ChCl], which was dried at 130 °C *in vacuo* and stored under nitrogen prior to use. The metal oxides iron(III) oxide (α-Fe_2O_3), magnesium oxide (MgO), cobalt(II) oxide (CoO), nickel(II) oxide (NiO), and zinc oxide (ZnO) were used as starting material for preparation by the DES

method and for the solid-state reaction of ferrite nanoparticles with the general formula MFe_2O_4.

DES preparation. The DESs were formed by mixing the two components in the respective molar ratio in a glass vial. The mixtures were heated up to 80 °C in an aluminum heating block until a homogeneous, colorless liquid was obtained.

Solubility experiments. Approximately 2.0 mg of the metal oxide was added to 5.0 g of the DES (ca. 0.05 wt%). The mixture was stirred at 80 °C for 2 h (and 24 h for Fe_2O_3) and the qualitative solubility evaluated by the appearance of the DES.

2.4.2 Thermal Process for the Synthesis of Spinel-Type Ferrites with DESs

Fe_2O_3 and the metal oxide MO (M = Mg, Co, Ni, Zn) were added to the DES in a molar ratio of 1:1, resulting in an overall amount of metal oxides in the melt of 0.5 wt %. After 2 h of stirring at 80 °C, the melts were transferred into a crucible and calcined in a muffle furnace in two steps: At first, the melts were heated at 230 °C for 2 h, in order to avoid extensive foaming. Then, the calcination of the mixtures was carried out at 400, 500, or 600 °C in air for 6 h. For the solid-state synthesis of spinel ferrite particles, Fe_2O_3 and MO (M = Mg, Co, Ni, Zn) were mixed in a 1:1 molar ratio, ground, and calcined at 900 °C in air for 3 days. The heating rate was set to 10 °C/min in all cases.

2.4.3 Characterization Methods

XRD imaging. The phase purity and crystal structure of the prepared ferrites were determined by powder X-ray diffraction (XRD). XRD patterns were recorded at r.t. on a STOE STADI P X-ray diffractometer (Stoe & Cie GmbH) with Cu$K\alpha_1$ (λ = 1.54059 Å) or Mo$K\alpha_1$ (λ = 0.70932 Å) radiation. The mean crystallite size of the powders was calculated from the diffraction line broadening by using the Williamson-Hall method.[46]

UV/Vis DRS measurements. UV/Vis DRS was carried out at r.t. on an Omega 20 UV/Vis spectrophotometer with Ulbricht sphere (Bruins Instruments) in the range λ = 380–800 nm. The UV/Vis spectra were processed with OriginPro software and the bandgap energy estimated by the Kubelka-Munk function, $F(R_\infty)$, which was extracted from the UV/Vis DRS absorbance.[42] The bandgap E_g was determined by finding the intercept of the

straight line in the low-energy rise of the plot of $[\mathrm{F}(R_\infty)hv]^{1/2}$ for the indirect allowed transition versus hv, where hv is the incident photon energy.

SEM imaging. Morphology studies were performed by a digital scanning electron microscope (Zeiss, DSM 940 A) operating in secondary imaging mode at 10 kV with a working distance of 10 mm. Incineration behavior was monitored by thermogravimetric analysis with a thermobalance (Mettler Toledo, TG50) at a heating rate of 10 °C/min in the temperature range of 25–500 °C.

2.5 References

[1] S. G. Mendo, A. F. Alves, L. P. Ferreira, M. M. Cruz, M. H. Mendonca, M. Godinho and M. D. Carvalho, *New J. Chem.*, **2015**, *39*, 7182-7193.

[2] A. W. Weimer, C. Perkins, J. Scheffe, S. M. George and P. Lichty, WO2009061795A1, **2009**.

[3] D. Makovec, A. Kosak, A. Znidarsic and M. Drofenik, *J. Magn. Magn. Mater.*, **2005**, *289*, 32-35.

[4] A. Sutka, M. Millers, M. Vanags, U. Joost, M. Maiorov, V. Kisand, R. Parna and I. Juhnevica, *Res. Chem. Intermed.*, **2015**, *41*, 9439-9449.

[5] A. Sutka and K. A. Gross, *Sens. Actuators, B*, **2016**, *222*, 95-105.

[6] I. Petrila and F. Tudorache, *Mater. Lett.*, **2013**, *108*, 129-133.

[7] H. W. Carpenter, US6909395B1, **2005**.

[8] S. Khilari, S. Pandit, J. L. Varanasi, D. Das and D. Pradhan, *ACS Appl. Mater. Interfaces*, **2015**, *7*, 20657-20666.

[9] L. J. Berchmans, R. K. Selvan and C. O. Augustin, *Mater. Lett.*, **2004**, *58*, 1928-1933.

[10] D. S. Mathew and R.-S. Juang, *Chem. Eng. J.*, **2007**, *129*, 51-65.

[11] O. M. Hemeda, K. R. Mahmoud and T. Sharshar, *Eur. Phys. J. Plus*, **2014**, *129*, 1-10.

[12] S. Gyergyek, D. Makovec, A. Kodre, I. Arcon, M. Jagodic and M. Drofenik, *J. Nanopart. Res.*, **2010**, *12*, 1263-1273.

[13] C. Liu, B. Zou, A. J. Rondinone and Z. J. Zhang, *J. Phys. Chem. B*, **2000**, *104*, 1141-1145.

[14] K. M. Reddy, L. Satyanarayana, S. V. Manorama and R. D. K. Misra, *Mater. Res. Bull.*, **2004**, *39*, 1491-1498.

[15] M. George, A. M. John, S. S. Nair, P. A. Joy and M. R. Anantharaman, *J. Magn. Magn. Mater.*, **2006**, *302*, 190-195.

[16] H. E. Zhang, B. F. Zhang, G. F. Wang, X. H. Dong and Y. Gao, *J. Magn. Magn. Mater.*, **2007**, *312*, 126-130.

[17] C. R. Vestal and Z. J. Zhang, *Nano Lett.*, **2003**, *3*, 1739-1743.

[18] G. Raja, S. Gopinath and K. Sivakumar, *Ceram. Int.*, **2016**, Ahead of Print.

[19] A. Doi, S. Matsushima, K. Obata, R. Maeda, A. Kajima and K. Kobayashi, *J. Ceram. Soc. Jpn.*, **2014**, *122*, 645-648, 644 pp.

[20] C. Ruß and B. König, *Green Chem.*, **2012**, *14*, 2969-2982.

[21] A. P. Abbott, D. Boothby, G. Capper, D. L. Davies and R. K. Rasheed, *J. Am. Chem. Soc.*, **2004**, *126*, 9142-9147.

[22] S. Stolte, J. Arning and J. Thoeming, *Chem. Ing. Tech.*, **2011**, *83*, 1454-1467.

[23] M. Petkovic, K. R. Seddon, L. P. N. Rebelo and C. S. Pereira, *Chem. Soc. Rev.*, **2011**, *40*, 1383-1403.

[24] G. Imperato, E. Eibler, J. Niedermaier and B. König, *Chem. Commun.*, **2005**, 1170-1172.

[25] G. Imperato, S. Hoger, D. Lenoir and B. König, *Green Chem.*, **2006**, *8*, 1051-1055.

[26] G. Imperato, R. Vasold and B. König, *Adv. Synth. Catal.*, **2006**, *348*, 2243-2247.

[27] F. Ilgen and B. König, *Green Chem.*, **2009**, *11*, 848-854.

[28] J. T. Gorke, F. Srienc and R. J. Kazlauskas, *Chem. Commun.*, **2008**, 1235-1237.

[29] B. N. Borse, V. S. Borude and S. R. Shukla, *Curr. Chem. Lett.*, **2012**, *1*, 59-68.

[30] E. L. Smith, A. P. Abbott and K. S. Ryder, *Chem. Rev.*, **2014**, *114*, 11060-11082.

[31] A. P. Abbott, G. Capper, D. L. Davies, K. J. McKenzie and S. U. Obi, *J. Chem. Eng. Data*, **2006**, *51*, 1280-1282.

[32] A. P. Abbott, G. Frisch, J. Hartley and K. S. Ryder, *Green Chem.*, **2011**, *13*, 471-481.

[33] A. P. Abbott, J. Collins, I. Dalrymple, R. C. Harris, R. Mistry, F. Qiu, J. Scheirer and W. R. Wise, *Aust. J. Chem.*, **2009**, *62*, 341-347.

[34] A. Söldner, J. Zach and B. König, *Green Chem.*, **2019**, *21*, 321-328.

[35] A. P. Abbott, G. Frisch and K. S. Ryder, *Annu. Rep. Prog. Chem., Sect. A: Inorg. Chem.*, **2008**, *104*, 21-45.

[36] A. P. Abbott, G. Capper, D. L. Davies, R. K. Rasheed and P. Shikotra, *Inorg. Chem.*, **2005**, *44*, 6497-6499.

[37] J. M. Hartley, C.-M. Ip, G. C. H. Forrest, K. Singh, S. J. Gurman, K. S. Ryder, A. P. Abbott and G. Frisch, *Inorg. Chem.*, **2014**, *53*, 6280-6288.

[38] Y. Dai, J. van Spronsen, G.-J. Witkamp, R. Verpoorte and Y. H. Choi, *Anal. Chim. Acta*, **2013**, *766*, 61-68.

[39] M. Azam, S. Riaz, A. Akbar and S. Naseem, *J. Sol-Gel Sci. Technol.*, **2014**, *74*, 340-351.

[40] I. Ibrahim, I. O. Ali, T. M. Salama, A. A. Bahgat and M. M. Mohamed, *Appl. Catal., B*, **2016**, *181*, 389-402.

[41] The syntheses of magnesium, cobalt, and nickel ferrites were also carried out by DES method at 700, 800, and 900 °C and resulted in particles of the same

crystalline phase as preparation at 500 and 600 °C. With rising calcination temperatures, an increase in particle size was observed.

[42] H. H. Kedesdy and A. Tauber, *J. Am. Ceram. Soc.*, **1956**, *39*, 425-431.

[43] A. M. Wahba and M. Bakr Mohamed, *J. Magn. Magn. Mater.*, **2015**, *378*, 246-252.

[44] M. Gateshki, V. Petkov, S. K. Pradhan and T. Vogt, *J. Appl. Crystallogr.*, **2005**, *38*, 772-779.

[45] K. Raju and D. H. Yoon, *J. Supercond. Novel Magn.*, **2014**, *27*, 1285-1292.

[46] G. K. Williamson and W. H. Hall, *Acta Metall.*, **1953**, *1*, 22-31.

[47] R. Koeferstein, T. Walther, D. Hesse and S. G. Ebbinghaus, *J. Mater. Sci.*, **2013**, *48*, 6509-6518.

[48] P. Kubelka and F. Munk, *Z. Techn. Phys.*, **1931**, *12*, 593-601.

[49] B. S. Holinsworth, D. Mazumdar, H. Sims, Q. C. Sun, M. K. Yurtisigi, S. K. Sarker, A. Gupta, W. H. Butler and J. L. Musfeldt, *Appl. Phys. Lett.*, **2013**, *103*, 082406/082401-082406/082404.

[50] F. S. Tehrani, V. Daadmehr, A. T. Rezakhani, R. H. Akbarnejad and S. Gholipour, *J. Supercond. Nov. Magn.*, **2012**, *25*, 2443-2455.

[51] Q.-C. Sun, H. Sims, D. Mazumdar, J. X. Ma, B. S. Holinsworth, K. R. O'Neal, G. Kim, W. H. Butler, A. Gupta and J. L. Musfeldt, *Phys. Rev. B*, **2012**, *86*, 205106.

[52] S. Brunauer, P. H. Emmett and E. Teller, *J. Am. Chem. Soc.*, **1938**, *60*, 309-319.

CHAPTER 3

3 Deep Eutectic Solvents as Potential Media for Optical Analysis and Separation of Trivalent Lanthanides

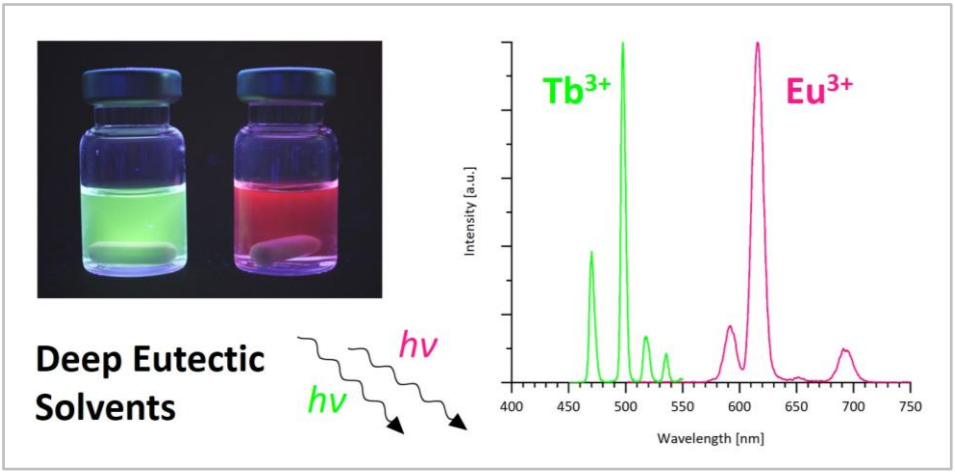

This chapter is a manuscript prepared for submission to the *Journal of Rare Earths*.

A. Söldner performed the experimental work and wrote the manuscript. B. König supervised the project and will be the corresponding author.

3.1 Introduction

The separation of lanthanides from one another still belongs to the most challenging tasks in separational science. Even though it is possible to commercially separate those elements since 1950,[1] the topic is still highly discussed for the exploration of more effective and environmentally friendly methods – especially since the separation problem no longer only applies to the processing of ores, but also to the recovery of lanthanides from synthetically produced materials and compounds that contain more than one rare earth element (Sc, Y, La–Lu). Multiple lanthanides are used in combination for example in magnets, catalysts, alloys, optical filters, neutron absorbers and for other applications (Table 14).[2, 3]

Table 14. Usage of rare earth elements by application in %.[3]

Application [%] [a]	Y	La	Ce	Pr	Nd	Sm	Eu	Gd	Tb	Dy	Other
magnets				23.4	69.4			2	0.2	5	
battery alloys		50	33.4	3.3	10	3.3					
metallurgy		26	52	5.5	16.5						
auto catalysts		5	90	2	3						
fluid catalytic cracking		90	10								
polishing powders		31.5	65	3.5							
glass additives	2	24	66	1	3						4
phosphors	69.2	8.5	11				4.9	1.8	4.6		
ceramics	53	17	12	6	12						
other	19	19	39	4	15	2		1			

(*a*) The percentages are estimated average consumption distributions by application; the actual distribution varies from manufacturer to manufacturer.

Due to the high resemblance of the chemical and physical properties of lanthanides to actinides, the issue is also of high interest for the reprocessing of nuclear waste, which means that suitable separation methods for rare earth elements may also be applicable for the radioactive f-block elements. The analogies between lanthanides and actinides include (a) the characteristic trivalence for both series of chemical elements, (b) the so-called lanthanide and actinide contraction as the consistent and greater-than-expected

decrease of the ionic radii Ln^{3+} and Ac^{3+} with the atomic mass (from 1.172 Å for La^{3+} to 1.001 Å for Lu^{3+}; from 1.26 Å for Ac^{3+} to 1.09 Å for Cf^{3+}), (c) the parallel curve progression of the magnetic moment of Ln^{3+} and Ac^{3+} ions, and (d) the remarkable similarity in the absorption spectra of the homologs of a series (*e.g.* Nd^{3+}/U^{3+}, Sm^{3+}/Pu^{3+}, Eu^{3+}/Am^{3+}).[4] The lanthanide contraction explains the natural occurrence of lanthanides in groups rather than individually and forms the basis for the majority of extraction and separation processes, *e.g.* countercurrent fractional solvent extraction,[5, 6] capillary electrophoresis[7, 8] and ion-exchange chromatography.[9, 10] Further, trivalent lanthanide ions show intense luminescence in the near-infrared (*e.g.* Nd^{3+}, Er^{3+}, Yb^{3+}) and visible regions (*e.g.* Eu^{3+}, Tb^{3+}) with long decay times and a large Stokes shift. This is explained by the shielding of the 4f valence shell from the environment around the lanthanide ion by higher lying closed shells. The weak intraconfigurational f–f transitions show characteristic narrow-line emission, which resembles more an atomic spectrum than a transition metal spectrum.[11] Figure 21 displays partial energy diagrams for lanthanide aquo ions.

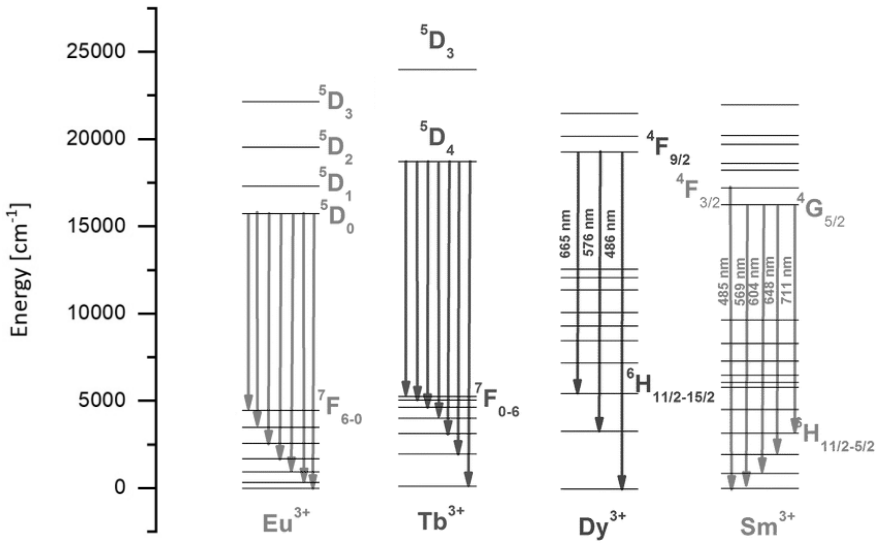

Figure 21. Partial energy diagrams for the aquo ions of europium(III), terbium(III), dysprosium(III), and samarium(III) and the respective main transition between the luminescent and the fundamental level.[12, 13]

Thus, lanthanide compounds gained a prominent position in lighting and light conversion technologies with the current focus on applications as lamp phosphors, organic light emitting diodes,[14-19] optical fibers,[20-24] single-molecule magnets,[25-29] functional complexes for biological assays,[30-35] and for medical imaging.[36-41] However, the

luminescence lifetime and quantum yield are hampered or even quenched completely in polar, protic solvents by coordination of the solvent molecules to the luminescent lanthanide centers. Non-radiative deactivation of the excited state takes place *via* vibronic coupling with the vibrational states of X–H oscillators (X = C, N, O). Therefore, it is important to avoid these quenchers in the first coordination sphere or even further away from the lanthanide ion.[42, 43] This fact strongly limits the application of luminescence measurements for the direct quantitative analysis of rare earth elements in solvent extraction processes. As a result, cost intensive plasma-based spectroscopy is usually used, *e.g.* inductively coupled plasma mass spectrometry (ICP-MS), microwave induced plasma and inductively coupled plasma optical emission spectroscopy (MIP-OES and ICP-OES).[44-46]

In 2004, Bünzli *et al.* introduced ionic liquids as promising solvents for near infrared emitting europium(III) complexes[47] and in the following years further investigations were made with other trivalent lanthanide ions.[48] It was shown that replacement of conventional solvents by ionic liquids leads to a dramatic increase of the luminescence quantum yields and lifetimes of the excited states.[13, 49-51] In addition, promising results on the use of ionic liquids for the separation of lanthanides were published.[52, 53] Recent studies have shown that some ionic liquids even display reasonable stability under α and γ irradiation,[54] thus reinforcing the potential of this type of solvent system for the usage in nuclear fuel industry.

We already published results that point out the extraction potential of deep eutectic solvents (DESs) – a solvent system closely related to ionic liquids – for the selective extraction of lanthanide compounds among other metal salts and oxides.[55] DESs are mixtures of a Lewis (or Brønsted-Lowry) acid with a Lewis base that results in a melting point lower than either of the individual components. The lower melting point in the eutectic mixture is the result of strong hydrogen bonds between the components, which typically involve an organic salt (*e.g.* choline chloride) as the hydrogen bond acceptor (HBA) mixed with a hydrogen bond donor (HBD). DESs and ionic liquids possess similar physicochemical properties, such as low vapor pressure, chemical and thermal stability, a large temperature range as a liquid, and a high dissolving power for a wide range of

compounds. Many DESs and ionic liquids are colorless or have only a slightly yellowish color and are optically transparent through almost the whole visible and near-infrared spectral regions. Further, both types of liquids can be designed as polar solvents, but without the high coordinating ability of typical polar solvents such as DMF, DMSO or water. However, DESs have an advantage over ionic liquids due to a simpler synthesis that does not require additional solvent or purification steps.[56]

In this respect, DESs become interesting solvents to investigate their separation abilities and optical properties for trivalent lanthanide compounds. DESs may provide an environment that allows selective separation of f-block elements as well as luminescence measurements for quantitative analysis at the same time. In the following chapter, the use of DESs based on natural compounds is evaluated on one side as media for spectroscopic quantitation of lanthanide ions and on the other side for the separation of lanthanide oxides with the overarching aim to combine both approaches.

3.2 Results and Discussion

The variety of DESs is vast due to the numerous amounts of compounds that were found suitable for the formation of eutectic solvents. Therefore, the selection of eutectic mixtures for luminescence, solubility, and separation experiments was limited and the DESs chosen based on two criteria: 1. Low to moderate viscous between r.t. and 100 °C for easy handling, and 2. thermal stable up to 100 °C over a long period of time. This limited the number of potential solvent systems to the DESs listed in Table 15 with either choline chloride (ChCl), choline bitartrate (ChBt), *N,N'*-dimethylurea (DMU), or DL-menthol as hydrogen-bond acceptor (HBA) (Figure 22). In addition to water-free DESs, eutectic melts containing hydrates were included in the selection to gain insight into the luminescence quenching effect of water in those solvents.

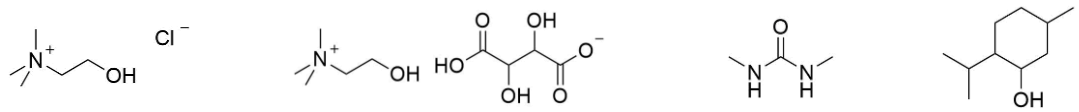

Figure 22. Hydrogen-bond acceptors (HBAs) for DES preparation: choline chloride (ChCl), choline bitartrate (ChBt), *N,N'*-dimethylurea (DMU), and DL-menthol (*from left to right*).

Table 15. DESs based on choline chloride (ChCl), choline bitartrate (ChBt), *N,N'*-dimethylurea (DMU), or DL-menthol for luminescence, solubility, and separation experiments with lanthanide compounds.

Entry	HBA	HBD	Structure [a]	Molar ratio	Processing temperature
1	ChCl	oxalic acid dihydrate	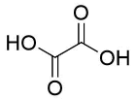	1 : 1	80 °C
2	ChCl	DL-lactic acid (~10% water)	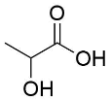	1 : 2	80 °C
3	ChCl	L-lactic acid	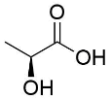	1 : 2	80 °C
4	ChCl	levulinic acid	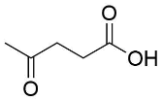	1 : 2	80 °C
5	ChCl	itaconic acid	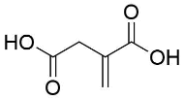	1 : 1	80 °C
6	ChCl	citric acid monohydrate	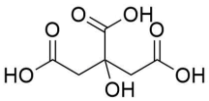	2 : 1	100 °C
7	ChCl	phenylacetic acid	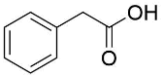	1 : 2	80 °C
8	ChCl	DL-mandelic acid	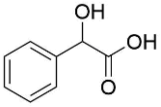	1 : 2	80 °C
9	ChCl	D-mandelic acid	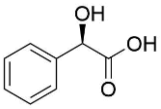	1 : 2	80 °C
10	ChCl	xylitol	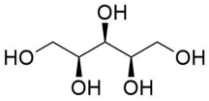	1 : 1	80 °C
11	ChCl	urea	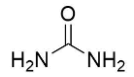	1 : 2	80 °C
12	ChCl	vanillin	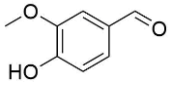	1 : 2	80 °C
13	ChBt	oxalic acid dihydrate	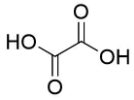	1 : 1	80 °C

14	DMU	citric acid anhydrous	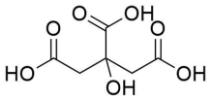	7 : 2	80 °C
15	DMU	citric acid monohydrate	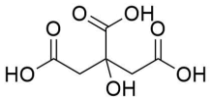	7 : 2	80 °C
16	DL-menthol	pyruvic acid	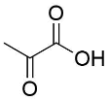	1 : 2	50 °C
17	DL-menthol	L-lactic acid	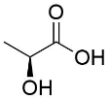	1 : 2	50 °C
18	DL-menthol	lauric acid	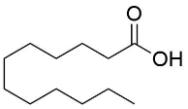	2 : 1	50 °C

(*a*) Structures do not contain hydrate molecules.

3.2.1 Spectroscopic Studies of Trivalent Lanthanides in DESs

In a first series of experiments, the spectroscopic characteristics of trivalent lanthanide chlorides $LnCl_3$ (Ln = Eu, Tb, Sm, Dy), respectively their aquo complexes, were investigated in DESs (Table 16). The effect of water in the DESs as well as the influence of temperature were examined for Eu^{3+} as a representative lanthanide ion and a homologue of Am^{3+} (an actinide of great interest in the nuclear fuel cycle). Further, the applicability of DESs as potential media for quantitation of europium(III) oxide was assessed.

Table 16. Trivalent lanthanide compounds used for luminescence studies in DESs and the general luminescence type of the trivalent ion.[13]

IUPAC name	Chemical formula	Luminescence type
europium(III) chloride	$EuCl_3$	phosphorescence
europium(III) chloride hexahydrate	$EuCl_3 \cdot 6\ H_2O$	
europium(III) oxide	Eu_2O_3	
terbium(III) chloride hexahydrate	$TbCl_3 \cdot 6\ H_2O$	phosphorescence
samarium(III) chloride hexahydrate	$SmCl_3 \cdot 6\ H_2O$	phosphorescence
dysprosium(III) chloride hexahydrate	$DyCl_3 \cdot 6\ H_2O$	phosphorescence

Europium(III)

The near-infrared emission spectra of anhydrous $EuCl_3$ (Figure 23) and $EuCl_3$ hexahydrate (Figure 24) in DESs show the characteristic emissions for Eu^{3+} at about 592, 616, and 692 nm for the transitions from the $^5D_0$ level to the ^7F_J levels (J = 1, 2, 4). The electronic dipole transition $^5D_0 \rightarrow {}^7F_2$ is in all DESs the strongest, indicating low symmetry around the Eu^{3+} ion.[57] The emission for the $^5D_0 \rightarrow {}^7F_3$ transition around 650 nm was too weak to be observed. Under identical experimental conditions, the phosphorescence emission intensities of Eu^{3+} in the DESs are compared to the emission spectra of anhydrous $EuCl_3$ in water and of $EuCl_3$ hexahydrate in water, methanol and ethanol; the respective phosphorescence characteristics at r.t. are listed in Table 17 and Table 18.

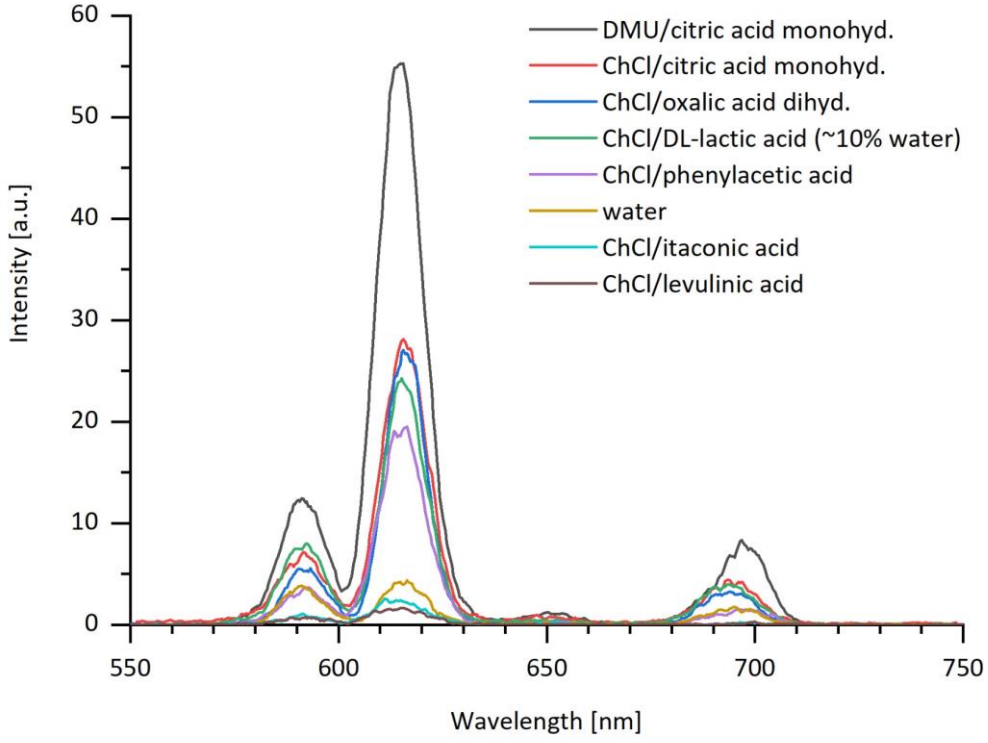

Figure 23. Phosphorescence emission spectra (λ_{ex} = 395 nm) of 1.00 mM solutions of anhydrous $EuCl_3$ in 7 different DESs and H_2O at r.t. (legend sorted according to emission intensity for the $^5D_0 \rightarrow {}^7F_2$ transition at around 616 nm).

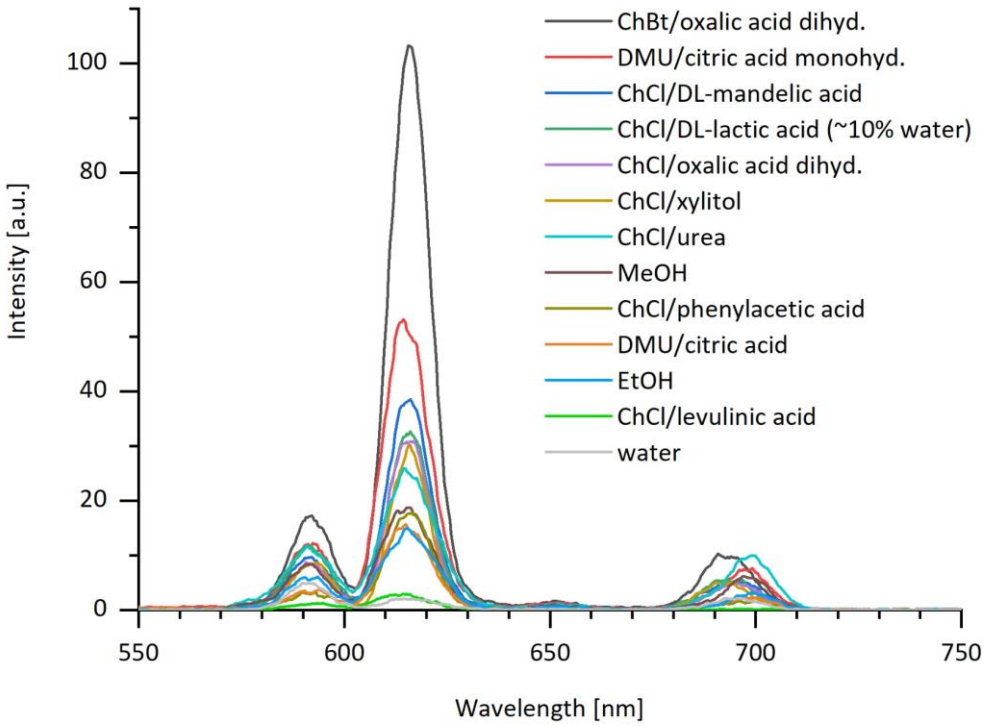

Figure 24. Phosphorescence emission spectra (λ_{ex} = 395 nm) of 1.00 mM solutions of $EuCl_3 \cdot 6\ H_2O$ in 10 different DESs, H_2O, MeOH, and EtOH at r.t. (legend sorted according to emission intensity for the $^5D_0 \rightarrow {}^7F_2$ transition at around 616 nm).

Table 17. Phosphorescence characteristics for anhydrous $EuCl_3$ in 7 different DESs and H_2O at λ_{ex} = 395 nm sorted by descending emission intensity of the strongest emission peak at around 616 nm.

Solvent	λ_{em} [nm]	Luminescence intensity [a.u.]	Transition
DMU/citric acid monohydrate	591	12	$^5D_0 \rightarrow {}^7F_1$
	616	55	$^5D_0 \rightarrow {}^7F_2$
	697	8	$^5D_0 \rightarrow {}^7F_4$
ChCl/citric acid monohydrate	592	7	$^5D_0 \rightarrow {}^7F_1$
	616	28	$^5D_0 \rightarrow {}^7F_2$
	694	4	$^5D_0 \rightarrow {}^7F_4$
ChCl/oxalic acid dihydrate	593	6	$^5D_0 \rightarrow {}^7F_1$
	616	27	$^5D_0 \rightarrow {}^7F_2$
	694	3	$^5D_0 \rightarrow {}^7F_4$
ChCl/DL-lactic acid (~10% water)	592	8	$^5D_0 \rightarrow {}^7F_1$
	615	24	$^5D_0 \rightarrow {}^7F_2$
	693	4	$^5D_0 \rightarrow {}^7F_4$
ChCl/phenylacetic acid	592	4	$^5D_0 \rightarrow {}^7F_1$
	616	19	$^5D_0 \rightarrow {}^7F_2$
	696	2	$^5D_0 \rightarrow {}^7F_4$

water	591	4	$^5D_0 \rightarrow {}^7F_1$
	616	4	$^5D_0 \rightarrow {}^7F_2$
	695	2	$^5D_0 \rightarrow {}^7F_4$
ChCl/itaconic acid	592	1	$^5D_0 \rightarrow {}^7F_1$
	611	3	$^5D_0 \rightarrow {}^7F_2$
ChCl/levulinic acid	592	1	$^5D_0 \rightarrow {}^7F_1$
	613	3	$^5D_0 \rightarrow {}^7F_2$

Table 18. Phosphorescence characteristics for $EuCl_3 \cdot 6\ H_2O$ in 10 different DESs, H_2O, MeOH, and EtOH at λ_{ex} = 395 nm; sorted by descending emission intensity of the strongest emission peak at around 616 nm.

Solvent	**λ_{em} [nm]**	**Luminescence intensity [a.u.]**	**Transition**
ChBt/oxalic acid dihydrate	592	17	$^5D_0 \rightarrow {}^7F_1$
	616	103	$^5D_0 \rightarrow {}^7F_2$
	691	5	$^5D_0 \rightarrow {}^7F_4$
DMU/citric acid monohydrate	592	12	$^5D_0 \rightarrow {}^7F_1$
	614	53	$^5D_0 \rightarrow {}^7F_2$
	699	7	$^5D_0 \rightarrow {}^7F_4$
ChCl/DL-mandelic acid	592	10	$^5D_0 \rightarrow {}^7F_1$
	616	38	$^5D_0 \rightarrow {}^7F_2$
	695	4	$^5D_0 \rightarrow {}^7F_4$
ChCl/DL-lactic acid (~10% water)	591	12	$^5D_0 \rightarrow {}^7F_1$
	616	33	$^5D_0 \rightarrow {}^7F_2$
	696	3	$^5D_0 \rightarrow {}^7F_4$
ChCl/oxalic acid dihydrate	591	9	$^5D_0 \rightarrow {}^7F_1$
	617	31	$^5D_0 \rightarrow {}^7F_2$
	695	3	$^5D_0 \rightarrow {}^7F_4$
ChCl/xylitol	593	9	$^5D_0 \rightarrow {}^7F_1$
	616	30	$^5D_0 \rightarrow {}^7F_2$
	693	2	$^5D_0 \rightarrow {}^7F_4$
ChCl/urea	591	12	$^5D_0 \rightarrow {}^7F_1$
	614	27	$^5D_0 \rightarrow {}^7F_2$
	700	9	$^5D_0 \rightarrow {}^7F_4$
MeOH	592	8	$^5D_0 \rightarrow {}^7F_1$
	616	19	$^5D_0 \rightarrow {}^7F_2$
	697	5	$^5D_0 \rightarrow {}^7F_4$
ChCl/phenylacetic acid	590	3	$^5D_0 \rightarrow {}^7F_1$
	616	18	$^5D_0 \rightarrow {}^7F_2$
	696	1	$^5D_0 \rightarrow {}^7F_4$
DMU/citric acid	594	4	$^5D_0 \rightarrow {}^7F_1$
	615	16	$^5D_0 \rightarrow {}^7F_2$
	700	2	$^5D_0 \rightarrow {}^7F_4$
EtOH	594	6	$^5D_0 \rightarrow {}^7F_1$
	615	15	$^5D_0 \rightarrow {}^7F_2$
	699	3	$^5D_0 \rightarrow {}^7F_4$

water	592	5	$^5D_0 \rightarrow {}^7F_1$
	615	2	$^5D_0 \rightarrow {}^7F_2$
	693	2	$^5D_0 \rightarrow {}^7F_4$
ChCl/levulinic acid	595	1	$^5D_0 \rightarrow {}^7F_1$
	614	3	$^5D_0 \rightarrow {}^7F_2$

Of the seven tested DESs with anhydrous $EuCl_3$, five showed significant higher luminescence intensity for Eu^{3+} than the reference medium water. For $EuCl_3$ hexahydrate, in seven out of ten DESs the emission of the trivalent lanthanide ion was considerably increased compared to water, ethanol, and methanol. The higher emission intensities for methanol and ethanol in comparison to water are owing to the distinct O–H oscillation of H_2O.

For both compounds, anhydrous $EuCl_3$ and $EuCl_3$ hexahydrate, it is conspicuous that especially DESs containing water result in a major increase in luminescence intensity compared to water-free DESs (*e.g.* DMU/citric acid monohydrate vs. DMU/citric acid). Further, there is little difference in the heights of the emission peaks for anhydrous $EuCl_3$ and its hexahydrate in the same DESs (*e.g.* ChCl/phenylacetic acid, DMU/citric acid monohydrate). In ChCl/oxalic acid dihydrate and ChCl/DL-lactic acid (~10% water), the luminescence intensity for $EuCl_3$ hexahydrate is actually stronger than for anhydrous $EuCl_3$. These findings are to some extend in contrast to our expectations and to related studies with ILs published in literature: In ILs, traces of water impair the luminescence of trivalent lanthanide ions as O–H vibrations lead to a rapid radiationless quenching.[51] Even the exposure of the samples to atmospheric moisture can result in a rapid decrease of the luminescence intensity to nearly zero for *e.g.* erbium(III) and neodymium(III).[11]

To gain further insight into the effect of water in DESs, Milli-Q water was subsequently added to 1.00 mM solutions of anhydrous $EuCl_3$ and $EuCl_3$ hexahydrate in water-free ChCl/levulinic acid. After each addition of 0.1 equivalent of water, the phosphorescence was measured and the resultant spectra interpreted. The plot of the emission intensity at 614 nm against the added water equivalents is depicted in Figure 25. The addition of up to one equivalent of water leads to an increase in luminescence intensity for anhydrous $EuCl_3$ in ChCl/levulinic acid. Above that amount, the emission intensity is slowly

decreasing. The luminescence of $EuCl_3$ hexahydrate in ChCl/levulinic acid is hardly affected by water addition up to one equivalent and also decreases after further addition. Throughout the series of experiments, the Eu^{3+} luminescence intensity of the hexahydrate is always higher than the luminescence of the anhydrous compound. This behavior indicates that DESs possess a higher stability towards water than ILs and that water may even have a supporting role towards luminescence in certain eutectic solvent systems. Further experiments will be necessary for a more conclusive statement.

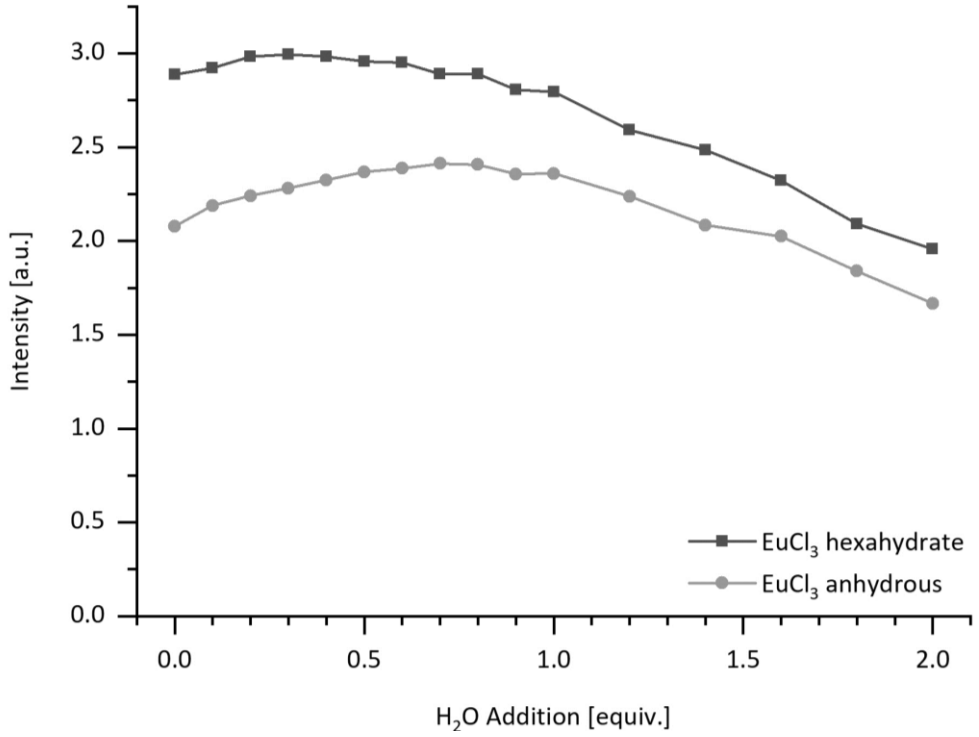

Figure 25. Phosphorescence emission intensity of $EuCl_3$ solutions at 614 nm (λ_{ex} = 395 nm) after subsequent addition of water.

In order to apply DESs for quantitation of lanthanide ions in fluorescence spectroscopy, a linear correlation between the fluorescence emission intensity I_F and the concentration c of the fluorophore in the DES is mandatory, according to the following approximation described by equation (2):

$$I_F \approx \Phi_F \cdot I_0 \cdot 2{,}303 \cdot \epsilon \cdot l \cdot c \qquad (2)$$

where Φ_F is the fluorescence quantum yield, I_0 is the intensity of the incident light, ϵ is the decadic molar extinction coefficient, and l is the length of the light path through the sample (for the mathematical description see Appendix 6.1). However, the decadic molar extinction coefficient ϵ and the fluorescence quantum yield Φ_F do not represent inherently constant parameters but are highly sensitive to their near environment and can vary *e.g.* with the solvent due to interactions between the analyte and the solvent molecules, or by formation of higher order aggregates in solution.[58, 59]

To evaluate the applicability of $EuCl_3$ in DESs for quantitation, a concentration series of $EuCl_3$ hexahydrate was exemplarily prepared with ChCl/xylitol and the concentration plotted against the phosphorescence intensity of the emission peaks at 529 and 615 nm (Figure 26).

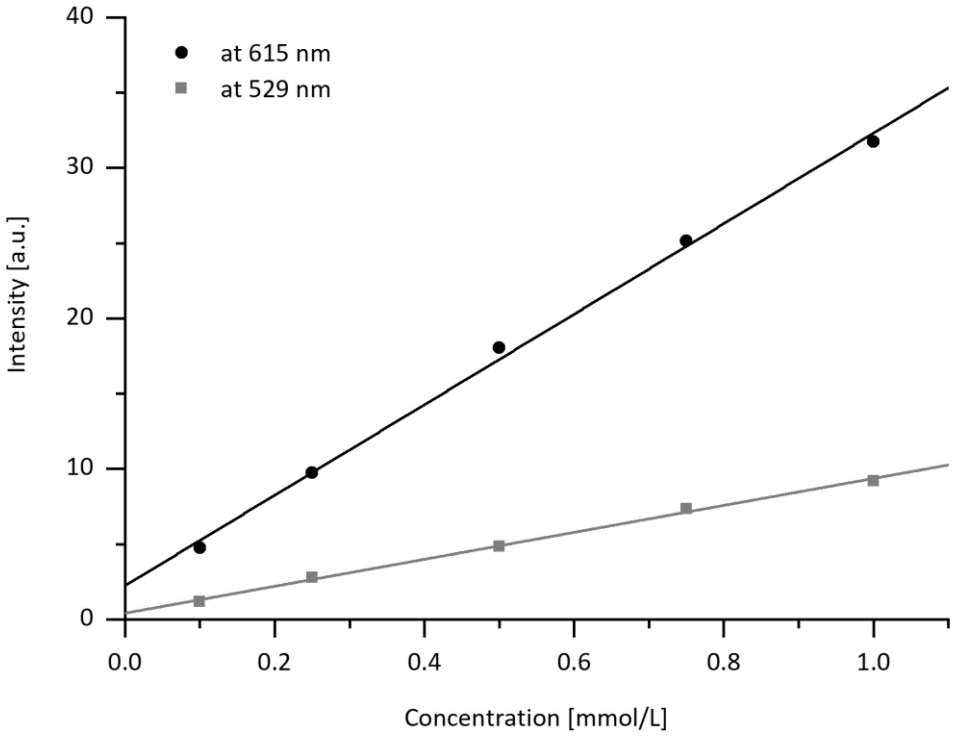

Figure 26. Phosphorescence emission intensity (λ_{ex} = 395 nm) of a concentration series of $EuCl_3$ hexahydrate in ChCl/xylitol and the linear fit of the emission peaks at 529 and 615 nm.

The graph shows linear correlation at both maxima verifying this specific solvent system for quantitation experiments of $EuCl_3$ and supporting the assumption of DESs being a promising solvent in quantitative analysis of trivalent lanthanide ions. However,

the correlation ought to be verified for each analyte–DES system separately prior to quantitation experiments ruling out possible interferences.

Further, luminescence is strongly influenced by the temperature and hence the viscosity of a medium as both parameters are closely connected to one another.[60, 61] Changes in temperature or the viscosity affect the number of quenching oscillations and collisions of an analyte in solution by defining the degrees of freedom for the system. Frequently, solutions of fluorophores are frozen with liquid nitrogen to improve the results by inhibiting these quenching effects.[62-64] In the processing temperature range of DESs between r.t. and 80 °C the viscosity can vary considerably – from about 15 to 13000 cP – as well as remain almost unchanged depending on the DES's composition.[61, 65] As a consequence, it is of high interest to gain insight into the luminescent behavior of trivalent lanthanide ions in DESs during a change in temperature. Figure 27 and Figure 28 show the phosphorescence dependency from the temperature of anhydrous $EuCl_3$ and its hexahydrate in DESs. Same results were obtained for cooling down from 20 to 80 °C and heating up from 20 to 80 °C. The curve progression with temperature is similar to that found in literature for other DESs and also for most ILs.[61, 65-69] Some DESs are highly affected by a change in temperature, *e.g.* ChCl/phenylacetic acid and ChCl/urea with an increase of up to 300% by cooling from 80 to 20 °C, whereas others are hardly influenced, *e.g.* ChCl/xylitol. Furthermore, it can be noticed that the temperature effect of ChCl/phenylacetic acid varies depending on the analyte; a stronger decrease in intensity is observed for $EuCl_3$ hexahydrate of up to 300% as opposed to anhydrous $EuCl_3$ of 200%. As the amount of water in the DESs may also have an influence of on the viscosity and therefore on the temperature dependency, experiments on the water content in context of viscosity may provide closer insight into the role of water in the eutectic solvents.

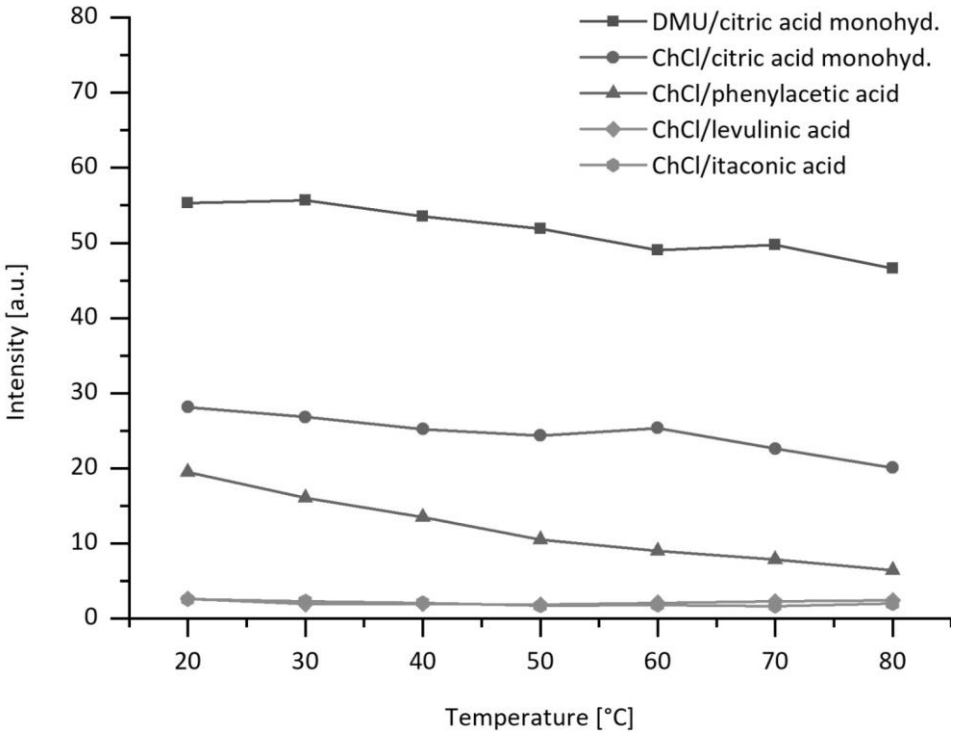

Figure 27. Phosphorescence emission intensity (λ_{ex} = 395 nm) of anhydrous $EuCl_3$ (1.00 mM) in 5 different DESs in the temperature range of 20–80 °C.

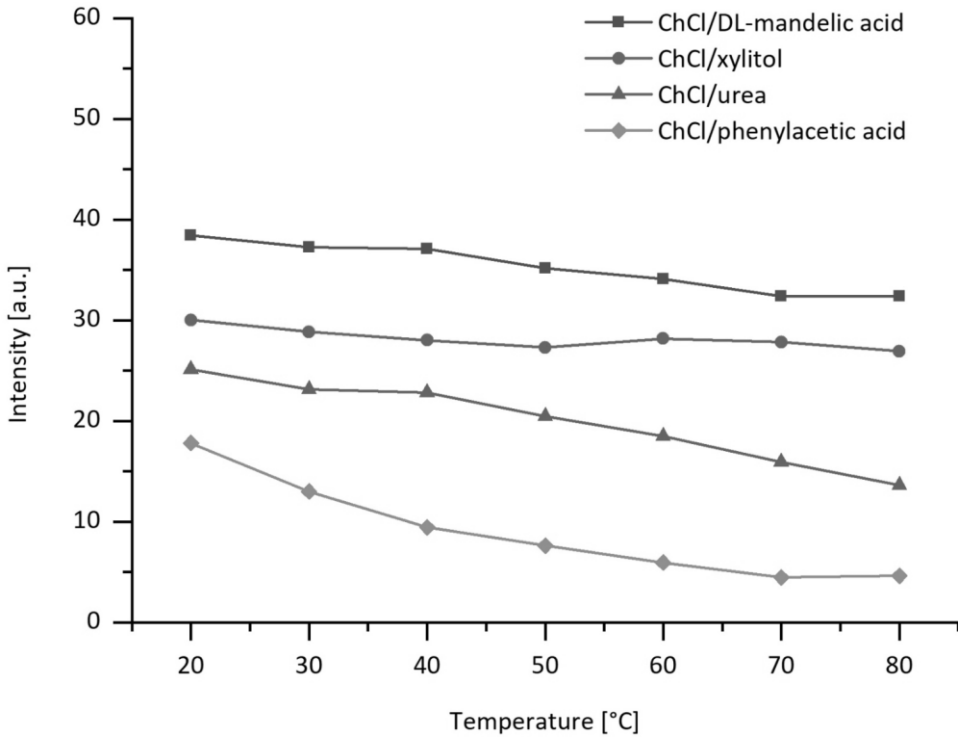

Figure 28. Phosphorescence emission spectra (λ_{ex} = 395 nm) of $EuCl_3 \cdot 6\ H_2O$ (1.00 mM) in 4 different DESs in the temperature range of 20–80 °C.

Spectroscopic studies were also performed for Eu_2O_3 in DESs as lanthanide oxides play an important role in the workup, processing and recovery of rare earth elements, and are hardly to non-soluble in most common solvents and mineral acids.[70, 71] However, lanthanide oxides possess a relatively high solubility in some DESs (see Chapter 3.2.2), even if the solvation process especially of oxides in DESs it is not fully understood yet.[72] For luminescence experiments, DESs were used that were able to dissolve a sufficient amount of Eu_2O_3. Under the same experimental conditions as $EuCl_3$, Eu_2O_3 in DESs shows the characteristic Eu^{3+} transitions from the $^5D_0$ level to the ^7F_J levels (J = 1, 2, 4) at about 592, 616, and 692 nm, while the electronic dipole transition $^5D_0 \rightarrow {}^7F_2$ is the strongest (Figure 29). In DMU/citric acid monohydrate, even the transition to the $^7F_3$ level around 652 nm was detectable (confer Figure 23 and Figure 24 for spectra of anhydrous $EuCl_3$ and $EuCl_3 \cdot 6\,H_2O$). The spectroscopic characteristics for the phosphorescence of Eu_2O_3 are listed in Table 19. Here again the DESs with complexed water results in the strongest luminescence.

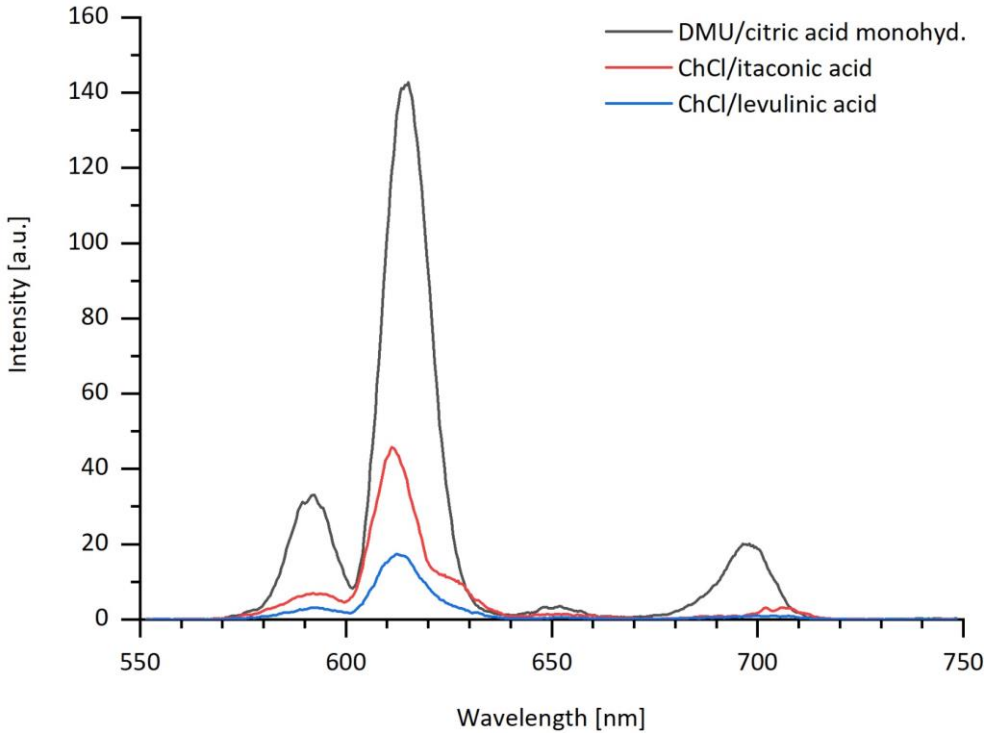

Figure 29. Phosphorescence emission spectra (λ_{ex} = 395 nm) of 1.00 mM solutions of Eu_2O_3 in 3 different DESs (legend sorted according to emission intensity for the $^5D_0 \rightarrow {}^7F_2$ transition at around 616 nm).

Table 19. Phosphorescence characteristics for anhydrous Eu_2O_3 in 3 different DESs at λ_{ex} = 395 nm sorted by descending emission intensity of the strongest emission peak at around 616 nm.

Solvent	λ_{em} [nm]	Luminescence intensity [a.u.]	Transition
DMU/citric acid monohydrate	592	33	$^5D_0 \rightarrow {}^7F_1$
	615	143	$^5D_0 \rightarrow {}^7F_2$
	652	3	$^5D_0 \rightarrow {}^7F_3$
	696	20	$^5D_0 \rightarrow {}^7F_4$
ChCl/itaconic acid	592	7	$^5D_0 \rightarrow {}^7F_1$
	611	46	$^5D_0 \rightarrow {}^7F_2$
	706	3	$^5D_0 \rightarrow {}^7F_4$
ChCl/levulinic acid	592	3	$^5D_0 \rightarrow {}^7F_1$
	612	17	$^5D_0 \rightarrow {}^7F_2$

It can be noted that the phosphorescence of Eu_2O_3 compared to $EuCl_3$ is much more intense in all three tested DESs – 2.6 times higher in DMU/citric acid monohydrate, 15.3 times higher in ChCl/itaconic acid, and 5.7 times higher in ChCl/levulinic acid. This can be explained by the counterion O^{2-}, which may prevent non-radiative energy transfer to a higher proportion than Cl^-.

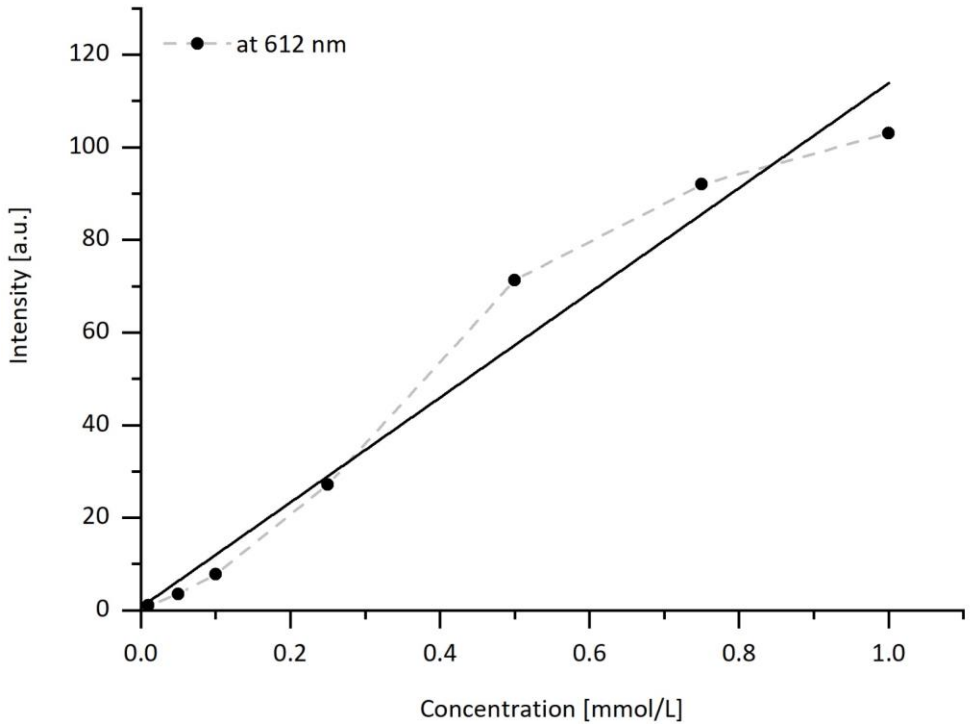

Figure 30. Phosphorescence emission intensity (λ_{ex} = 395 nm) of a concentration series of Eu_2O_3 in ChCl/levulinic acid and the linear fit of the emission peaks at 612 nm.

Further, the correlation between the phosphorescence intensity and the concentration of Eu_2O_3 in DESs was exemplarily assessed in ChCl/levulinic acid for a conceivable application in quantitative analysis. Figure 30 shows the comparison between the series of the measurements and the linear fit. The experiment was repeated three times with the same outcome: The single values differ significantly from the straight line pointing out that the system of Eu_2O_3 and ChCl/levulinic acid as solvent is not suitable for quantitation experiments.

Terbium(III)

The luminescence behavior of $TbCl_3 \cdot 6\ H_2O$ was studied in eleven different DESs (Figure 31). Characteristic phosphorescence was observed for the transitions around 490 ($^5D_4 \rightarrow {}^7F_6$), 544 ($^5D_4 \rightarrow {}^7F_5$), 584 ($^5D_4 \rightarrow {}^7F_4$), and 620 nm ($^5D_4 \rightarrow {}^7F_3$); the respective data are listed in Table 20.

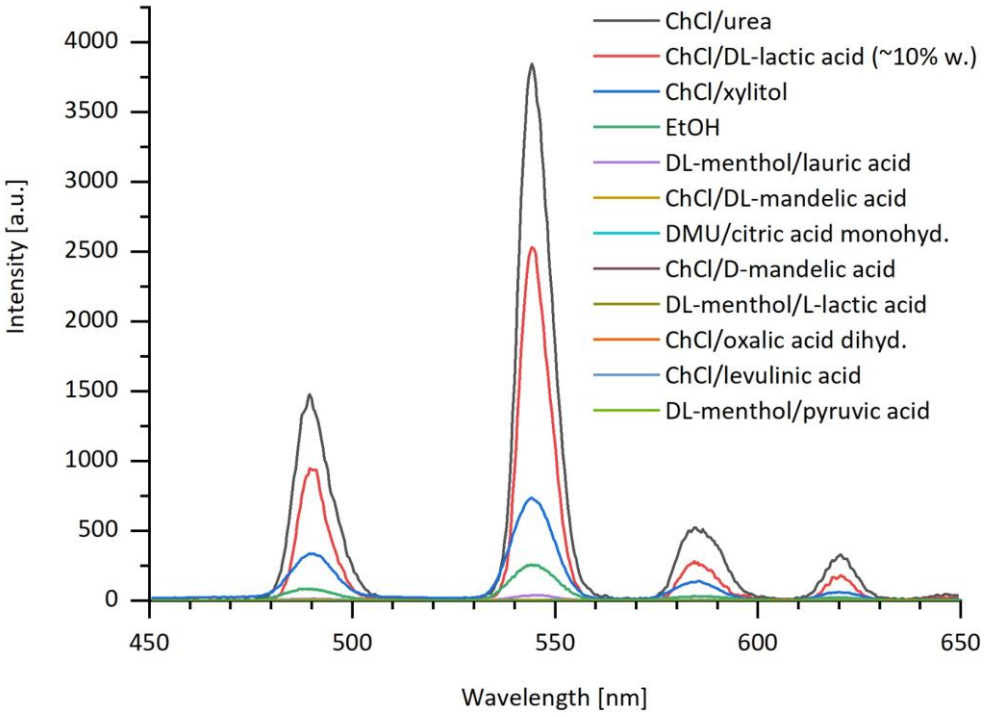

Figure 31. Phosphorescence emission spectra (λ_{ex} = 266 nm) of 1.00 mM solutions of $TbCl_3 \cdot 6\ H_2O$ in 11 different DESs and EtOH at r.t. (legend sorted according to emission intensity for the $^5D_0 \rightarrow {}^7F_2$ transition at around 616 nm).

Table 20. Phosphorescence emission characteristics for $TbCl_3 \cdot 6\ H_2O$ in 11 different DESs and EtOH at λ_{ex} = 266 nm; sorted by descending emission intensity of the strongest emission peak at around 544 nm.

Solvent	λ_{em} [nm]	Luminescence intensity [a.u.]	Transition
ChCl/urea	490	1478	$^5D_0 \rightarrow {}^7F_6$
	544	3844	$^5D_0 \rightarrow {}^7F_5$
	584	522	$^5D_0 \rightarrow {}^7F_4$
	620	328	$^5D_0 \rightarrow {}^7F_3$
ChCl/DL-lactic acid (~10% water)	490	946	$^5D_0 \rightarrow {}^7F_6$
	544	2530	$^5D_0 \rightarrow {}^7F_5$
	584	278	$^5D_0 \rightarrow {}^7F_4$
	620	179	$^5D_0 \rightarrow {}^7F_3$
ChCl/xylitol	490	337	$^5D_0 \rightarrow {}^7F_6$
	544	732	$^5D_0 \rightarrow {}^7F_5$
	586	140	$^5D_0 \rightarrow {}^7F_4$
	620	61	$^5D_0 \rightarrow {}^7F_3$
EtOH	488	83	$^5D_0 \rightarrow {}^7F_6$
	544	258	$^5D_0 \rightarrow {}^7F_5$
	584	32	$^5D_0 \rightarrow {}^7F_4$
	621	22	$^5D_0 \rightarrow {}^7F_3$
DL-menthol/lauric acid	490	13	$^5D_0 \rightarrow {}^7F_6$
	546	38	$^5D_0 \rightarrow {}^7F_5$
	588	6	$^5D_0 \rightarrow {}^7F_4$
	620	3	$^5D_0 \rightarrow {}^7F_3$
ChCl/DL-mandelic acid	488	2	$^5D_0 \rightarrow {}^7F_6$
	546	3	$^5D_0 \rightarrow {}^7F_5$
DMU/citric acid monohydrate	543	2	$^5D_0 \rightarrow {}^7F_5$
ChCl/D-mandelic acid	---	---	---
DL-menthol/L-lactic acid	---	---	---
ChCl/oxalic acid dihydrate	---	---	---
ChCl/levulinic acid	---	---	---
DL-menthol/pyruvic acid	---	---	---

Three of the eleven tested DESs (*i.e.* ChCl/urea, ChCl/DL-lactic acid (~10% water), ChCl/xylitol) lead to a major increase in the phosphorescence emission intensity of Tb^{3+} compared to ethanol as detection medium. However, these three DESs gave only moderate results for Eu^{3+} and the DESs most suitable for Eu^{3+} (*e.g.* DMU/citric acid monohydrate, ChCl/DL-mandelic acid, ChCl/oxalic acid dihydrate) yielded merely in mediocre luminescence or even complete quenching for Tb^{3+}. It is notable that the DES ChCl/DL-lactic acid containing 10% water lead also to an effective medium for

phosphorescence measurement of Tb^{3+}, which is supporting the assumption that some DESs are stable towards water regarding luminescence.

Further Trivalent Lanthanides (Sm^{3+}, Dy^{3+})

Spectroscopic studies were also performed for the trivalent lanthanide chlorides of samarium and dysprosium. For $SmCl_3 \cdot 6\ H_2O$ and $DyCl_3 \cdot 6\ H_2O$, no phosphorescence emission could be observed and unfortunately, the fluorescence measurements for Sm^{3+} and Dy^{3+} revealed that the light diffusion in the DESs is very high so that an evaluation of the fluorescence emission spectra of the lanthanide ions was not possible (see Figure A.3, Figure A.4, and Figure A.5 in Appendix 6.4). Similar results are reported in literature for Sm^{3+} and Dy^{3+} doped ionic liquid crystals.[73] In fact, NADES are similar to liquid crystals in which all molecules are arranged through hydrogen bonding and other physical intermolecular binding forces.[74]

3.2.2 Solubility and Separation Experiments of Trivalent Lanthanide Oxides in DESs

In Chapter 1, we already illustrated that the kinetics of an extraction varies with the composition of a DES as well as the composition of the sample to be separated.[55] This means that the individual solubilities of a sample's components in DESs can only be taken as an orientation for the choice of a suitable DES as extraction medium. For each separation problem, the applicability of a DES as an extractant has to be assessed separately and an individual optimization is necessary to reach the desired efficiency and selectivity. Therefore, the following solubility experiments on trivalent lanthanide oxides in DESs represent merely a rough estimation in order to narrow down potential DESs for subsequent investigations on the separation process. It should be noted that the solvation process of oxides in DESs is not fully understood yet and may also be attributed to high dispersion. However, the terms "soluble" and "dissolved" are used in the following.

The lanthanide oxides for the qualitative solubility study were limited to selected representatives for the so-called light (La–Gd) and heavy (Tb–Lu, Y) rare earth elements – abbreviated LREE and HREE – with focus on the LREE.[75-80] The qualitative solubility of the selected compounds in water and some mineral acids is listed in Table 21.

Table 21. Selected trivalent lanthanide oxides Ln_2O_3 (Ln = La, Nd, Sm, Eu, Gd, Tb, Dy) and their qualitative solubility (sol. = soluble, n.s. = not soluble) of about 0.05 wt% in water, diluted and undiluted nitric acid, and aqua regia (nitric acid and hydrochloric acid in a molar ratio of 1:3). The lanthanide oxides are divided into light rare earth elements (LREE) and heavy rare earth elements (HREE).

Qualitative solubility		**LREE**					**HREE**	
Entry	**Solvent**	**La_2O_3**	**Nd_2O_3**	**Sm_2O_3**	**Eu_2O_3**	**Gd_2O_3**	**Tb_2O_3**	**Dy_2O_3**
1	H_2O	n.s.	n.s.	n.s.	n.s.	n.s.	n.s.	n.s.
2	5% HNO_3	**sol.**	**sol.**	**sol.**	**sol.**	**sol.**	n.s.	n.s.
3	65% HNO_3	**sol.**	**sol.**	**sol.**	**sol.**	**sol.**	n.s.	n.s.
4	aqua regia	**sol.**	**sol.**	**sol.**	**sol.**	**sol.**	**sol.**	**sol.**

Abbreviations: sol. = soluble, n.s. = not soluble.

Table 21 shows that the two classes LREE and HREE can already be separated from one another using conventional acids. However, these acids provide a restricted capability of separation within a category as either the complete class is soluble or none of a group.

In preliminary experiments an approximate amount of 0.05 wt% of the respective sesquioxide Ln_2O_3 (Ln = La, Nd, Sm, Eu, Gd, Tb, Dy) was added to the DESs listed in Table 22 and stirred for 24 h at the processing temperature from Table 15. We compared the appearance of the sample right after the addition with the end of the stirring time. If a clear melt was obtained, the lanthanide oxide was assumed to be soluble in the DES; if the DES stayed turbid, the lanthanide oxide was stated as not soluble. The results are summarized in Table 22. If an entry is empty, the experiment was not performed for this combination of lanthanide oxide and DES.

Table 22. Estimated qualitative solubility of trivalent lanthanide oxides Ln_2O_3 (Ln = La, Nd, Sm, Eu, Gd, Tb, Dy) in DESs. DESs that are used for following experiments are highlighted with a grey background.

Qualitative solubility		**LREE**					**HREE**	
Entry	**DES**	**La_2O_3**	**Nd_2O_3**	**Sm_2O_3**	**Eu_2O_3**	**Gd_2O_3**	**Tb_2O_3**	**Dy_2O_3**
1	ChCl/ oxalic acid dihydrate	-	n.s.	n.s.	n.s.	-	n.s.	n.s.
2	ChCl/ DL-lactic acid (~10% water)	-	-	n.s.	n.s.	-	-	-
3	ChCl/ L-lactic acid	n.s.	**sol.**	n.s.	n.s.	n.s.	n.s.	n.s.
4	ChCl/ levulinic acid	**sol.**	**sol.**	**sol.**	**sol.**	**sol.**	n.s.	n.s.
5	ChCl/ citric acid monohydrate	**sol.**	**sol.**	**sol.**	n.s.	n.s.	n.s.	n.s.
6	ChCl/ itaconic acid	**sol.**	**sol.**	**sol.**	**sol.**	**sol.**	n.s.	n.s.
7	ChCl/ phenylacetic acid	n.s.	n.s.	n.s.	n.s.	n.s.	n.s.	n.s.
8	ChCl/ DL-mandelic acid	-	n.s.	n.s.	n.s.	-	n.s.	-
9	ChCl/ D-mandelic acid	**sol.**	**sol.**	n.s.	n.s.	n.s.	n.s.	n.s.
10	ChCl/xylitol	-	n.s.	n.s.	n.s.	-	n.s.	n.s.
11	ChCl/urea	-	n.s.	n.s.	n.s.	-	n.s.	n.s.
12	ChCl/vanillin	-	n.s.	n.s.	-	-	-	n.s.
13	ChBt/ oxalic acid dihydrate	-	n.s.	n.s.	-	-	-	n.s.
14	DL-menthol/ pyruvic acid	n.s.	n.s.	n.s.	n.s.	n.s.	n.s.	n.s.
15	DL-menthol/ L-lactic acid	-	-	-	n.s.	-	n.s.	n.s.
16	DL-menthol/ lauric acid	-	n.s.	n.s.	n.s.	-	n.s.	n.s.
17	DMU/ citric acid monohydrate	**sol.**	**sol.**	**sol.**	**sol.**	**sol.**	n.s.	n.s.

Abbreviations: sol. = soluble, n.s. = not soluble, - = not tested.

None of the HREE was soluble in the DESs, but for the tested LREE several DESs were able of dissolving the sesquioxides (*i.e.* ChCl/L-lactic acid, ChCl/levulinic acid, ChCl/citric acid monohydrate, ChCl/itaconic acid, ChCl/D-mandelic acid, DMU/citric acid monohydrate). Some tendencies can already be concluded from these experiments: Only a part of the LREE were soluble in ChCl/citric acid monohydrate or ChCl/D-mandelic acid, and in ChCl/L-lactic acid only Nd_2O_3 could be dissolved. In general, DESs containing carboxylic acids such as citric acid or lactic acid combined with ChCl or DMU as melt components proved to be potent media for dissolving light lanthanide oxides. These results are in accordance with our previous findings published in *Green Chemistry*.[55]

In a further series of experiments, the solubility of the LREE was investigated more closely in the six DESs that were able to dissolve these compounds. The approximate maximum solubility as mass fraction ω_{max} of lanthanide oxide in the DES was determined by subsequent addition of the respective oxide to the DES. The results from Table 22 for sesquioxides that were not soluble in any of these DESs (*i.e.* ω_{max} less than 0.05 wt%) were included in the overview in Table 23. Figure 32 shows exemplarily the appearance of the samples during the quantitative experiments for Nd_2O_3. The slightly yellowish color of samples a) and c) derives from the DES itself.

Table 23. Approximated quantitative solubility as maximum mass fraction ω_{max} of trivalent lanthanide oxide Ln_2O_3 (Ln = La, Nd, Sm, Eu, Gd, Tb, Dy) in DESs.

Quantitative solubility ω_{max} **[wt%]** [a]		LREE					HREE	
Entry	**DES**	**La_2O_3**	**Nd_2O_3**	**Sm_2O_3**	**Eu_2O_3**	**Gd_2O_3**	**Tb_2O_3**	**Dy_2O_3**
1	ChCl/ L-lactic acid	<0.05	0.39	<0.05	<0.05	<0.05	<0.05	<0.05
2	ChCl/ levulinic acid	0.78	3.26	>0.62 [b]	>5.74 [b]	0.51	<0.05	<0.05
3	ChCl/ citric acid monohydrate	0.10	0.10	0.11	<0.05	<0.05	<0.05	<0.05
4	ChCl/ itaconic acid	0.37	0.81	>0.51 [b]	>1.19 [b]	0.24	<0.05	<0.05
5	ChCl/ D-mandelic acid	0.38	0.59	<0.05	<0.05	<0.05	<0.05	<0.05

6	DMU/ citric acid monohydrate	0.29	1.37	0.18	>3.69 [b]	0.53	<0.05	<0.05

(*a*) Amount of Ln_2O_3 before a saturation was reached by further addition. Time of dissolution were 24 h. (*b*) Saturation was not yet reached for these Ln_2O_3.

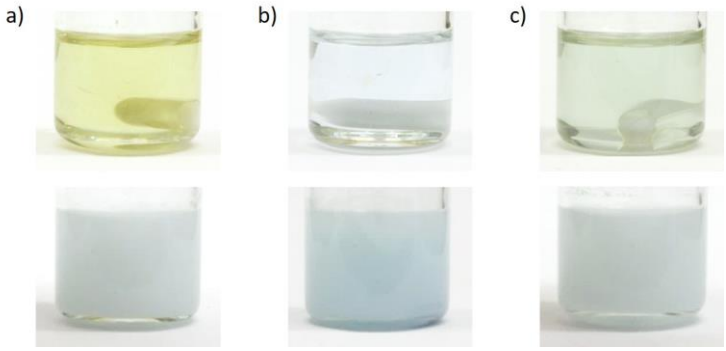

Figure 32. Samples of Nd_2O_3 in a) DMU/citric acid monohydrate, b) ChCl/L-lactic acid, c) ChCl/D-mandelic acid (*from left to right*) in comparison right after the addition of the sesquioxide to the DES (*bottom row*) and afterwards when dissolved (*top row*).

The DESs are able to dissolve more than 5 wt% of Eu_2O_3 and also up to 3.26 wt% of Nd_2O_3. Furthermore, the solubility in a DES differs between some LREE by an order of magnitude (*e.g.* in ChCl/levulinic acid and DMU/citric acid monohydrate). These results provide the selectivity that is essential for separation procedures and suggest that separation of LREE may be feasible with DESs.

In the next step, the solid–liquid separation of LREE was investigated with the six DESs from Table 23 using a mixture of the sesquioxides Ln_2O_3 (Ln = La, Nd, Sm, Eu, Gd) in a molar ratio of 1:1:1:1:1. The intention is to find out, which DES leads to an accumulation or depletion of which LREE and to what extent. The experiments were performed according to the following processes: 1.5 wt% of the LREE mixture was added to each DES, stirred for 2 h at 80 °C, and filtered by a hot filtration apparatus. All obtained filtrates were analyzed *via* ICP-OES for their resulting molar ratio of lanthanides (Figure 33).

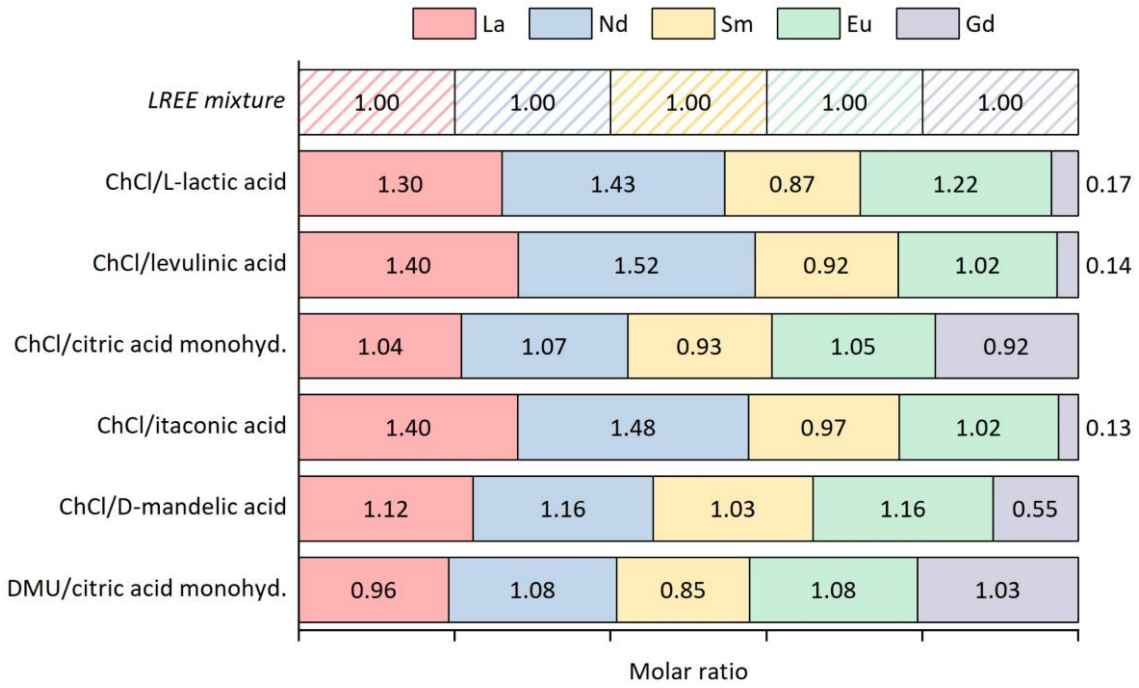

Figure 33. Molar ratio of lanthanides La, Nd, Sm, Eu, and Gd in the filtrate of the separation process compared to the starting material, namely the LREE mixture.

An accumulation of neodymium(III) to 1.5 equiv. and at the same time depletion of gadolinium(III) down to 0.1 equiv. took place in the DESs ChCl/levulinic acid and ChCl/itaconic acid. In ChCl/L-lactic acid, an accumulation of europium(III) up to 1.4 equiv. occurred additionally. There was hardly any change in the molar ratio in ChCl/citric acid monohydrate and DMU/citric acid monohydrate. These results correspond only in part with the tendencies from the solubility experiments in Table 23.

Even if an accumulation or depletion of some lanthanides was achieved by treatment with DES, an optimization of the separation process is still necessary. This may be accomplished by either additional trials using further DESs or adjustments on the process itself (*e.g.* stirring time, processing temperature, hot filtration, supplementary separation steps).

3.3 Conclusion

In conclusion, we verified the use of DESs as potent media for luminescence measurements of europium(III) and terbium(III) chlorides. The luminescence intensity significantly increased in the DESs as polar and weakly coordinating solvent compared to water, methanol or ethanol. The emission intensity in DESs shows linear correlation to the concentration of the lanthanide chlorides, but unfortunately not for the tested oxide. It was demonstrated, that the luminescence of the trivalent lanthanide ion is relatively stable in some DESs towards external influences as change in temperature or water contend. Addition of water even enhanced the emission intensity in ChCl/levulinic acid in contrast to ILs, where traces of water can result in rapid emission quenching. Future studies regarding the viscosity may provide closer insight into the role of water in the DESs and the impact on the luminescence of trivalent lanthanide ions. Degassing of the samples prior to the measurements may be used to improve the results on the phosphorescence of samarium(III) and dysprosium(III) as dissolved oxygen can lead to luminescence quenching.[47, 57]

Further, we have shown that DESs effectively dissolve light lanthanide sesquioxides. The considerably different solubilities in the DESs may be used for solid–liquid separation of light rare earth elements. However, further optimization is required to establish a practical separation process.

3.4 Experimental

3.4.1 General Procedures and Materials

***Chemicals*.** All chemicals were of analytical reagent grade and used as received without further purification except for choline chloride [$HOC_2H_4N(CH_3)_3^+Cl^-$ or ChCl], which was dried at 130 °C *in vacuo* and stored under nitrogen prior to use. The lanthanide salts and oxides were of at least 99.9% trace metal basis. All organic solvents used were purified by standard methods.

***Sample preparation*.** The deep eutectic solvents were formed by mixing the two components in the respective molar ratio in a glass vial. The mixtures were heated up to

50, 80, or 100 °C (according to information in Table 15) in an aluminum heating block until a homogeneous, colorless liquid was obtained. The lanthanide salts or oxides were dissolved by adding them to the DES at the processing temperature in the respective concentration or amount and further stirring until the DES had a clear appearance. If water was added to a DES–lanthanide mixture, deionized water was used (Milli-Q water, Millipore deionization system, ω = 18.3 MΩ cm^{-1}).

3.4.2 Spectroscopic Methods for Luminescence Studies

***Phosphorescence measurements*.** Phosphorescence emission spectra were recorded on a Varian Cary Eclipse fluorescence spectrophotometer with temperature control using 10 mm Hellma fluorescence quartz cuvettes. If not stated otherwise, then the spectra were taken at r.t. For experiments regarding the temperature dependence, the samples were tempered for 20 min. The same results were obtained for cooling the samples from 80 to 20 °C and for heating from 20 to 80 °C. Settings for Eu^{3+}: total decay time 0.020 s, delay time 0.1 ms, gate time 5.0 ms, slit 10 nm. Settings for Tb^{3+}: total decay time 0.001 s, delay time 0.1 ms, gate time 5.0 ms, slit 10 nm.

***Fluorescence measurements*.** Fluorescence emission spectra were performed at r.t. on a Horiba Fluoromax4 spectrophotometer using 10 mm Hellma fluorescence quartz cuvettes.

3.4.3 Procedures and Analytical Methods for Solubility and Separation Experiments

Solubility experiments. For qualitative experiments, approximately 0.05 wt% of a lanthanide compound were added to the respective solvent and the appearance evaluated after stirring for 24 h at the processing temperature for DESs according to the information in Table 15 or at r.t. for water and mineral acids. For quantitative experiments, the lanthanide sesquioxide was added gradually to the DES in defined proportions of 0.05 wt%. The mixture was stirred at the processing temperature from Table 15 for 24 h before further addition of the next proportion until saturation was reached. The amount before saturation was taken as approximated quantitative solubility ω_{max} of a lanthanide oxide.

Separation process. 1.5 wt% of the LREE mixture (Ln_2O_3 of Ln = La, Nd, Sm, Eu, and Gd in a molar ratio of 1:1:1:1:1) was added to a DES and stirred for 2 h at 80 °C. The suspension was filtered through a hot filtration apparatus at 80 °C. The hot filtration apparatus consists of an adapted extruder (LiposoFastBasic) by Avestin and a heating block with control panel. The original PTFE-blocks (polytetrafluoroethylene) of the extruder were exchanged with PEEK-blocks (polyetheretherketone). The outlet was widened up to 1.60 mm and adjusted to 1 mL Hamilton Gastight syringes with Luer-Lock and shortened HSW ECO cannulas (1.60 × 3.00 mm) from Henke-Sass, Wolf GmbH. No. 41 Whatman filter paper used with a pore size of 20–25 μm and a filter net by Avestin used as pre-filter.

ICP-OES measurements. The concentration of the lanthanides in DESs was determined using a SpectroFlame-EOP, FSMEA85C S/N 4G/0002 by SPECTRO Analytical Instruments of solutions with diluted nitric acid (5%).

3.5 References

[1] F. T. Fitch and D. S. Russell, *The separation of the rare earths by ion-exchange procedures*, **1951**.

[2] H. Sicius, *Seltenerdmetalle: Lanthanoide und dritte Nebengruppe: Eine Reise durch das Periodensystem*, Springer Fachmedien, Wiesbaden, **2015**.

[3] K. Binnemans, P. T. Jones, B. Blanpain, T. Van Gerven, Y. Yang, A. Walton and M. Buchert, *J. Clean. Prod.*, **2013**, *51*, 1-22.

[4] A. F. Hollemann and N. Wiberg, *Lehrbuch der Anorganischen Chemie*, Walter de Gruyter & Co., Berlin, 102 edn., **2007**.

[5] S. A. Ansari, D. R. Prabhu, R. B. Gujar, A. S. Kanekar, B. Rajeswari, M. J. Kulkarni, M. S. Murali, Y. Babu, V. Natarajan, S. Rajeswari, A. Suresh, R. Manivannan, M. P. Antony, T. G. Srinivasan and V. K. Manchanda, *Sep. Purif. Technol.*, **2009**, *66*, 118-124.

[6] T. Takeuchi, Y. Kabasawa and T. Tanimura, *J. Chromatog. A*, **1991**, *538*, 125-131.

[7] A. Nilchi, M. Edalat, M. Taghiof and S. Rasouli Garmarodi, *Anal. Chem.*, **2012**, *67*, 378-385.

[8] P. Janoš, *Electrophoresis*, **2003**, *24*, 1982-1992.

[9] M. Reza Pourjavid, P. Norouzi, H. Rashedi and M. Reza Ganjali, *Separation and direct detection of heavy lanthanides using new ion-exchange chromatography: Fast Fourier transform continuous cyclic voltammetry system*, **2010**.

[10] L. W. McKeen, *Chemistry*, **1970**, *43*, 28-31.

[11] K. Binnemans, *Chem. Rev.*, **2007**, *107*, 2592-2614.

[12] S. Shuvaev, V. Utochnikova, Ł. Marciniak, A. Freidzon, I. Sinev, R. Van Deun, R. O. Freire, Y. Zubavichus, W. Grünert and N. Kuzmina, *Dalton Trans.*, **2014**, *43*, 3121-3136.

[13] J.-C. G. Bünzli and C. Piguet, *Chem. Soc. Rev.*, **2005**, *34*, 1048-1077.

[14] A. Ugale, T. N. Kalyani and S. J. Dhoble, in *Lanthanide-Based Multifunctional Materials*, eds. P. Martín-Ramos and M. Ramos Silva, Elsevier, **2018**, 59-97.

[15] J. H. S. K. Monteiro and A. de Bettencourt-Dias, in *Lanthanide-Based Multifunctional Materials*, eds. P. Martín-Ramos and M. Ramos Silva, Elsevier, **2018**, 99-131.

[16] K. Jinnai, R. Kabe and C. Adachi, *Chem. Commun.*, **2017**, *53*, 5457-5460.

[17] J. Xue, Q. Liang, Y. Zhang, R. Zhang, L. Duan and J. Qiao, *Adv. Funct. Mater.*, **2017**, *27*, 1703283.

[18] G. Yu, F. Ding, H. Wei, Z. Zhao, Z. Liu, Z. Bian, L. Xiao and C. Huang, *J. Mater. Chem. C*, **2016**, *4*, 121-125.

[19] R. C. Evans, P. Douglas and C. J. Winscom, *Coord. Chem. Rev.*, **2006**, *250*, 2093-2126.

[20] M. Vermillac, J.-F. Lupi, H. Fneich, J. Turlier, M. Cabié, C. Kucera, D. Borschneck, F. Peters, S. Chaussedent, P. Vennéguès, D. R. Neuville, A. Mehdi, J. Ballato and W. Blanc, *Thalium-doped nanoparticles and their properties in silica-based optical fibers*, SPIE, **2018**.

[21] J. Li, H. Ebendorff-Heidepriem, B. C. Gibson, A. D. Greentree, M. R. Hutchinson, P. Jia, R. Kostecki, G. Liu, A. Orth, M. Ploschner, E. P. Schartner, S. C. Warren-Smith, K. Zhang, G. Tsiminis and E. M. Goldys, *APL Photonics*, **2018**, *3*, 100902.

[22] P. Miluski, M. Kochanowicz, J. Zmojda, T. Ragin and D. Dorosz, *Opt. Mater.*, **2018**.

[23] J. Ballato, H. Ebendorff-Heidepriem, J. Zhao, L. Petit and J. Troles, *Fibers*, **2017**, *5*, 11.

[24] E. P. Schartner, G. Tsiminis, A. François, R. Kostecki, S. C. Warren-Smith, L. V. Nguyen, S. Heng, T. Reynolds, E. Klantsataya, K. J. Rowland, A. D. Abell, H. Ebendorff-Heidepriem and T. M. Monro, *Int. J. Appl. Glass Sci.*, **2015**, *6*, 229-239.

[25] D. Prodius, V. Mereacre, P. Singh, Y. Lan, S. Mameri, D. D. Johnson, W. Wernsdorfer, C. E. Anson and A. K. Powell, *J. Mater. Chem. C*, **2018**, *6*, 2862-2872.

[26] A. Dey, P. Kalita and V. Chandrasekhar, *ACS Omega*, **2018**, *3*, 9462-9475.

[27] C. A. P. Goodwin, F. Ortu, D. Reta, N. F. Chilton and D. P. Mills, *Nature (London, U. K.)*, **2017**, *548*, 439-442.

[28] K. S. Pederson, D. N. Woodruff, J. Bendix and R. Clerac, *Experimental aspects of lanthanide single-molecule magnet physics*, Wiley-VCH Verlag GmbH & Co. KGaA, **2015**.

[29] R. A. Layfield, *Organometallics*, **2014**, *33*, 1084-1099.

[30] W. You, D. Tu, W. Zheng, X. Shang, X. Song, S. Zhou, Y. Liu, R. Li and X. Chen, *Nanoscale*, **2018**, *10*, 11477-11484.

[31] S. A. Diaz, G. Lasarte-Aragones, R. G. Lowery, Aniket, J. N. Vranish, W. P. Klein, K. Susumu and I. L. Medintz, *ACS Appl. Nano Mater.*, **2018**, *1*, 3006-3014.

[32] E. M. Surender, S. J. Bradberry, S. A. Bright, C. P. McCoy, D. C. Williams and T. Gunnlaugsson, *J. Am. Chem. Soc.*, **2017**, *139*, 381-388.

[33] P. Huang, D. Tu, W. Zheng, S. Zhou, Z. Chen and X. Chen, *Sci. China Mater.*, **2015**, *58*, 156-177.

[34] S. Zhou, W. Zheng, Z. Chen, D. Tu, Y. Liu, E. Ma, R. Li, H. Zhu, M. Huang and X. Chen, *Angew. Chem., Int. Ed.*, **2014**, *53*, 12498-12502.

[35] M. V. DaCosta, S. Doughan, Y. Han and U. J. Krull, *Anal. Chim. Acta*, **2014**, *832*, 1-33.

[36] A. J. Talib, M. Alkahtani, L. Jiang, F. Alghannam, R. Brick, C. L. Gomes, M. O. Scully, A. V. Sokolov and P. R. Hemmer, *Opt. Mater. Express*, **2018**, *8*, 3277-3287.

[37] C. Cruje, D. W. Holdsworth, E. R. Gillies and M. Drangova, *High-concentration gadolinium nanoparticles for pre-clinical vascular imaging*, SPIE, **2018**.

[38] J.-C. G. Bünzli, *J. Lumin.*, **2016**, *170*, 866-878.

[39] J. He, C. S. Bonnet, S. V. Eliseeva, S. Lacerda, T. Chauvin, P. Retailleau, F. Szeremeta, B. Badet, S. Petoud, É. Tóth and P. Durand, *J. Am. Chem. Soc.*, **2016**, *138*, 2913-2916.

[40] D. Yang, C. Li and J. Lin, *Nanomedicine*, **2015**, *10*, 2573-2591.

[41] Y. I. Park, K. T. Lee, Y. D. Suh and T. Hyeon, *Chem. Soc. Rev.*, **2015**, *44*, 1302-1317.

[42] T. Kimura, R. Nagaishi, Y. Kato and Z. Yoshida, *J. Alloys Compd.*, **2001**, *323–324*, 164-168.

[43] T. Kimura and Y. Kato, *J. Alloys Compd.*, **1998**, *278*, 92-97.

[44] L. Whitty-Léveillé, K. Turgeon, C. Bazin and D. Larivière, *Anal. Chim. Acta*, **2017**, *961*, 33-41.

[45] F. Ardini, F. Soggia, F. Rugi, R. Udisti and M. Grotti, *Anal. Chim. Acta*, **2010**, *678*, 18-25.

[46] S. Riaño, M. Petranikova, B. Onghena, T. Vander Hoogerstraete, D. Banerjee, M. R. S. Foreman, C. Ekberg and K. Binnemans, *RSC Adv.*, **2017**, *7*, 32100-32113.

[47] I. Billard, S. Mekki, C. Gaillard, P. Hesemann, G. Moutiers, C. Mariet, A. Labet and J.-Claude G. Bünzli, *Eur. J. Inorg. Chem.*, **2004**, 1190-1197.

[48] K. Driesen, P. Nockemann and K. Binnemans, *Chem. Phys. Lett.*, **2004**, *395*, 306-310.

[49] L. Zheng, L.-L. Yang, N.-N. Xing, Y. Pan, H.-X. Ji, J. Wei and W. Guan, *RSC Advances*, **2017**, *7*, 35814-35818.

[50] K. Lunstroot, K. Driesen, P. Nockemann, K. Hecke, L. Meervelt, C. C. Görller-Walrand Gorllerwalrand, K. Binnemans, S. Bellayer, L. Viau, J. Le Bideau and A. Vioux, *Lanthanide-doped luminescent ionogels*, *Dalton Trans.*, **2009**, 298-306.

[51] A.-V. Mudring, A. Babai, S. Arenz, R. Giernoth, K. Binnemans, K. Driesen and P. Nockemann, *J. Alloys Compd.*, **2006**, *418*, 204-208.

[52] S. A. Ansari, P. K. Mohapatra, A. Leoncini, J. Huskens and W. Verboom, *Dalton Trans.*, **2017**, *46*, 11355-11362.

[53] A.-V. Mudring and S. Tang, *Eur. J. Inorg. Chem.*, **2010**, 2569-2581.

[54] B. J. Mincher and J. F. Wishart, *Solvent Extr. Ion Exch.*, **2014**, *32*, 563-583.

[55] A. Söldner, J. Zach and B. König, *Green Chem.*, **2019**, *21*, 321-328.

[56] C. Ruß and B. König, *Green Chem.*, **2012**, *14*, 2969-2982.

[57] K. Binnemans, *Coord. Chem. Rev.*, **2015**, *295*, 1-45.

[58] M. Sauer, J. Hofkens and J. Enderlein, *Handbook of Fluorescence Spectroscopy and Imaging: From Single Molecules to Ensembles*, Wiley-VCH, Weinheim, **2011**.

[59] P. Atkins and J. de Paula, *Physical Chemistry*, W. H. Freeman and Company, New York, NY, 8th edn., **2006**.

[60] C. V. Raman, *Nature*, **1923**, *111*, 532-533.

[61] F. S. Mjalli and J. Naser, *Asia-Pac. J. Chem. Eng.*, **2015**, *10*, 273-281.

[62] G. von Foerster, *J. Chem. Phys.*, **1964**, *40*, 2059-2060.

[63] K. Tokumasu, M. Harada and T. Okada, *Langmuir*, **2016**, *32*, 527-533.

[64] A. Stepanov, S. Nikitina and E. Preobrazhenskaya, *Sov. Radiochem.(Engl. Transl.)*, **1985**, *26*.

[65] A. Popescu, C. Donath and V. Constantin, *Density, viscosity and electrical conductivity of three choline chloride based ionic liquids*, **2014**.

[66] A. P. Abbott, D. Boothby, G. Capper, D. L. Davies and R. K. Rasheed, *J. Am. Chem. Soc.*, **2004**, *126*, 9142-9147.

[67] O. Ciocirlan, O. Iulian and O. Croitoru, *Effect of Temperature on the Physico-chemical Properties of Three Ionic Liquids Containing Choline Chloride*, **2010**.

[68] A. P. Abbott, G. Capper, D. L. Davies, R. K. Rasheed and V. Tambyrajah, *Chem. Commun.*, **2003**, 70-71.

[69] J. G. Huddleston, A. E. Visser, W. M. Reichert, H. D. Willauer, G. A. Broker and R. D. Rogers, *Green Chem.*, **2001**, *3*, 156-164.

[70] N. Swain and S. Mishra, *J. Clean. Prod.*, **2019**, *220*, 884-898.

[71] S. Sinha, D. Abhilash, P. Meshram and B. Pandey, *Metallurgical processes for the recovery and recycling of lanthanum from various resources—A review*, **2015**.

[72] J. M. Hartley, C.-M. Ip, G. C. H. Forrest, K. Singh, S. J. Gurman, K. S. Ryder, A. P. Abbott and G. Frisch, *Inorg. Chem.*, **2014**, *53*, 6280-6288.

[73] A. Getsis and A.-V. Mudring, *Z. Anorg. Allg. Chem.*, **2010**, *636*, 1726-1734.

[74] Y. Dai, J. van Spronsen, G.-J. Witkamp, R. Verpoorte and Y. H. Choi, *Anal. Chim. Acta*, **2013**, *766*, 61-68.

[75] *There can be found some inconsistency in literature for the classification of the rare earth elements. In some books and articles, they are subdivided into light and heavy rare earth elements, whereas in others, a group of middle rare earth elements is recognized. The attribution of the elements differs depending on the chemical or physical properties that are considered. Although light, yttrium is typically included with the heavy rare earth elements due to its very similar chemical behavior.*

[76] D. A. Atwood, *The Rare Earth Elements: Fundamentals and Applications*, Wiley, Wests Sussex, **2013**.

[77] B. Zhou, Z. Li and C. Chen, *Global Potential of Rare Earth Resources and Rare Earth Demand from Clean Technologies*, **2017**.

[78] S. M. Jowitt, *Criticality of the Rare Earth Elements: Current and Future Sources and Recycling*, MDPI AG, Basel, **2018**.

[79] N. Haque, A. Hughes, S. Lim and C. Vernon, *Resources*, **2014**, *3*, 614-635.

[80] N. Sui, K. Huang, C. Zhang, N. Wang, F. Wang and H. Liu, *Ind. Eng. Chem. Res.*, **2013**, *52*, 5997-6008.

SUMMARY

4 Summary

This thesis presents novel approaches and applications for deep eutectic solvents (DESs) based on readily available, renewable, and inexpensive compounds as extraction, reaction and detection media for inorganic compounds.

Chapter 1 focuses on the selective extraction of metal salts and oxides, specifically phosphates, from incinerated sewage sludge ash (ISSA) using DESs that are based on natural products. The solubility behavior of the main components of ISSA as well as several metal salts and metal oxides in DESs is investigated and an empirical basis for possible applications is provided. The solubility can partly be correlated with the approximated pH value of the DESs: the tested phosphates and metal chlorides dissolve preferably in DESs containing urea or *N,N'*-dimethyl urea (DMU), which offer neutral to slightly basic conditions; in general, metal oxides enrich in DESs with carboxylic acids at strongly acidic pH value; and acetates dissolve best in DESs based on choline chloride (ChCl). From these findings, DESs were tested as environmentally friendly extraction media for phosphorus from ISSA. The first results show the feasibility of the approach, which may lead to a low-energy process. With the DES of DMU/mannose, an accumulation of phosphorus up to 31% was achieved, emphasizing the capability of biodegradable DESs as extraction media.

In **Chapter 2**, DESs are introduced that are able to dissolve metal oxides and are used as reaction media to synthesize spinel-type ferrite nanoparticles MFe_2O_4 (M = Mg, Zn, Co, Ni). By employing DESs, the reactions towards phase-pure spinel ferrites proceed at much lower temperatures than usual for the respective solid-state reaction of the metal oxides and at the same temperatures as a synthesis with comparable calcination processes using metal salts. Best results for spinel-type ferrite nanoparticles were obtained with the DES consisting of ChCl/maleic acid. The method therefore reduces the overall required energy for the nanoparticle synthesis. The analysis of the cation distribution, particle size, band gap, and morphology showed that the properties of the gained nanoparticles are comparable to particles obtained by other methods, which illustrates the potential of DESs for the processing of metal oxides.

Chapter 3 presents DESs as promising solvents for light rare earth elements (LREE) in solid–liquid separation on one hand and potent media for luminescence measurements of trivalent lanthanide ions in quantitative analysis on the other hand. The spectroscopic characteristics of lanthanide chlorides $LnCl_3$ (Ln = Eu, Tb), respectively their aquo complexes, are described in a comprehensive study that demonstrates the significant enhancement of the phosphorescence emission intensity in DESs as polar and weakly coordinating solvent. Several DESs proved to be a stable environment for luminescent lanthanide ions towards external influences such as changes in temperature and moisture, which gives them an advantage over ionic liquids. It was found that water may even have a supporting role in certain eutectic systems that leads to a further increase in phosphorescence emission. By investigating the solubility of lanthanide sesquioxides Ln_2O_3 (Ln = La, Nd, Sm, Eu, Gd, Tb, Dy) in DESs, selectivities were identified that provide the basis for subsequent development of a separation process for LREE.

ZUSAMMENFASSUNG

5 Zusammenfassung

Diese Arbeit behandelt neuartige Konzepte und Anwendungsmöglichkeiten von tiefeutektischen Lösungsmitteln (DESs) als Extraktions-, Reaktions- und Messmedium für anorganische Verbindungen.

Kapitel 1 beschäftigt sich mit der selektiven Extraktion von Metallsalzen und -oxiden mithilfe von DESs, beispielhaft gezeigt für Phosphate aus Klärschlammasche. Es wurden sowohl Lösungsverhalten der Hauptbestandteile von Klärschlammasche als auch anderer Metallsalze und Metalloxide untersucht und damit eine Grundlage für mögliche Anwendungen geschaffen. Es konnte festgestellt werden, dass zum Teil ein Zusammenhang zwischen der Löslichkeit der Verbindungen in DESs und dem abgeschätzten pH-Wert besteht: Die getesteten Phosphate und Metallchloride lösen sich bevorzugt in DESs, die Harnstoff oder *N*,*N*'-Dimethylharnstoff (DMU) enthalten und somit ein neutrales bis leicht basisches Milieu bieten; Metalloxide lassen sich generell eher in DESs mit Carbonsäuren und einem stark sauren pH anreichern; das Lösen von Acetaten hingegen wird durch Cholinchlorid-haltige DES begünstigt. Ausgehend von diesen Erkenntnissen wurden DESs in der Verwendung als umweltfreundliche Extraktionsmittel für Klärschlammasche erprobt. Erste Ergebnisse zeigen die Machbarkeit des Ansatzes, der zu einem Verfahren mit ausgesprochen niedrigem Energieverbrauch führen kann. Mit dem DES bestehend aus DMU und Mannose konnte eine Phosphatanreicherung um 31% erreicht werden, was die Leistungsfähigkeit von biologisch abbaubaren DESs als Extraktionsmedium belegt.

In **Kapitel 2** werden DESs genutzt, um Metalloxide zu lösen und mithilfe dieser Suspensionen nanopartikuläre Eisenspinelle (auch bekannt als Ferrite) mit der allgemeinen Formel MFe_2O_4 (M = Mg, Zn, Co, Ni) zu synthetisieren. Durch die Verwendung von DESs erfolgt die Reaktion bei wesentlich niedrigeren Temperaturen als bei der entsprechende Festphasenreaktion der Metalloxide und bei gleichen Temperaturen, wie bei einer vergleichbaren Kalzinierung von Metallsalzen. Die besten Ergebnisse bei der Herstellung von phasenreinen Eisenspinellen wurden mit dem DES aus Cholinchlorid und Maleinsäure erzielt. Somit kann mit der entwickelten Methode die insgesamt benötigte

Energie für die Nanopartikelsynthese reduziert werden. Bei der Analyse von Kationenverteilung, Partikelgröße, Bandlücke und Morphologie der Eisenspinelle konnte zudem gezeigt werden, dass die Eigenschaften der synthetisierten Partikel mit denen, die durch andere Verfahren hergestellt wurden, vergleichbar sind. Zusammenfassend wird das Potenzial von DESs als innovatives Reaktionsmedium für anorganische Verbindungen mit der vorgestellten Methode veranschaulicht.

Kapitel 3 beschreibt DESs als vielversprechendes Lösungsmittel sowohl für Lumineszenzmessungen von dreiwertigen Lanthanoiden in der quantitativen Analyse als auch für die Fest-Flüssig-Trennung von leichten Seltenerdmetallen (LREE). Die spektroskopischen Eigenschaften von Lanthanoidchloriden $LnCl_3$ (Ln = Eu, Tb) bzw. ihrer Aquokomplexe wurden in einer umfangreichen Studie untersucht. Es konnte dargelegt werden, dass es in diesem polaren und schwach koordinierenden Lösemittel zu einer signifikanten Steigerung der Phosphoreszenzintensität kommt. Einige DESs erwiesen sich zudem als stabiles Medium für lumineszente Lanthanoidionen gegenüber äußeren Einflüssen, wie beispielsweise Temperaturänderungen oder Feuchtigkeit, was einen Vorteil gegenüber ionischen Flüssigkeiten darstellt. Die Ergebnisse lassen vermuten, dass Wasser eine unterstützende Funktion im eutektischen System haben kann, die zu einem weiteren Anstieg der Phosphoreszenzemission führt. Anhand von Löslichkeitsversuchen der Lanthanoidsesquioxiden Ln_2O_3 (Ln = La, Nd, Sm, Eu, Gd, Tb, Dy) in DESs, konnten Selektivitäten identifiziert werden, die für die Entwicklung eines Separationsverfahrens für LREE genutzt werden können.

APPENDIX

6 Appendix

6.1 References for Renewable DES Compounds

Table A.1. References for used DES compounds that can be extracted or produces from plants.

Compound	Reference
tartaric acid, malic acid	M. Palma, C. G. Barroso, *Anal. Chim. Acta* **2002**, *458*, 119-130.
citric acid	F. H. Verhoff, H. Bauweleers, *Citric Acid. Ullmann's Encyclopedia of Industrial Chemistry*, Wiley-VCH, 2014.
malonic acid	J. Chlopicka, J. Dobrowolska-Iwanek, M. Wozniakiewicz, P. Zagrodzki, *Food Analytical Methods* **2014**, *7*, 1323-1327.
oxalic acid	H. Werner, A. Waehling, K. Kabrodt, NIG Nahrungs-Ingenieurtechnik G.m.b.H., Germany; Prof. Hellriegel Institut e.V. **1999**, p. 8 pp.
xylitol	H. Jain, S. Mulay, *International Journal of Food Sciences and Nutrition* **2014**, *65*, 135-143.
D-sorbitol	H. H. Strain, *J. Am. Chem. Soc.* **1934**, *56*, 1756-1759.
D-fructose	T. Becker, D. Breithaupt, *Biotechnology. Ullmann's Encyclopedia of Industrial Chemistry*, Wiley-VCH, **2011**.
D-glucose	P. J. Fellows, *Food Processing Technology*, Woodhead Publishing, **2016**.
mannose	X. Hu, Y. Shi, P. Zhang, M. Miao, T. Zhang, B. Jiang, *Comprehensive Reviews in Food Science and Food Safety* **2016**, *15*, 773-785.
galactose	Z. M. Senu, M. Husin, A. R. Li, R. Samsuddin, M. R. Ahmad, N. R. Nik Abd Rashid, N. Z. Mohd Taza, Springer Singapore, Singapore, **2015**, pp. 123-130.
choline	H. Müller, *Fette, Seifen, Anstrichmittel* **1977**, *79*, 259-261.

6.2 Degree of Inversion of the Prepared $MgFe_2O_4$ Nanoparticles

The distribution of the metal cations occupying the octahedral (O) and tetrahedral voids (T) of the cubic closely packed crystal structure of spinel type ferrites, and hence the degree of inversion, is defined as followed:

$$[Mg_{1-\lambda}Fe_{\lambda}]^{T}[Mg_{\lambda}Fe_{2-\lambda}]^{O}O_4$$

with $\lambda = 0$: normal and $\lambda = 1$: inverse. The recorded X-ray diffraction pattern for $MgFe_2O_4$ nanoparticles prepared at 600 °C *via* the DES-method were compared with the best matching pattern from the Inorganic Crystal Structure Database – ICSD (ICSD CODE 152470, Table 1).[1, 2] The degree of inversion λ was estimated to $\lambda \approx 0.76$ based on the

refined lattice parameter *a* = 8.388(3) Å by using the Software WinX^{POW} from STOE & Cie GmbH,[3] giving the formula

$$[Mg_{0.24}Fe_{0.76}]^{T}[Mg_{0.76}Fe_{1.24}]^{O}O_4$$

Table A.2. Structural data of $MgFe_2O_4$ from ICSD CODE 152470, *a* = 8.390(1) Å.

Atom		Wyckoff	*x*	*y*	*z*	Occupation
Mg1	Mg^{2+}	8*a*	0.125	0.125	0.125	0.30(1)
Fe1	Fe^{3+}	8*a*	0.125	0.125	0.125	0.70(1)
Mg2	Mg^{2+}	16*d*	0.5	0.5	0.5	0.350(5)
Fe2	Fe^{3+}	16*d*	0.5	0.5	0.5	0.650(5)
O1	O^{2-}	32*e*	0.254(1)	0.254(1)	0.254(1)	1

In order to get an additional insight into the degree of inversion of the prepared $MgFe_2O_4$ nanoparticles an inverse and a normal spinel type structure were simulated, and the X-ray diffraction patterns were calculated.

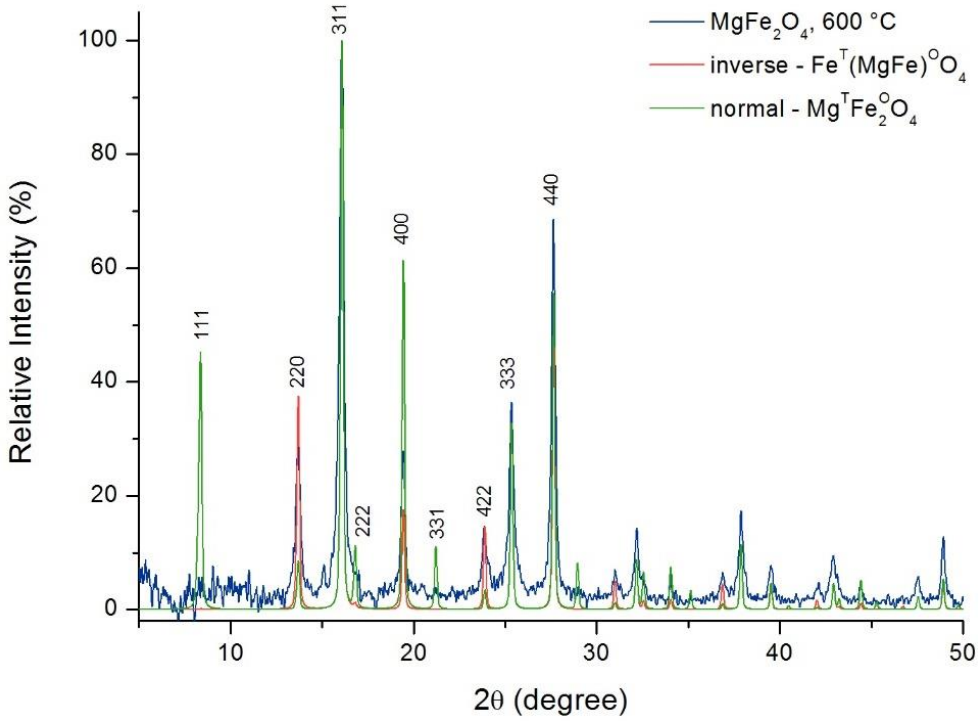

Figure A.1. Comparison of recorded X-ray powder diffraction pattern of $MgFe_2O_4$ prepared at 600 °C *via* the DES method (blue) and the simulated X-ray powder diffraction patterns of normal (λ = 0, green) and inverse (λ = 1, red) spinel type ferrites.

The comparison of the intensities of the reflections 111, 220, 400, 331, and 422 shows that the recorded data fits best for the pattern of a mostly inverse spinel type ferrite, with a = 8.388(3) Å (Table A.2). The slightly smaller lattice parameter also indicates a higher degree of inversion according to [1].

[1] FIZ Karlsruhe, Inorganic Crystal Structure Database (ICSD), https://icsd.fiz-karlsruhe.de/search/index.xhtml (accessed 01.07.2016).

[2] M. Gateshki, V. Petkov, S. K. Pradhan and T. Vogt, *J. Appl. Crystallogr.*, **2005**, *38*, 772-779.

[3] Stoe & Cie GmbH, WinX^{POW}, Version 3, Darmstadt, **2014**.

6.3 Concentration Dependence of the Fluorescence Intensity

The following description explains the mathematical derivation of the correlation between fluorescence intensity and the concentration of a fluorophore.[1-4]

The radiant intensity I and number of photons N are proportional to each other and are linked by the variables energy E, time t, and area A:

$$I = \frac{E}{t \cdot A} = \frac{N}{t \cdot A} h\nu = \frac{N}{t \cdot A} \frac{hc}{\lambda} \tag{A.1}$$

where h is the Planck's constant, ν is the frequency, c is the speed of light in vacuum, and λ is the wavelength.

The fluorescence quantum yield Φ_F is the ratio of the emitted intensity I_F to the absorbed intensity I_A :

$$\Phi_F = \frac{I_F}{I_A} \tag{A.2}$$

As the absorbed intensity I_A is the difference between the intensities in front I_0 and behind I the cuvette, the following can be derived for the emitted intensity I_F:

$$I_F = \Phi_F \cdot I_A = \Phi_F \cdot (I_0 - I) \tag{A.3}$$

According to the Lambert-Beer law, the concentration c of the fluorophore, the length l of the light path through the sample, and the decadic molar extinction coefficient ϵ are related to the absorbance A:

$$A = log\frac{I_0}{I} = \epsilon \cdot l \cdot c \quad \Rightarrow \quad I = I_0 \cdot 10^{-\epsilon lc} \tag{A.4}$$

When I is inserted into equation A.3, the fluorescence intensity can be expressed as:

$$I_F = \Phi_F \cdot (I_0 - I_0 \cdot 10^{-\epsilon lc}) = \Phi_F \cdot I_0 \cdot (1 - 10^{-\epsilon lc}) \tag{A.5}$$

This shows that the intensity of the fluorescence emission I_F does not correlate linearly with the concentration c of the fluorescent analyte, but exponentially. The equation can be rearranged and the term ϵlc replaced by the absorbance A, resulting in the normalized description:

$$\frac{I_F}{\Phi_F \cdot I_A} = 1 - 10^{-A} \tag{A.6}$$

According to the *Taylor series* T_∞, a function $f(x)$ can be represented by an infinite sum of terms at the point a:

$$T_\infty f(x;a) = \sum_{n=0}^{\infty} \frac{f^{(n)}(a)}{n!}(x-a)^n \tag{A.7}$$

where $f^{(n)}$ denotes the n-th derivative of f and $n!$ denotes the factorial of n. The derivative of order zero $f^{(0)}$ is defined to be f itself, and $(x-a)^0$ and $0!$ are both defined to be 1.

It is possible to create a linear approximation for the function in the specific point $a = 0$ by development of only the first two terms of the series $(n = 0, 1)$, called *Maclaurin series*:

$$T_1 f(x;a) = f(a) + f'(a)(x-a) \tag{A.8}$$

Applying the Maclaurin series to the normalized function of the absorbance A:

$$f(A) = 1 - 10^{-A} \tag{A.9}$$

$$\Longrightarrow T_1 f(A; A_0) = f(A_0) + f'(A_0)(A - A_0)$$

and calculation of the first derivative of f with respect to A at $A_0 = 0$ and $f(A_0) = 0$:

$$f'(A) = \frac{d}{dA}(1 - 10^{-A}) = (-1) \cdot \ln(10) \cdot 10^{-A} \cdot (-1) = \ln(10) \cdot 10^{-A}$$

$$\Longrightarrow f'(A_0) = \ln(10) \cdot 10^{-0} = \ln(10)$$

results in the following linear approximation:

$$T_1 f(A; A_0) = 0 + \ln(10) \cdot (A - 0) = \ln(10) \cdot A \tag{A.10}$$

$$\Longrightarrow I_F \approx \Phi_F \cdot I_0 \cdot 2{,}303 \cdot \epsilon \cdot l \cdot c \tag{A.11}$$

The plot of equations A.9 and A.10 is depicted in Figure A.2.

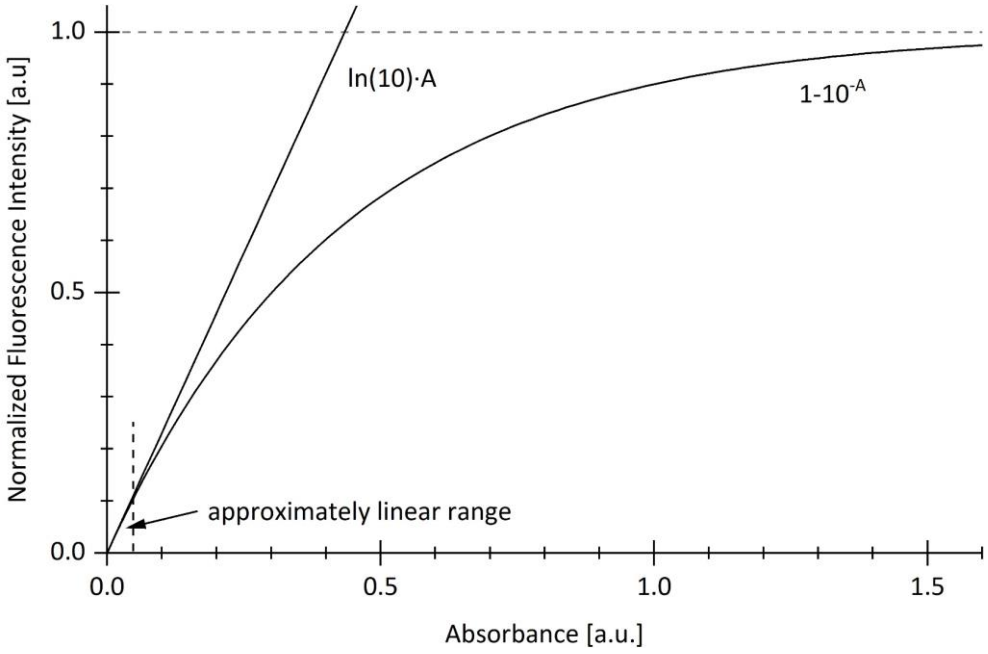

Figure A.2. Normalized fluorescence intensity as function of the absorbance A compared to the approximated linear function.

One can see that the linear approximation complies with the actual function for low absorbance values. Consequently, the emitted fluorescence intensity I_F is proportional to the concentration c of the fluorophore, if the following conditions are fulfilled:

1. The fluorescence quantum yield Φ_F is constant (ensured at constant excitation wavelength but mostly dependent on the solvent).
2. The intensity of the excitation light I_0 is constant (usually automatically ensured due to the reference channel of the spectrometer).
3. The decadic molar extinction coefficient ϵ is constant (ensured at constant excitation wavelength, pH, and temperature but mostly dependent on the solvent).
4. The length l of the light path through the sample is constant (ensured by usage of the same cuvettes).
5. The absorbance $A = \epsilon \cdot l \cdot c$ of the diluted sample is ≤ 0.05 (confer Figure A.2).

[1] P. Atkins and J. de Paula, *Physical Chemistry*, W. H. Freeman and Company, New York, NY, 8th edn., **2006**.

[2] M. Sauer, J. Hofkens and J. Enderlein, *Handbook of Fluorescence Spectroscopy and Imaging: From Single Molecules to Ensembles*, Wiley-VCH, Weinheim, **2011**.

[3] J. Lakowicz, *Principles of Fluorescence Spectroscopy*, Springer, Baltimore, MD, **2010**.

[4] T. Biskup, PCG-Fluoreszenz, https://www.radicals.uni-freiburg.de/de/ak/mitarbeiterinnen/biskup/pcg-fluoreszenz, (accessed 10.03.2019).

6.4 Fluorescence Spectra of Samarium(III) and Dysprosium(III) Chlorides in DESs

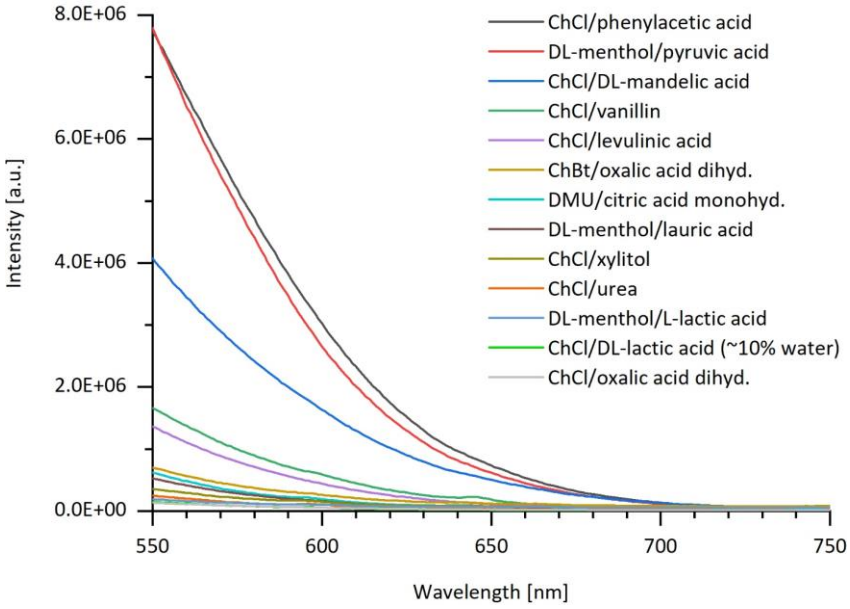

Figure A.3. Fluorescence emission spectra (λ_{ex} = 404 nm) of 1.00 mM solutions of $SmCl_3 \cdot 6\ H_2O$ in 13 different DESs at r.t. (legend sorted according to intensity).

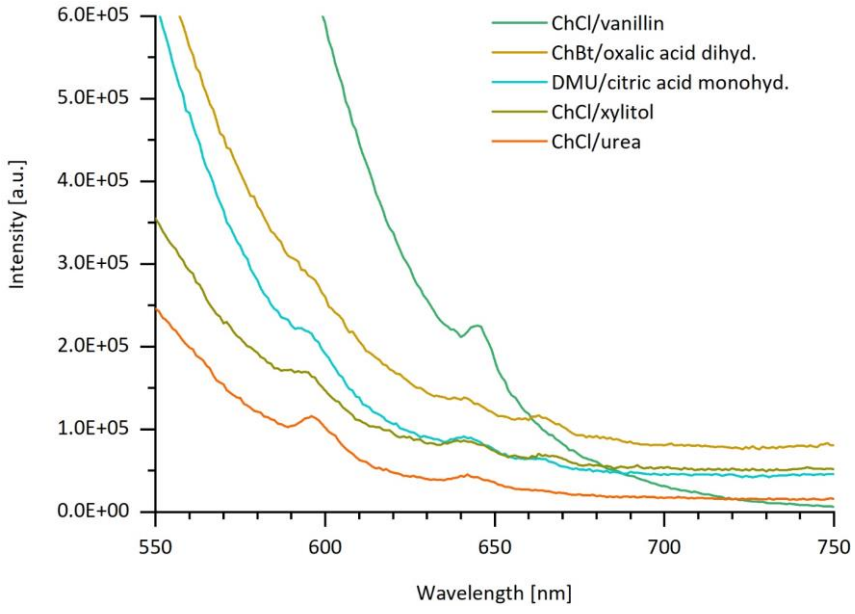

Figure A.4. Section of Figure A.3 of $SmCl_3 \cdot 6\ H_2O$ (1.00 mM) in the DESs in which fluorescence peaks of Sm^{3+} were observed (legend sorted according to intensity). Fluorescence emission peaks of Sm^{3+} were observed for at around 595 ($^4G_{5/2} \rightarrow {}^6H_{7/2}$) and 642 nm ($^4G_{5/2} \rightarrow {}^6H_{9/2}$).

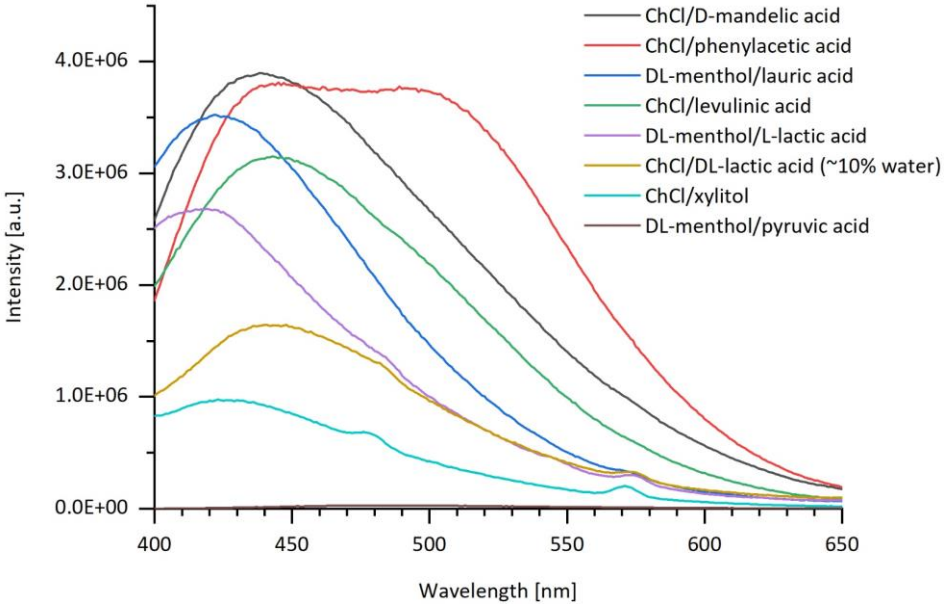

Figure A.5. Fluorescence emission spectra (λ_{ex} = 350 nm) of 1.00 mM solutions of $DyCl_3 \cdot 6\ H_2O$ in 8 different DESs at r.t. (legend sorted according to intensity). Fluorescence emission peaks of Dy^{3+} were observed for DL-menthol/L-lactic acid, ChCl/DL-lactic acid (~10% water), and ChCl/xylitol at around 481 ($^4F_{9/2} \rightarrow {}^6H_{15/2}$) and 573 nm ($^4F_{9/2} \rightarrow {}^6H_{13/2}$).

6.5 Abbreviations

°C	degrees Celsius
Å	Ångström (10^{-10} m)
a.u.	arbitrary unit
anhyd.	anhydrous
c	concentration
ChBt	choline bitartrate
ChCl	choline chloride
cm	centimeter
cP	centipoise
dec.	decomposition of the DES
DES	deep eutectic solvent
dihyd.	dihydrate
DMF	dimethylformamide
DMSO	dimethyl sulfoxide
DMU	*N,N'*-dimethyl urea
DRS	diffuse reflectance spectroscopy
DTGA	differential thermogravimetric analysis
ϵ	decadic molar extinction coefficient
e.g.	for example (*lat.* exempli gratia)
equiv.	equivalent
et al.	and others (*lat.* et alii)
EU	European Union
eV	electron volt
Φ_F	fluorescence quantum yield
g	gram
h	hour
HBA	hydrogen-bond acceptor
HBD	hydrogen-bond donor

hv	incident photon energy
HREE	heavy rare earth elements
i.e.	that is (*lat.* id est)
I_0	intensity of the incident light
ICP-MS	inductively coupled plasma mass spectrometry
ICP-OES	inductively coupled plasma optical emission spectroscopy
I_F	fluorescence emission intensity
IL	ionic liquid
IR	infrared
ISCD	inorganic crystal structure database
ISSA	incinerated sewage sludge ash
kg	kilogram
λ	wavelength
l	length
L	liter
λ_{em}	emission wavelength
λ_{ex}	excitation wavelength
LREE	light rare earth elements
M	molar (mol/L)
mg	milligram
min	minute
MIP-OES	microwave induced plasma optical emission spectroscopy
mL	milliliter
mM	millimolar (mmol/L)
mm	millimeter
mmol	millimole
monohyd.	monohydrate
MΩ	megaohm
n.a.	not available
n.q.	not quantifiable

n.s.	not soluble
nm	nanometer
ns	nanosecond
p.s.	partly soluble
PEEK	polyetheretherketone
ppm	parts per million
PTFE	polytetrafluoroethylene
r.t.	room temperature
R_∞	reflectance
s	second
SEM	scanning electron microscopy
sol.	soluble
T	temperature
TEM	transmission electron microscopy
TGA	thermogravimetric analysis
T_m	melting point
T_s	solidification point
UV	ultra violet
Vis	visible light
vs.	against (*lat.* versus)
wt%	weight percent
XRD	powder X-ray diffraction
µm	micrometer
ω_{max}	maximum of a soluble mass fraction / maximum solubility

DANKSAGUNG

7 Danksagung

Mein erster Dank gilt meinem Doktorvater Herrn Prof. Dr. Burkhard König, der es mir ermöglicht hat, meine Dissertation auf einem so vielseitigen, spannenden und zukunftsweisenden Thema anzufertigen, das mir sogar Auftritte in Politik und Fernsehen verschafft hat. Ich bedanke mich herzlich für seine Unterstützung während der gesamten Zeit, seine positive und motivierende Art und die mir gewährten Freiheiten.

Für die Übernahme des Zweitgutachtens, sowie die erfolgreiche Kooperation bei der Synthese von Eisenspinellen danke ich Prof. Dr. Arno Pfitzner. Vielen Dank an Prof. Dr. Frank-Michael Matysik und Prof. Dr. Alexander Breder, dass sie sich die Zeit genommen haben in meinem Prüfungsausschuss mitzuwirken.

Ich danke dem Bayerischen Staatsministerium für Umwelt und Verbraucherschutz für die Finanzierung meiner Promotion im Rahmen des Projektverbundes „ForCYCLE I – Rohstoffwende Bayern“ sowie den Betreuern des Projekts an der Universität Augsburg Prof. Dr. Armin Reller und Dr. Julia Fendt für die Organisation und die außergewöhnlichen Workshops und Events. Weiter danke ich Dr. Petra Hilgers für die angenehme Zusammenarbeit auf dem Projekt.

Mein Dank gilt besonders Dipl. Ing. Julia Zach für den motivierenden Austausch, die kreative Unterstützung in den unterschiedlichsten Bereichen und das Korrekturlesen meiner Arbeit.

Joachim Rewitzer danke ich für die zahlreichen Einsätze am ICP-OES. Bei Melanie Iwanow, Dr. Tobias Gärtner und Dr. Mark Schlosser möchte ich mich für die gute Kooperation sowie die SEM-Aufnahmen und XRD-Messungen bedanken.

Meinen Praktikanten Alexander Wimmer, Sebastian Graf, Norman Schramm, Dominik Oswald, Stephan Wensauer, Manuela Zobel, Dominik Wichner, Karsten Donabauer, Theresa Fischer, Johanna Schwarz, Fabian Teubl, Maria Haimerl, Christoph Ziegler, Franziska Urban, Jutta Lehnfeld, Natalja Moor und Oliver Sarosi danke ich für ihre Mitarbeit an meinen Forschungsprojekten.

Für ihre Hilfsbereitschaft, die gemeinsamen Kaffeepausen, spaßigen Abende und Ausflüge danke ich den derzeitigen und ehemaligen Mitarbeitern des Arbeitskreises, insbesondere: Thea, Caro, Willi, Natascha, Tomas, Anna E., Flo, Benno, Andi M., Josef, Susa, Peter, Tamal, Alex, Andi G., Anna B., Karin, Tonda, Nadja, Stefano, Amrita und Martin.

Vielen lieben Dank an meine Studienkollegen, ganz besonders an Steffi sowie Jens, Stefan W., Stefan V., Melli, Julian und Simon für die gegenseitige Unterstützung und Eure Freundschaft! Ihr habt das Studium zu einer großartigen Zeit gemacht und langweilige in kurzweilige Momente verwandelt.

Von ganzem Herzen danke ich meinen Eltern für die Unterstützung auf jeder Ebene, für den Rückhalt und für Euer Vertrauen. Ich danke meinem Bruder, meiner Caro und meinen Stiefeltern, dass Ihr mich auf meinem Weg begleitet und für mich da seid.

Richard, ich danke Dir, dass Du mit mir gemeinsam durchs Leben gehst und mit Dir einfach alles so viel schöner, leichter, besser und lustiger ist.

Danke